Experimental and numerical study of the impact behaviour of an adhesively bonded automotive structure

by *Nelson Diogo Dias Silva*

Master Dissertation

Supervised by: Prof. Lucas Filipe Martins da Silva
Co-supervised by: Eduardo André de Sousa Marques
José Joaquim da Mota Machado

U.PORTO
FEUP FACULDADE DE ENGENHARIA
UNIVERSIDADE DO PORTO

Integrated Master in Mechanical Engineering

Porto, June of 2019

To my family and friends

Abstract

Reduction in fuel consumption and pollutant gases emission are nowadays the main challenges faced by the automotive industry. Therefore, car manufacturers began to produce lighter body structures, encouraging the use of aluminium alloys or composites, and searching for connection processes that do not imply the use of fasteners and/or rivets, such as adhesive bonding. So that the application of this technique is possible, it is fundamental to guarantee that adhesive joints fulfil the requirements demanded by the automotive industry, mainly those related to impact, ensuring passengers' safety. Studies of adhesively bonded automotive structures are crucial for the consolidation of this promising technology in the market, allowing the manufacturing of lighter, yet equally strong structures that are able to satisfy the goals mentioned above.

The aim of the present work is the experimental and numerical analysis of a real-scale, adhesively bonded automotive structure belonging to the Aston Martin's DB11 model. The physical tests were conducted at room temperature (RT) and at different displacement rates, regarding quasi-static (1 mm/min) and impact (3 m/s) conditions. The data previously collected by ADFEUP's group regarding the epoxy system used to bond the structure allowed the definition of cohesive laws that were applied to predict the behaviour of the real component through numerical simulations using cohesive zone modelling (CZM) of the adhesive layer. The results were then compared to the experimental data to validate the numerical models. Since the adhesive layer thickness necessary for bonding the component's substrates was 1.6 mm, higher than the 0.2 mm commonly used in the study of adhesive joints, single-lap joints (SLJs) with these thicknesses were produced and tested. The objective was to analyse the effect of adhesive's thickness in the mechanical behaviour of these joints. For this purpose, the experimental tests were also conducted at RT and three displacement rates were applied, namely 1 mm/min, 0.1 m/s and 3 m/s. Numerical studies were also conducted for this case. Lastly, the adaptation of a test device for impact conditions was performed, which will allow to complement the mechanical characterization of adhesive systems in the future.

The tests performed on the automotive structure revealed that its response is ruled by the behaviour of the aluminium substrates and that the adhesive does not compromise its integrity, with the numerical analysis showing good accordance with the experimental data. Facing these results, a polyurethane was also considered to bond the structure, showing promising results in comparison with the epoxy. When it comes to the SLJs, it was possible to conclude that higher displacement rates and lower thicknesses lead to an increase in the failure load of the joint. The numerical models were also found to be in agreement with the experimental data for this study.

Resumo

A redução do consumo de combustível e da emissão de gases poluentes representam atualmente os principais desafios na indústria automóvel. Assim, os fabricantes começaram a apostar na produção de estruturas mais leves, privilegiando materiais como alumínio ou compósitos, e em processos de ligação alternativos aos parafusos e/ou rebites, como a ligação adesiva. Para que a aplicação deste método seja possível, é impreterível que as juntas adesivas cumpram os requisitos impostos pela indústria automóvel, principalmente aqueles relacionados com impacto, assegurando a segurança dos passageiros. O estudo de componentes automóveis unidos com recurso a adesivos torna-se assim fundamental para a consolidação desta promissora tecnologia no mercado, permitindo obter estruturas mais leves, mas igualmente resistentes, que satisfaçam os objetivos referidos inicialmente.

O objetivo do presente trabalho consiste na análise experimental e numérica de um componente automóvel, em escala real, pertencente ao modelo DB11 da Aston Martin Lagonda Limited®. Os testes físicos foram conduzidos à temperatura ambiente e a diferentes velocidades, nomeadamente em condições quase-estáticas (1 mm/min) e ao impacto (3 m/s). A informação reunida previamente pelo grupo ADFEUP acerca do epóxido utilizado para unir a estrutura, permitiu a definição de leis coesivas que foram aplicadas para a previsão do comportamento do componente real através de simulações numéricas usando modelação coesiva no adesivo, cujos resultados foram validados experimentalmente. Uma vez que a espessura da camada adesiva requerida na ligação dos substratos do componente foi de 1.6 mm, superior aos 0.2 mm comumente utilizados no estudo de juntas adesivas, foram desenvolvidas e testadas juntas de sobreposição simples com estas espessuras. Este estudo pretendeu aferir a influência da espessura de adesivo no comportamento mecânico destas juntas. As mesmas foram testadas à temperatura ambiente e sujeitas a três velocidades distintas, nomeadamente 1 mm/min, 0.1 m/s e 3 m/s. Estudos numéricos foram igualmente conduzidos acerca deste tópico. Por último, um dispositivo de teste foi adaptado para condições de impacto, o que futuramente irá permitir complementar a caracterização mecânica de adesivos.

Os testes realizados na estrutura automóvel revelaram que a sua resposta é dominada pelo comportamento dos substratos de alumínio e que o adesivo não compromete a sua integridade. Adicionalmente, um poliuretano foi também considerado para unir a junta automóvel, originando resultados promissores face ao epóxido. Relativamente às juntas de sobreposição simples, foi possível concluir que velocidades mais elevadas e espessuras de adesivo menores conduzem a maiores capacidades de carga nas juntas. Os modelos numéricos revelaram bons resultados face aos dados experimentais para ambos os estudos.

Acknowledgements

First of all, I would like to express my sincere gratitude to Professor Lucas da Silva, for giving me the opportunity to collaborate with ADFEUP and for all his support, consideration and advice.

I also want to give a special thanks to my co-supervisors, Eduardo Marques and José Machado, for all their shared experience, excellent guiding and assistance during this project. The accomplishment of this work would certainly not be possible without their support. A big thanks also goes to Diogo Antunes, for all the availability and crucial help given during the dynamic experimental procedures. My greetings are also extended to the remaining elements of the group, especially Paulo Nunes, for all their assistance when needed. A word of gratitude is also directed to Professor Marco Parente, for the good advices given about the numerical models, and to LOME, in the name of Pedro Moreira, Paulo Tavares and Nuno Viriato, for the kindness of providing the high-speed video camera used in the impact tests.

I am extremely thankful to my parents and friends, for all their support, patient and encouragement in the most difficult moments and throughout this long journey.

Finally, I gratefully acknowledge the funding of Project NORTE-01-0145-FEDER-000022 - SciTech - Science and Technology for Competitive and Sustainable Industries, co-financed by Programa Operacional Regional do Norte (NORTE2020), through Fundo Europeu de Desenvolvimento Regional (FEDER).

Contents

Abstract iii

Resumo iv

Acknowledgements v

Contents vi

List of acronyms viii

Notation ix

List of Figures x

List of Tables xiii

1 Introduction 1

1.1 Background and motivation 1

1.2 Problem definition 1

1.3 Testing an adhesively bonded automotive structure at ADFEUP 2

1.4 Objectives of the project 2

1.5 Project planning 2

1.6 Master dissertation structure/outline 3

2 Literature review 5

2.1 Aluminium alloys 5

2.1.1 Strain rate dependence 6

2.2 Adhesive bonding 7

2.3 Adhesives 11

2.3.1 Classification 11

2.3.2 Adhesives in the automotive industry 12

2.3.3 Crash-resistant adhesives 13

2.3.4 Fracture mechanics 14

2.3.5 Mechanical properties 15

2.3.6 Temperature and strain rate dependence 16

2.3.7 Numerical modelling: CZM 18

2.4 Automotive structures 21

3 Arcan device for impact 24

3.1 Design of the Arcan 24

3.2 Numerical analysis under impact 27

3.3 Adhesive's initial stress (due to Arcan's weight) 31

3.4 Mould for Arcan specimens 33

4 Study of aluminium SLJs bonded with a crash-resistant adhesive 36

4.1 Materials 37

4.1.1 Aluminium 37

4.1.2 Adhesive 39

4.2 Numerical details 41

4.3 Experimental details 42

5 Analysis of an adhesively bonded automotive structure 46

5.1 Structural support 47

5.2 Impactor 49

5.3 Materials 50

5.3.1 Aluminium 50

5.3.2 Adhesives 51

5.4 Numerical analysis 52

5.5 Experimental details 52

6 Conclusions 56

7 Future work 58

References 60

Appendix A: Paper 1 66

Appendix B: Paper 2 94

List of acronyms

4ENF	Four-Point End-Notched Flexure
ADFEUP	Grupo de Adesivos da Faculdade de Engenharia da Universidade do Porto
CM	Center of Mass
CZM	Cohesive Zone Modelling
DCB	Double Cantilever Beam
DIN	Deutsches Institut für Normung
DLJ	Double Lap Joint
ELS	End Loaded Split
ENF	End-Notched Flexure
FE	Finite Element
FEM	Finite Element Method
HAZ	Heat Affected Zone
LEFM	Linear Elastic Fracture Mechanics
LOME	Laboratório de Ótica e Mecânica Experimental
RP	Reference Point
RT	Room Temperature
RTV	Room Temperature Vulcanizing
SDEG	Scalar Stiffness Degradation
SF	Safety Factor
SHPB	Split Hopkinson Pressure Bar
SLJ	Single Lap Joint
TAST	Thick Adherend Shear Test
TDCB	Tapered Double Cantilever Beam
VCCT	Virtual Crack Closure Technique
VM	Von Mises

Notation

E	Young's modulus
G	Shear modulus
G_c	Critical strain energy release rate
G_I / G_n	Energy release rate in mode I
G_{II} / G_s	Energy release rate in mode II
G_{IC} / G_n^c	Critical strain energy release rate in mode I
G_{IIC} / G_s^c	Critical strain energy release rate in mode II
K	Stress intensity factor
$\boldsymbol{K}$	Elastic constitutive matrix
K_c	Fracture toughness
T_g	Glass transition temperature
t_n^0	Tensile/normal strength
t_n	Cohesive tensile/normal stress
t_s^0	Shear strength
t_s	Cohesive shear stress
δ_n^0	Initial tensile/normal displacement
δ_s^0	Initial shear displacement
δ_n^f	Final tensile/normal displacement
δ_s^f	Final shear displacement
ε_n	Tensile/normal strain
ε_s	Shear strain
$\dot{\varepsilon}$	Strain rate
$\dot{x}$	Displacement rate
ν	Poisson's ratio

List of Figures

Figure 1 - Project's workplan 3

Figure 2 - Aluminium components (painted in green, blue and red) in the body structure of Audi's Q8 [12] 6

Figure 3 - Stress-strain results obtained by Chen et al. [16], suggesting a strain rate-insensitive behaviour of the AA6xxx alloys and a moderate dependency of the AA7xxx alloys 7

Figure 4 - Types of failure in adhesive joints [21] 9

Figure 5 - Non-reinforced area and stress distribution in adhesive and riveted joints [21] 9

Figure 6 - Types of stresses acting in adhesive joints: a) normal/tensile, b) shear, c) cleavage, d) peel and e) torsion stress (adapted from [26]) 10

Figure 7 - Aston Martin's V12 Vanquish model [28] 11

Figure 8 - Stress distribution along the overlap for a stiff and a flexible adhesive [26] 12

Figure 9 - Mechanical behaviour of a crash-suitable structural adhesive [21] 14

Figure 10 - Diagram of an impact peel test for a structural and a crash-suitable adhesive [21] 14

Figure 11 - Load modes in fracture mechanics: a) mode I, b) mode II, c) mode III (adapted from [35]) 15

Figure 12 - Tensile stress-strain curves as a function of temperature and test speed obtained by Banea et al. [24] 17

Figure 13 - Stress-strain curves as a function of temperature and displacement rate for the epoxy adhesive tested by Machado et al. [2] 18

Figure 14 - Different CZM shapes: a) triangular and exponential laws; b) trapezoidal law (adapted from [41]) 20

Figure 15 - Schematic of the damage zone in an adhesively bonded joint and corresponding triangular law [45] 20

Figure 16 – Traction-separation laws for pure-mode and mixed-mode conditions: a) triangular [47] and b) trapezoidal [44] 21

Figure 17 - Body cover analyzed by Golzar et al. [49] 22

Figure 18 - Example of a side-door impact beam, developed by DuPont® [54] 23
Figure 19 - Configuration of the existent Arcan device, used in static tests 24
Figure 20 - Initial adaptation of the Arcan for impact tests 25
Figure 21 - 3D model of the a) old and b) new Arcan device 26
Figure 22 - Final design of the Arcan device to perform impact tests 27
Figure 23 - Configuration of the Arcan for quasi-static tests 27
Figure 24 - Encastre boundary condition in the right-side of the specimen 28
Figure 25 - Maximum VM stress on the half-Arcan 29
Figure 26 - Maximum VM stress on the steel parts of the specimen 29
Figure 27 - Maximum VM stress on the pins that connect the specimen to the Arcan 29
Figure 28 - Maximum VM stress on the inferior component 30
Figure 29 - Maximum VM stress on the inferior extractors 30
Figure 30 - Suspended structure that the adhesive needs to hold before impact tests 31
Figure 31 - Schematic of the simulated geometry 32
Figure 32 - Adhesive's initial stress 32
Figure 33 - Stress distribution along the bondline 32
Figure 34 - Stress distribution vs time at the tops of the adhesive layer for a bondline of 15 mm and impact conditions 33
Figure 35 - Existent mould to produce the Arcan specimens 34
Figure 36 - 3D model of the new mould, designed to be compatible with all specimens 34
Figure 37 – Dimensions (in mm) of the specimens for the existent Arcan 35
Figure 38 – Dimensions (in mm) of the specimens for the designed/new Arcan 35
Figure 39 - Joint configurations: a) SLJ, b) DLJ, c) Double scarf joint, d) Double stepped-lap joint (adapted from [59]) 36
Figure 40 - Schematic of the tested SLJs 37
Figure 41 - Load vs displacement curve of a SLJ with an overlap of 25 mm, indicating failure exclusively by plastic deformation of the aluminium substrates 37
Figure 42 - Stress-strain curves at different strain rates for the 6082-T6 alloy [65] 39

Figure 43 - Anodizing process: a) setup and b) closer look 42

Figure 44 - Aluminium substrates after anodizing 43

Figure 45 - Schematic of the SLJ configuration in the mould 43

Figure 46 - Manufacturing of SLJs using a mould 44

Figure 47 – Hot plate press used to cure the adhesive layer 44

Figure 48 - Universal machines used to perform tests under a) quasi-static and b) 0.1 m/s conditions 45

Figure 49 - Drop-weight machine used to perform impact tests 45

Figure 50 – Front header in the body structure of an Aston Martin's DB-11 model [66] 46

Figure 51 - Substrates of the automotive front header 47

Figure 52 - 3D model of the component in Hypermesh® (supplied by Aston Martin Lagonda Limited®) 47

Figure 53 - Designed structural support with clamps being used to fix the automotive front header 48

Figure 54 - Steel parts that allow the connection of the structural support with a) the drop-weight and b) universal testing machines 48

Figure 55 - Schematic of the new approach to fix the geometry of the automotive component 49

Figure 56 - Impactor's configuration for a) impact and b) quasi-static tests 50

Figure 57 - Influence of strain-rate on stress-strain curves of 6016-T4 alloy, for two different temperatures [67] 51

Figure 58 - Plastic behaviour of the 6016-T6 aluminium alloy 51

Figure 59 - Acrylic plates used in the test (left) and application of the adhesive (right) 53

Figure 60 – Adhesive's shape before (left) and after (right) the test 53

Figure 61 - Oven used to manufacture the front header joints 54

Figure 62 - Evolution of the temperature inside and measured by the oven, for a set temperature of 210 °C 54

List of Tables

Table 1 - Gantt diagram of the workplan 3

Table 2 - Properties of AV-138 adhesive used in the numerical simulation 28

Table 3 - Mechanical properties of PM300 steel at 20 ºC, supplied by Ramada Aços® [58] ... 30

Table 4 - Safety factors of the Arcan device components under impact 31

Table 5 - Mechanical properties of 6016 and 6082 aluminium alloys [62-64] 38

Table 6 - Yield and tensile strength of 6082-T6 alloy for the tested strain rates (adapted from [65]) 39

Table 7 - Mechanical properties of XNR6852 E-3, at 24 °C, for quasi-static and impact conditions [1, 2] 40

Table 8 – Stipulated mechanical properties of XNR6852 E-3, at 24 °C, for 0.1 m/s condition 41

Table 9 - General characteristics of XNR6852 E-3 adhesive 52

Table 10 - General properties and characteristics of the polyurethane used to bond the automotive structure 52

1 Introduction

1.1 Background and motivation

The rising concerns and new restrictions regarding the emission of polluting gases, together with the desire to obtain highly efficient cars, have led the automotive industry to adopt a light-weight manufacturing concept. To fulfil these requirements, light-weight materials, like aluminium, are being increasingly used instead of traditional materials such as steel. The weight saving is also extended to joining processes, which has led to the consolidation of adhesive bonding as an excellent alternative to other processes for joining both similar and dissimilar materials. Still, as all joining methods, adhesive joints for automotive applications must behave well under extreme conditions, especially under impact, so that passengers' safety can be ensured. The combination of safety standards and weight savings is not easy and therefore poses the biggest challenge for engineers when designing automotive components. Studies of real-scale adhesively bonded automotive structures, using numerical approaches with experimental data validation, are necessary to evaluate its behaviour and verify the application of adhesives in this field.

1.2 Problem definition

Although significant research has been done in the mechanical characterization of adhesives and adhesive joints, the analysis of real components, which is not very common in the literature, is of extreme importance and should also be considered to enable better designs. Therefore, the use of adhesive bonding in "real-life" structures requires further investigation and testing, not only to prove that this joining process can be successfully applied but also to show that its application do not compromise the structure's integrity during a crash. By analysing the behaviour of a real bonded component, the present master thesis attempts to give a valuable contribution to this area of expertise and encourage further studies.

1.3 Testing an adhesively bonded automotive structure at ADFEUP

The activities related to the project took place at ADFEUP's laboratory and installations, located in the Mechanical Engineering department of Faculty of Engineering of University of Porto. The main activities of the group are the experimental and numerical study of adhesive joints as an alternative to other joining processes such as fastening, riveting and welding. An extensive work was already developed and published by the group regarding this subject, but a full scale, automotive bonded component was never previously studied and experimentally tested. This represents the main purpose of the current project.

1.4 Objectives of the project

The main objective of the project is to numerically and experimentally test a real adhesively bonded automotive structure supplied by Aston Martin Lagonda Limited®. The tests will be performed at two displacement rates (quasi-static and impact conditions) and at RT. So that the experimental tests can be performed with the equipment available in the laboratory, a structural support to fix the component had to be developed. The information collected in previous works [1, 2] regarding the applied crash-resistant epoxy system allowed the definition of cohesive laws that can be used to predict the behaviour of the automotive frame through finite element method (FEM) simulations using CZM in the adhesive. These numerical results could then be compared to the experimental ones to validate the models.

Because the adhesive layer thickness used to bond the automotive frame is significantly different from the known optimal adhesive thickness for structural bonding (0.2 mm), SLJs made of aluminium substrates bonded with this specified thickness are proposed to be manufactured and tested.

Additionally, testing procedures and equipments need to be adapted by the group in order to complement the characterization of adhesives under impact. In this work, a device is meant to be designed for these conditions, using its configuration in static tests as reference.

1.5 Project planning

The tasks of the project were planned as presented in Figure 1 and Table 1.

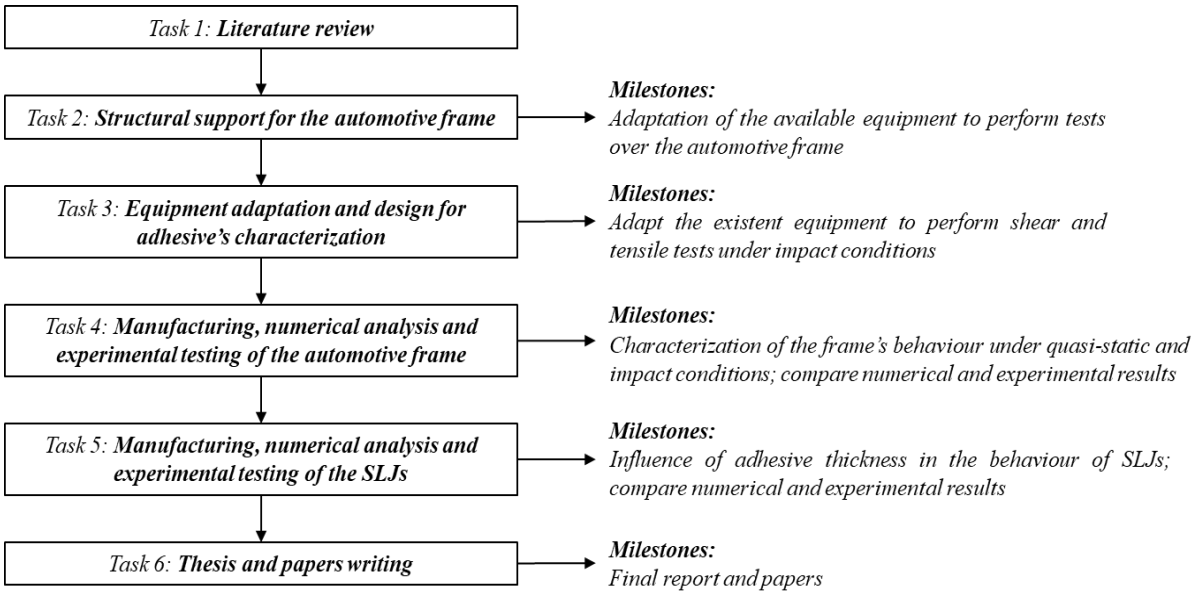

Figure 1 - Project's workplan

Table 1 - Gantt diagram of the workplan

Task	*February*	*March*	*April*	*May*	*June*
1					
2					
3					
4					
5					
6					

1.6 Master dissertation structure/outline

The work conducted in the context of this master dissertation can be divided into three major topics, as already introduced in section 1.4, namely:

1. Design of testing equipment to perform shear and tensile tests under impact conditions, allowing the mechanical characterization of adhesive's shear and tensile properties;
2. Numerical and experimental study of SLJs made of aluminium substrates bonded with a crash-resistant epoxy adhesive, for adhesive layer thicknesses of 0.2 and 1.6 mm;

3. Numerical and experimental analysis of a real, adhesively bonded automotive structure/frame under quasi-static and impact conditions at RT.

In the following sections, each one of these topics will be presented in separated chapters. Therefore, chapters 3, 4 and 5 will be dedicated to points 1, 2 and 3, respectively. Since two papers were also written in the context of the dissertation, these chapters generally describe the tasks and only include the information that is not available in the papers, so that repetitions could be avoided. The structure of the papers is similar, as they both include information regarding the automotive structure and the SLJs. While paper 1 focus on all procedures and results at static conditions, paper 2 presents the same but for the impact load. The topic 1, about the design of the testing equipment, is mentioned on the master thesis document only.

Finally, it is worth mentioning that both papers were already submitted to international journals. The first paper, named "Experimental and numerical study of the quasi-static response of an adhesively bonded automotive structure" was submitted to the "Engineering Failure Analysis" journal and the second, designated as "Experimental and numerical study of the dynamic response of an adhesively bonded automotive structure", was sent to the "International Journal of Impact Engineering".

2 Literature review

2.1 Aluminium alloys

Reduction in fuel consumption and CO_2 emissions is one of the most challenging concerns faced by automotive manufacturers worldwide. A solution to achieve this goal is the manufacture of lighter structures, encouraging the use of materials such as aluminium and composites in opposition to the traditional steel in vehicle's body structure, which represents 20-30% of its total weight [3]. Despite the excellent strength and stiffness to weight ratios of composite materials, their application in high volume structural automotive applications is still limited, mainly due to high material and manufacturing costs and some uncertainty related to functionality and long-term durability [4-7]. On the other hand, aluminium is a well-studied material and its low density in comparison to steel, associated to high corrosion resistance and good formability [1, 8, 9], makes it attractive for body frame construction. The lower strength and stiffness can be successfully compensated with the design of the spaceframes and the use of thicker sections [3], with high strength aluminium alloys being able to satisfy the torsion and stiffness requirements of an automotive component [10]. Aluminium is available in several varieties of semi-finished forms (such as sheet, extrusions and shape castings). Highly integrated and compact parts lead to the cost-efficient manufacturability, quality and high performance demanded by this sector. In fact, it was estimated that the average European car had 140 kg of aluminium content in 2012 [11]. The applications of aluminium in automotive components is very diverse and can cover body structure, chassis and power trains [9]. A good example of the application of aluminium in the body structure of an automobile is the Audi's Q8 model (Figure 2).

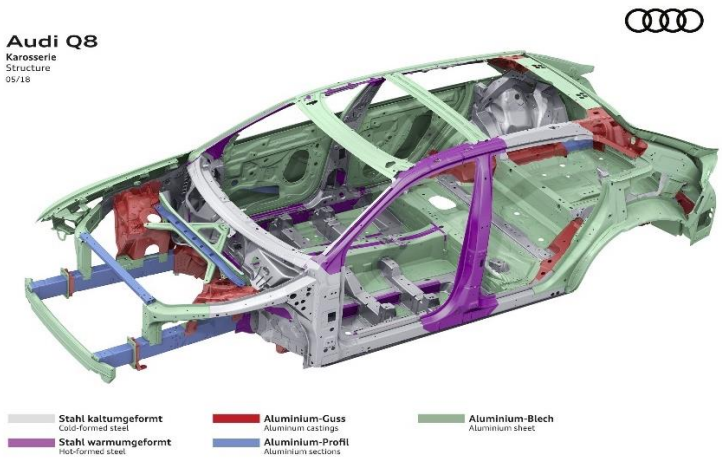

Figure 2 - Aluminium components (painted in green, blue and red) in the body structure of Audi's Q8 [12]

The most common aluminium alloys used in automobiles belong to the 5xxx and 6xxx series [13]. The first ones, highly deformable, are mostly used for inner panel applications, while the second ones, heat-treatable, are preferred for outer panels [9]. Within the 6xxx series, AA6016 (Europe) and AA6111 (USA) alloys are frequently used for body structures. The AA6016 alloy is preferred in Europe because it shows a superior formability and corrosion resistance compared to AA6111 [10, 11].

2.1.1 Strain rate dependence

The strain rate sensitivity of aluminium alloys used in the automotive industry has been studied by several authors over the years, for different alloys and surface treatments. This dependence appears to be alloy and heat treatment dependent [14], with a decrease being observed with an increase of the alloy content and with tempering [15].

Oosterkamp et al. [15] analysed the behaviour of the AA6082 and AA7108 alloys in T6 and T79 tempers at different strain rates, in a range from 0.1 to 3000 s^{-1}. It was concluded that the strain rate sensitivity of both alloys is very low.

Tensile tests from low to high strain rates were conducted by Chen et al. [16] on aluminium alloys belonging to the AA6xxx and AA7xxx series in T6 temper, namely AA6082, AA6060, AA7003 and AA7108 alloys. A standard tensile test machine was used to perform the tests from low to intermediate strain rates, while high strain rates were achieved with a split-Hopkinson tension bar. The AA6xxx alloys were found to exhibit no significant strain rate sensitivity in the stress-strain behaviour, while moderate dependence was observed for the AA7xxx alloys. Therefore, the authors concluded that the alloys belonging to the AA6xxx series can be modelled as strain rate-insensitive with good accuracy and strain rate dependence should be included for better results when it comes to the AA7xxx series alloys.

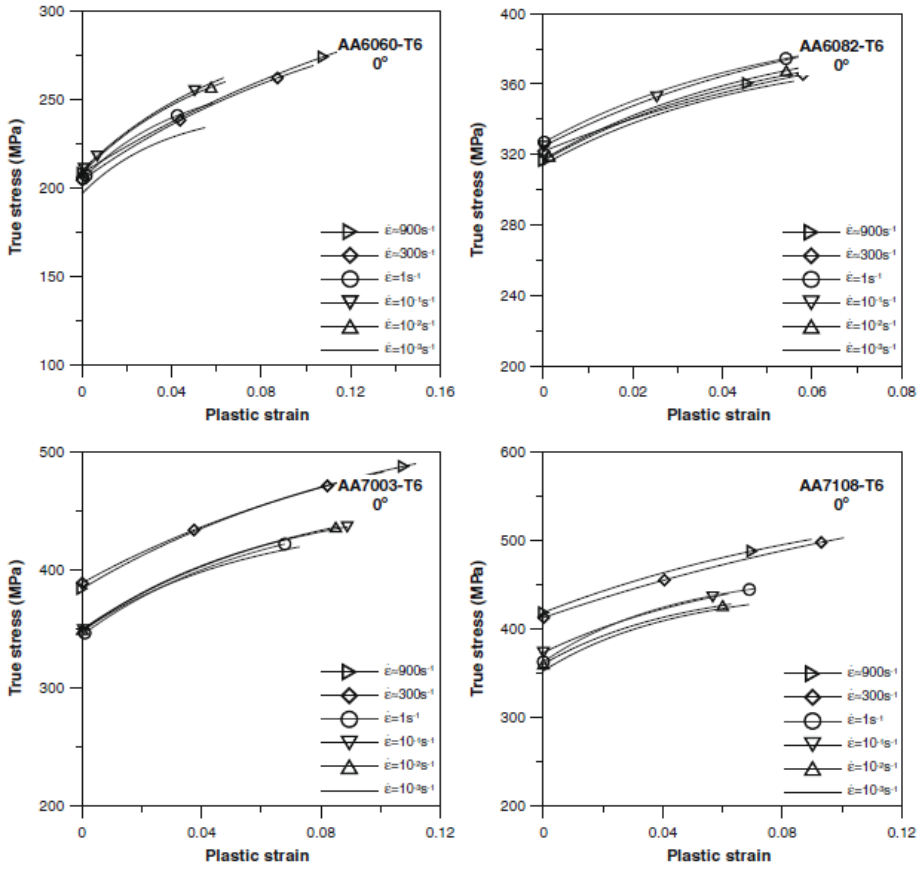

Figure 3 - Stress-strain results obtained by Chen et al. [16], suggesting a strain rate-insensitive behaviour of the AA6xxx alloys and a moderate dependency of the AA7xxx alloys

Tensile tests at different strain rates, namely $3.3x10^{-3}$ (quasi-static conditions), 600, 1100 and 1500 s^{-1}, were also performed by Smerd et al. [14] for the AA5754 and AA5182 alloys. For this case as well, both aluminium alloys showed low strain rate sensitivity.

From the results presented above, the strain rate dependence of the aluminium alloys used in the automotive industry seems to be insignificant, especially considering the AA6xxx series, and its mechanical behaviour can therefore be considered and modelled as strain rate independent.

2.2 Adhesive bonding

Despite the advantages associated with lighter body frames, weight reduction must not be followed by a decrease in strength, the end goal being to achieve lighter yet strong structures. Load bearing automotive components must perform well under complex loading situations and ensure safety requirements. This often leads to an increase in the complexity and new manufacturing difficulties. Thus, joining different components has become a major subject in this industry and a topic of constant research. Several techniques to join different parts of both similar or dissimilar materials can be used. Fasteners and rivets were the very first approach

and still represent a common solution in worldwide applications. Although they allow disassembly without damaging the components and do not require prior surface preparation, the use of fasteners and/or rivets causes discontinuity of the materials, increase in total weight and local stress concentrations, which may compromise the structures' integrity. Welding represents another option to join two components, but heat distortions and residual stresses appear in the heat affected zone (HAZ), which leads to deterioration of material properties [7]. Premature failure due to corrosion is another frequent problem, demanding more regular inspections [17]. Furthermore, it is difficult to weld aluminium properly as it tends to react with oxygen, forming an oxide layer in the surface that, although protecting against corrosion, has a higher melting point than aluminium [18]. Welding composite materials is also a difficult process and a matter of intense research over the last years, as existing processes and technologies cannot be directly transferred to these materials [19]. For these reasons, the automotive industry (as others like the aerospace and naval industries) started looking for alternatives leading to an increased and renewed interest in adhesive bonding. Over the last decades, this method for joining different parts has been gained importance, as it represents an excellent alternative to the methods presented above.

In adhesive bonding, an adhesive is used to bond two materials, which are called *substrates*. Basically, an adhesive may be defined as a material that allows the joining between different surfaces when applied between them and resist separation [20]. After bonding, the substrates are generally called *adherends*. To understand the principal phenomena that supports adhesive bonding, it is important to distinguish the concepts of *adhesion* and *cohesion*. The first is defined as the attraction between two substances resulting from the established intermolecular forces between them, while the second only involves intermolecular forces inside one substance. *Adhesion* can then be described as the ability of the adhesive to establish and maintain interactions with the substrates and *cohesion* can be assumed to determine the ability of the joint to effectively contribute to the solidity of the assembly. The main intermolecular forces that are present in both adhesion and cohesion are van der Waals type forces [21].

Two failure mechanisms can be observed in adhesive joints with aluminium substrates (and metallic substrates in general), namely cohesive and adhesive failure (Figure 4). The last one happens in the interface between the adherend and the adhesive and should not occur in a joint, since it often means a poor surface preparation during manufacturing. This type of failure is common when adherend's surface is contaminated (with rust or other particles) or its superficial energy is much lower than that of the adhesive. Cohesive failure, in the other hand, can happen in both the adhesive or the adherend, being the last the desired case as it means that

the adhesive doesn't compromise the strength of the joint. Cohesive failure in the adhesive can be caused by reasons such as the presence of voids, thermal stresses or the use of an inadequate overlap length, while cohesive failure in the adherend occurs when its strength limits are reached [1].

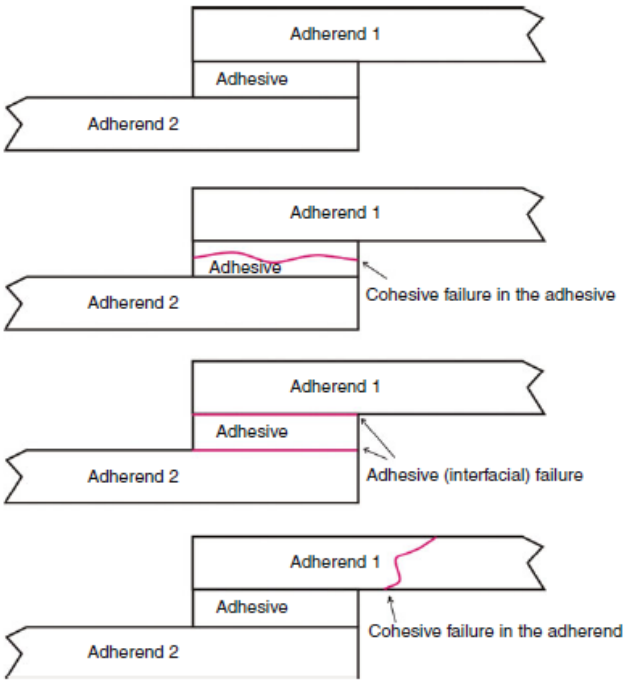

Figure 4 - Types of failure in adhesive joints [21]

Adhesive joints allow the manufacture and assembly of structures that would be impossible otherwise, can be readily automated [18] and generate smoother stress distribution along the bonded length, with a reduction of stress concentrations (Figure 5) [17-19, 22], thus enhancing fatigue resistance [2, 18, 23]. Additionally, the use of adhesives leads to reduction of noise and vibrations [3, 18], improved damage tolerance and lower fabrication costs [24].

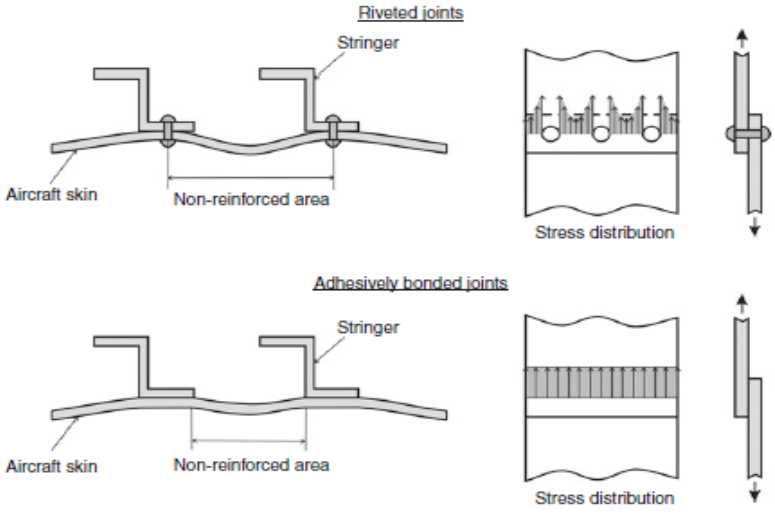

Figure 5 - Non-reinforced area and stress distribution in adhesive and riveted joints [21]

However, they also present some disadvantages that can limit their application and encourage further investigation, being the most significant the following [21]:

- Poor behaviour under peeling and cleavage stresses, as they concentrate the load in a small area;
- Limited resistance to extreme humidity and temperature conditions due to its polymeric nature;
- Prior surface preparation is often required to allow good adhesion;
- Need of fixtures to hold the substrates during the curing process;
- High curing temperatures are necessary for many adhesives, demanding the use of equipment such as ovens and autoclaves;
- Disassembly of the bonded structures is not possible without damage;
- Quality control is difficult to perform.

Of all types of loads that can be applied to a bonded joint, peel and cleavage stresses are indeed the ones that cause more damage and should therefore be avoided as much as possible [25]. Peel stresses are mainly due to eccentric loads and appear on the edges of the adhesive layer, while cleavage is caused by bending moments or offset tensile loads. Besides these, other common stresses acting in a joint are normal (tensile or compressive), torsion and shear stresses, with the last ones being more suited for adhesive joints (Figure 6).

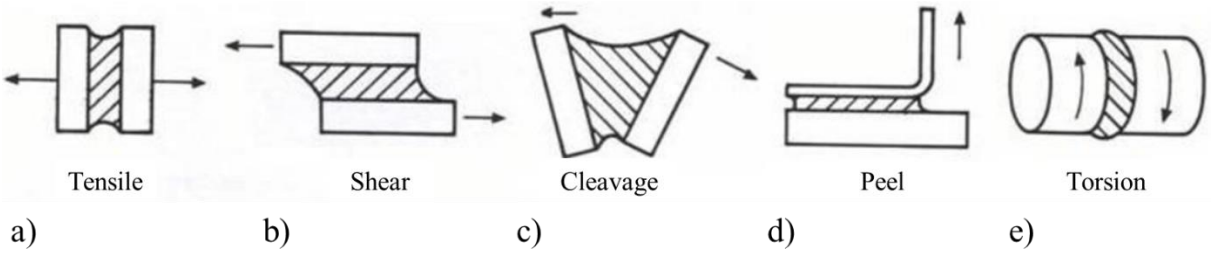

Figure 6 - Types of stresses acting in adhesive joints: a) normal/tensile, b) shear, c) cleavage, d) peel and e) torsion stress (adapted from [26])

In an attempt to reduce fuel consumption and gases emission, the automotive industry has become one of the leaders in the use of adhesive bonding for structural purposes, with lighter materials being bonded with this technique. Several car manufacturers have already shown the benefits of adhesive bonding with the production of concept cars like Ford's AIV, Jaguar's XJ220, Rover's ECV3, Honda's NSX, Audi's A2 and A8, BMW's Z8 and the Lotus Elise [11, 18]. The 2002 Aston Martin's V12 Vanquish (Figure 7), one of the most technically advanced cars of its time, had a space-frame made of extruded aluminium and adhesive bonding was

chosen to join the entire vehicle together, with a single-component epoxy toughened adhesive used to bond the aluminium extrusions [27].

Figure 7 - Aston Martin's V12 Vanquish model [28]

2.3 Adhesives

2.3.1 Classification

Adhesives can be classified according to several parameters, being the most important its origin, structure and function. Adhesives' origin can be either natural or synthetic. Natural adhesives are obtained from natural resources and casein-based adhesives or natural rubber are some examples belonging to this group. Synthetic adhesives are the most common and all types of epoxies, silicones, acrylics, phenolics or polyesters are part of these.

In terms of structure, adhesives are often classified as thermosets, thermoplastics, elastomers or hybrid. Thermosetting adhesives cannot be melted again after curing, as they consist of prepolymers in a viscous or soft solid state that irreversibly change into an insoluble polymer network. Thermoplastic adhesives have that possibility if heated up to temperatures above glass transition temperature (T_g), with further cooling leading to the return of the solid state [1]. Therefore, they can be repeatedly softened or hardened by an increase or decrease in temperature, respectively. Thermosetting materials are usually stronger than thermoplastics and are more suited to high-strength and high-temperature applications. The main advantages of elastomers are their high toughness, elongation and peel strength, but they are not very strong. Hybrid formulations result from a combination of different types of adhesives, allowing to obtain the best properties of each one [21].

Adhesives can still be divided in structural or non-structural, depending on their function. Structural adhesives are used to transfer loads between adherends during service and its shear strength can vary from 5 MPa for a polyurethane to 50 MPa for an epoxy, being the most

interesting in this engineering context. They are mainly one- or two-component thermosetting resins and present good resistance to high temperatures, solvents and creep. A two-component system usually consists of a resin and a hardener, with the possible addition of additives such as accelerators, resin modifiers, plasticizers, reactive diluents and fillers. While one-component systems often cure at high temperature and present reduced shelf life, two-component systems cure at RT and have longer shelf life, although its working temperature is lower [21]. Structural adhesives can be more ductile and flexible or present a stiff behaviour. Ductile adhesives are generally weaker than the stiffer ones, but when applied in a joint their ductility is used to redistribute the stress along the overlap length. Joints bonded with ductile adhesives can therefore present higher strength than others bonded with stronger but less ductile adhesives [26].

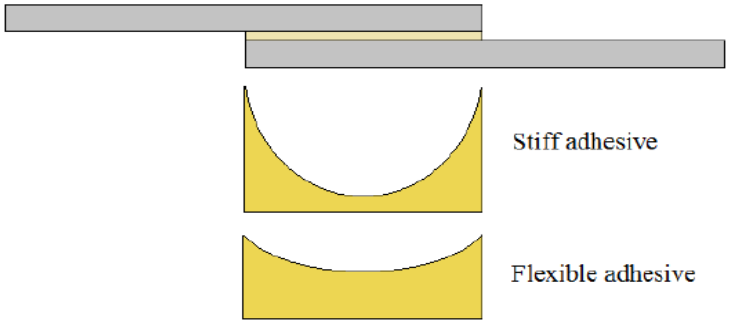

Figure 8 - Stress distribution along the overlap for a stiff and a flexible adhesive [26]

2.3.2 Adhesives in the automotive industry

Epoxy systems represent the most common types of adhesive used in automotive structural applications [29]. Besides being synthetic, epoxies can be classified as thermoset, structural adhesives and are the most important and versatile of their kind. They are successfully used to bond a variety of substrates and can be formulated to cure under dry or wet conditions and at a range of temperatures. Their success is mainly due to [21]:

- High strength;
- Good heat and solvent resistance;
- Relatively low-cost;
- Good gap-filling capabilities;
- Wide range of formulations;

and their principal drawbacks are [21]:

- Short pot life;
- Exothermic reaction;

- Optimum properties require exact material proportions.

Although strong, conventional epoxies are very brittle and therefore have insufficient energy absorption properties, leading to reduced shear strength and peel resistance under impact [29, 30]. During the 1990s, toughened, crash-resistant epoxy adhesives were developed to present superior energy absorption capabilities and good strength at high strain rates [31]. The toughening is usually achieved with the addition of flexible polymer or rubber particles to epoxy-based formulations. Crash-resistant epoxy adhesives are able to combine high ductility with high strength and stiffness, allowing the absorption of significant amounts of energy in comparison to standard adhesives [23]. For instance, an epoxy adhesive was used to bond load carrying components of the Lamborghini's Murcièlago model due to its capability to guarantee a stiff bond and joint stability [32], and to bond the extruded aluminium sections that shape the chassis of Lotus' Elise and Evora models [7]. Borsellino et al. [18] analysed the joint resistance of an aluminium alloy sheet with several adhesives (orthophtalic polyester, vinylester and epoxy resins) and concluded that the epoxy resin joint was the most resistant, due to the intrinsic strength of the adhesive, the enhanced stability of aluminium oxide in alkaline environment and the effect of mixing with catalyst.

In addition to epoxy systems, polyurethanes and acrylics represent other frequent types of adhesives used in the automotive industry. Polyurethanes are known for their high toughness, peel strength, durability and good fatigue behaviour, but its mechanical strength and heat resistance is lower in comparison to epoxies. Acrylics present good flexibility, peel and shear strengths and are especially useful to join dirty/less prepared surfaces as surface preparation is usually not required. The low strength at high temperature, flammability and toxicity are their major drawbacks [1, 21]. Adhesives belonging to this family are often applied in humid environments due to its resistance in this conditions [33].

2.3.3 Crash-resistant adhesives

A crash-resistant adhesive should present a behaviour similar to the one showed in Figure 9, where three distinct sections can be found. Initially, section 1, the adhesive reveals a linear-elastic behaviour, where the strength and deformation can be predicted using constitutive relations. Section 2 represents a zone where the adhesive should be able to withstand, without damage, high loads for short periods of time, characteristic of impact conditions. Sections 1 and 2 are typical for high strength structural adhesives, including the brittle ones. What really distinguishes a crash-suitable adhesive from these is section 3, where a wide deformation should occur, allowing the absorption of a significant amount of energy and the failure delay.

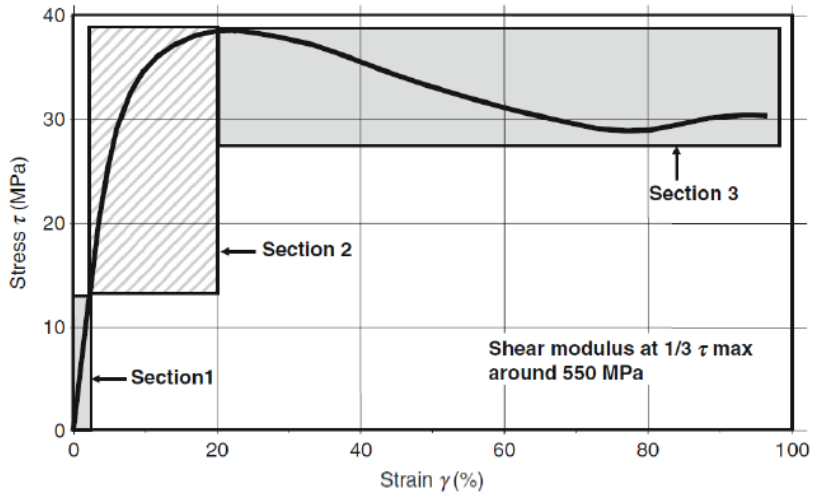

Figure 9 - Mechanical behaviour of a crash-suitable structural adhesive [21]

The difference between a crash-resistant and a very good structural adhesive can be clearly seen in the diagram of an impact peel test (Figure 10). While a standard structural adhesive presents an average peel resistance of 400 N during 15 miliseconds (ms), the crash-resistant one provides an average resistance of 900 N for almost 20 ms. As the area below a curve is a measurement of the absorbed energy, it is possible to conclude about the superior energy-absorption capabilities of the crash-resistant adhesive.

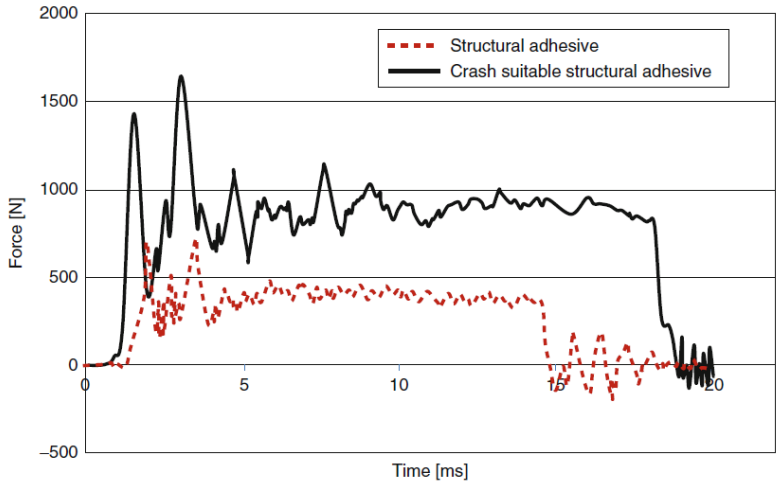

Figure 10 - Diagram of an impact peel test for a structural and a crash-suitable adhesive [21]

2.3.4 Fracture mechanics

With the goal of presenting the most relevant mechanical properties of the adhesives, some concepts related to fracture mechanics must be introduced beforehand. In a fracture mechanics approach, the materials are assumed to be non-perfect, in the way that defects are present and affect the mechanical behaviour of solids. The fracture is considered to initiate in the most critical defect and two major definitions are often applied to characterize this

phenomenon, namely an energy-based and a stress intensity-based criterion. Both criteria state that fracture will occur when a certain parameter in the defect reaches a maximum, often referred as the critical value. Therefore, the stress intensity-based theory states that fracture will initiate when the stress intensity factor (often designated as K) around the defect is equal to the critical one (called fracture toughness, K_c), while the energetic criterion states that the same will occur when the energy release rate (often designated as G) reaches the critical value (G_c). While the first approach is frequently applied in fracture mechanics of metallic materials, the second one, initially proposed by Alan Griffith [34], is more common in adhesives [20] and composites.

Three loading modes can be distinguished depending on the orientation of the load with regards to the crack's plane: mode I, mode II and mode III (Figure 11). In mode I, the load is applied perpendicularly to crack's plane, leading to a tensile solicitation, while in mode II and III the applied load is parallel to this plane. The difference between mode II and III is that the load is perpendicular and parallel to crack's front edge, respectively. This way, mode II leads to an in-plane solicitation and mode III to an out-of-plane solicitation.

In adhesively bonded joints, modes I and II loadings are the most common. The forces acting on a bonded joint can therefore lead to the adhesive being loaded in pure mode I, pure mode II or a combination of both modes (I+II), often known as mixed-mode.

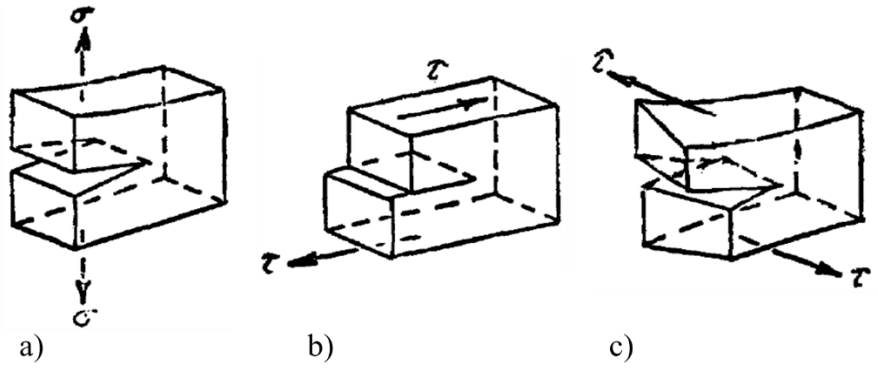

Figure 11 - Load modes in fracture mechanics: a) mode I, b) mode II, c) mode III (adapted from [35])

2.3.5 Mechanical properties

The most relevant mechanical properties of the adhesives can be defined as:

- Tensile strength (t_n^0);
- Young's modulus (E);
- Shear strength (t_s^0);
- Shear modulus (G);
- Critical strain energy release rate in mode I (G_{IC});

- Critical strain energy release rate in mode II (G_{IIC}).

Tensile strength and Young's modulus are commonly obtained by performing tensile tests on bulk specimens of adhesive. To determine shear strength and modulus, several testing procedures can be applied, such as the Notched plate shear method (Arcan) test, the torsion test, the Thick Adherend Shear Test (TAST) and the Iosipescu test [2]. The critical strain energy release rate in mode I and mode II are often known with the use of Double Cantilever Beam (DCB) and End-Notched Flexure (ENF) tests, respectively. An alternative to find G_{IC} is the Tapered Double Cantilever Beam (TDCB) test and G_{IIC} can also be determined using Four-Point Notched Flexure (4ENF) or End Loaded Split (ELS) tests [21].

2.3.6 Temperature and strain rate dependence

Due to its viscoelastic behaviour, adhesives have shown to be highly sensitive to both temperature and strain rate [1, 2, 24, 36].

The maximum service temperature range of the adhesives mainly depend on its type and can be defined as follows [21]:

1. Low Temperature (under 121°C): polyesters, polyurethanes;
2. Medium Temperature (121-260°C): epoxies, phenolics, silicones;
3. High Temperature (over 260°C): bismaleimides, polyimides.

The maximum service temperature of an adhesive is closely related to its T_g, that can be defined as the temperature from which the behaviour of the adhesive changes from glass- to rubber-like. Working at temperatures above T_g is unacceptable for structural applications as the stress relaxation in the adhesive leads to a decrease in modulus and strength [37]. Additionally, when designing a bonded joint to work at high temperatures, it is important to consider the difference in the thermal expansion coefficients between the adhesive and the substrates. A large difference may create additional stresses in the joint, leading to a decrease in its load capacity [38].

The response of adhesive joints under impact conditions is of extreme importance for the automotive industry, due to crash situations. When designing an adhesive joint for this industry, it is therefore necessary to investigate how the performance of a joint varies from static conditions. High values of strain to failure should be verified in a joint well suited for impact, so that energy absorption can be enhanced and the damage resistance increased. Impact conditions can be understood as discontinuous loadings that are normal during working conditions and to which the mechanisms should resist, or as punctual, impulsive situations that

are extraordinary and unusual during service conditions. The second case corresponds, for example, to an accident and is of more interest for the automotive manufacturers. The behaviour of adhesive joints under impact can be evaluated using several tests, being the most applied the drop-weight, wedge-peel, block impact and split Hopkinson pressure bar (SHPB) tests. Depending on the loading rate, the tests can be classified as [30, 39]:

- Low velocity: impact rates below 5 m/s, usually achieved with pendulum impact testers (ex: Charpy test) or with drop-weight machines;
- Medium velocity: obtained with drop-weight tests, for loading rates up to 10 m/s;
- High velocity: impact rates up to 100 m/s can be accomplished with the use of SHPB test.

Several studies were conducted in the last decade about the effect of temperature and strain rate on adhesives' properties. Banea et al. [24] investigated the combined effect of temperature and test speed on the tensile properties of an epoxy adhesive. It was concluded that both ultimate tensile stress and Young's modulus decreased with temperature and increased with strain rate. The effect of temperature was found to be more significant than that of the strain rate.

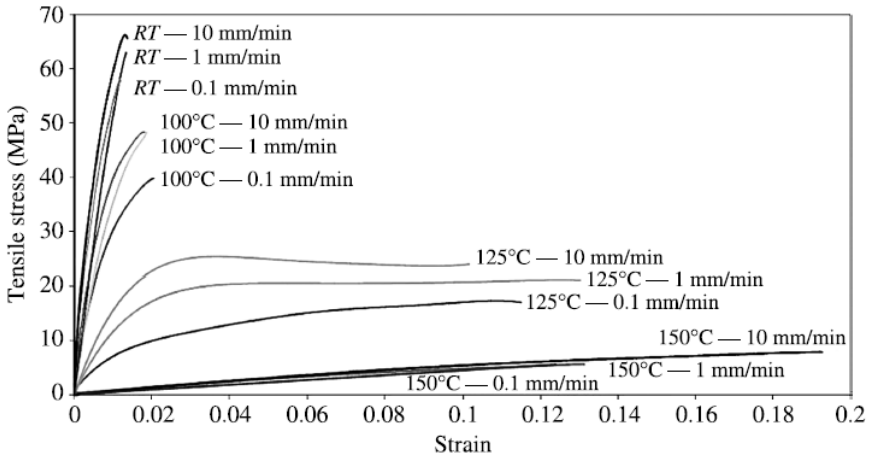

Figure 12 - Tensile stress-strain curves as a function of temperature and test speed obtained by Banea et al. [24]

In another work [40], the same author studied the effect of temperature in the shear strength of two flexible adhesives, a polyurethane and a room temperature vulcanizing (RTV) silicone rubber. A decrease in shear strength was found with increasing temperature for both adhesives.

Machado et al. [2] tested a crash-resistant epoxy at different temperatures and strain rates. Higher tensile strength and Young's modulus were observed with the increase of strain rate and the decrease of temperature. The G_{IC} was found to increase with both temperature and strain

rate. Higher values of G_{IC} for higher temperatures can be explained by the approach of T_g, which causes the adhesive to be more ductile and tough. An increase in strain rate also led to an increase in shear strength.

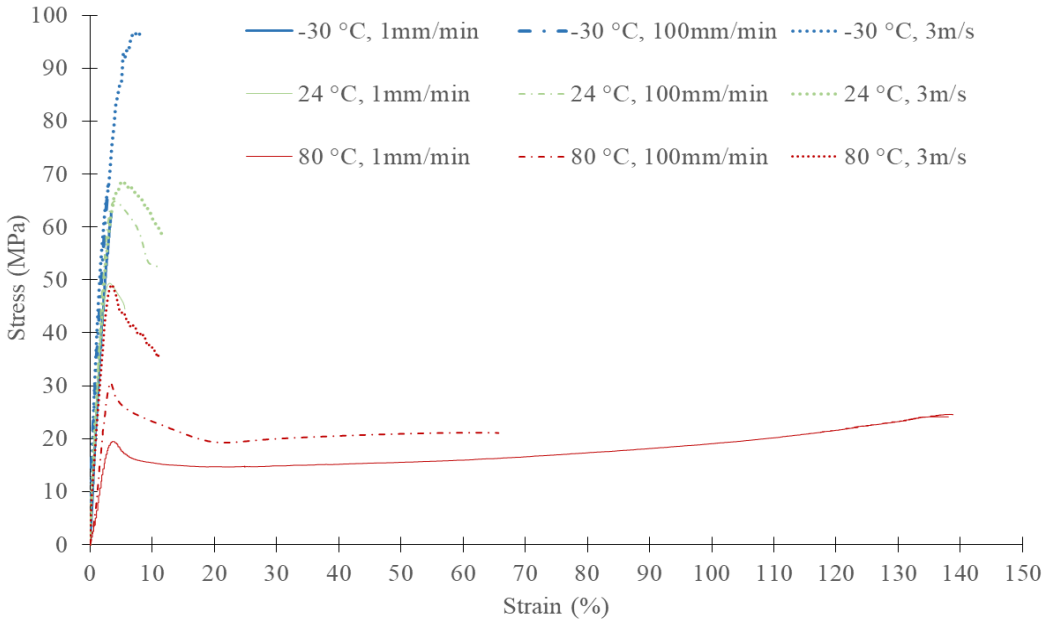

Figure 13 - Stress-strain curves as a function of temperature and displacement rate for the epoxy adhesive tested by Machado et al. [2]

2.3.7 Numerical modelling: CZM

Failure load prediction of bonded joints can be achieved analytically, numerically or experimentally. The use of analytical approaches, although being simple and direct, is limited to well defined geometries and loading conditions. Experimental data is the best source of information to obtain the mechanical behaviour of adhesive joints but carrying out experimental testing is not always possible or desired, as it requires time consuming manufacturing processes, material consuming and specific testing equipment. Therefore, numerical modelling through finite element (FE) analysis represents an excellent alternative to characterize joint's behaviour, especially for complex geometries or when a parametric study must be performed.

So that these numerical models can be applied, it becomes necessary to correctly predict both the stresses and the propagation of damage in the adhesive when loaded, which is often achieved using a technique called cohesive zone modelling (CZM). The initial FE models applied to adhesive joints considered fracture mechanics or stress/strain (continuum mechanics) criteria for failure prediction. Fracture mechanics criteria such as the Virtual Crack Closure Technique (VCCT) can only be applied to Linear Elastic Fracture Mechanics (LEFM), where the nonlinear area in front of the crack tip is negligible and an initial crack is required [41, 42]. The first statement cannot be assumed in presence of ductile materials, as the size of the

nonlinear zone (introduced by plasticity or microcracking) is relevant in comparison with the cracked geometry, and even for brittle materials (where this assumption is acceptable), the need of an initial crack stands as a limitation. Regarding stress/strain criteria, failure predictions are dependent of the mesh refinement at the critical regions [41].

These limitations encouraged the development and application of CZM, following a damage mechanics approach which was originally applied by Hillerborg [43] to concrete and cementitious composites, but can also be successfully applied to other materials, including adhesives. Besides being able to deal with the nonlinear zone ahead of the crack tip, the cohesive zone model is able to predict the behaviour of uncracked structures and not only the response of bodies with cracks [42]. This method has been used in adhesive joints as an add-in to FE analysis to simulate damage growth and evaluate joint strength, by making use of energetic principles. The use of this technique requires the establishment of traction-separation laws with a pre-defined shape at the failure paths. Several shapes can be developed for cohesive laws to model the behaviour of the adhesive. The most common CZM shapes are the triangular, trapezoidal and exponential laws, by this order, represented in Figure 14. The triangular law is often the first choice as it is the easiest to formulate and implement in FE codes and has less convergence problems. To apply any of these laws, material properties (G_{IC} and G_{IIC}, t_n^0 and t_s^0, E and G) are required, as they define the zones of elastic behaviour and damage initiation. For all laws, an initial linear evolution, with E / G as slope, is observed until t_n^0 / t_s^0 is reached, corresponding to an initial displacement δ_n^0 / δ_s^0 (points A and C in Figure 14). This evolution is characterized by the elastic behaviour of the material and no damage is caused within this zone. The current stresses and strains can be related by an elastic constitutive matrix using the following relation [41]:

$$\boldsymbol{t} = \begin{Bmatrix} t_n \\ t_s \end{Bmatrix} = \begin{bmatrix} K_{nn} & K_{ns} \\ K_{ns} & K_{ss} \end{bmatrix} \begin{Bmatrix} \varepsilon_n \\ \varepsilon_s \end{Bmatrix} = \boldsymbol{K\varepsilon} \tag{2.1}$$

Where t_n and t_s represent the cohesive traction values in tension and shear, respectively, corresponding to the strains in traction and shear, namely ε_n and ε_s. The stiffness parameters of the adhesive are contained in the stiffness matrix, $\boldsymbol{K}$, and for thin adhesive layers this matrix can be approximated doing $K_{nn}=E$, $K_{ss}=G$ and $K_{ns}=0$ [44]. From points A and C forward the damage initiates and its propagation is different depending on the law. For the triangular and exponential laws, the damage follows a linear and an exponential evolution, respectively, until total failure occurs (points B and B'). In the case of the trapezoidal law, a stage at t_n^0 / t_s^0 is observed prior to degradation, corresponding to a zone where the damage doesn't lead to a decrease in the material strength. After this stage (point D forward), the softening starts until

the maximum damage is reached (point E), leading to material failure. These traction-separation laws can be constructed for all loading modes presented before. Therefore, the tensile properties are used for the laws when in mode I loading conditions, while shear properties are used for mode II. Depending on the mode, the total area below a law is defined as G_{IC} (or G_n^c), in tension, and G_{IIC} (or G_s^c), in shear, meaning the maximum energy the material is able to withstand. This being said, the definition of the normal or shear maximum relative displacements (δ_n^f or δ_s^f, respectively) can be achieved by equalizing the values of the energy release rate in tension and shear to the critical ones ($G_n = G_n^c$ and $G_s = G_s^c$, respectively).

Experimental and numerical studies developed by Campilho et al. [41] showed that joints bonded with ductile adhesives are influenced by the CZM shape in the accuracy of the strength prediction, with the trapezoidal shape having the best agreement with experimental data. For brittle adhesives, the influence of the CZM shape was found to be negligible.

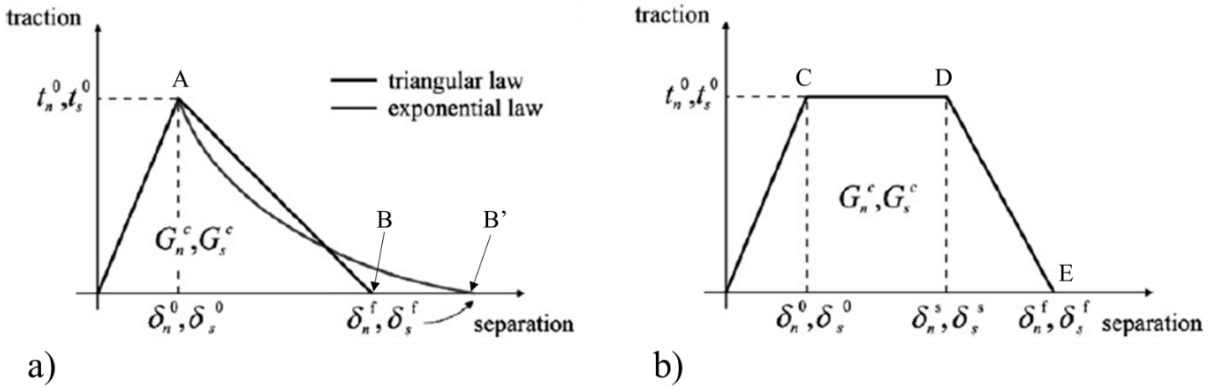

Figure 14 - Different CZM shapes: a) triangular and exponential laws; b) trapezoidal law (adapted from [41])

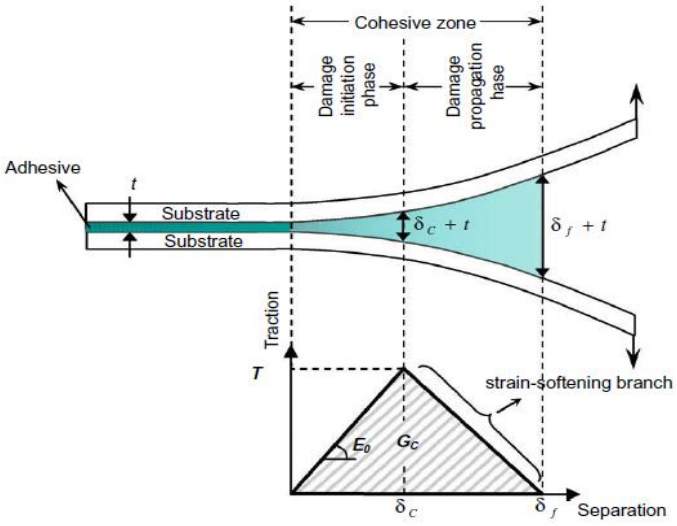

Figure 15 - Schematic of the damage zone in an adhesively bonded joint and corresponding triangular law [45]

When in the presence of a mixed-mode I+II condition, common in adhesive joints as mentioned earlier, a mixed-mode damage model is required, resulting from a combination

between the two modes, and the strength of the adhesive in this combined state will be lower than the one in presence of a standalone mode (Figure 16). Several mixed-mode models can be used to evaluate damage initiation and propagation, the most common being the quadratic nominal stress criterion [41], expressed in Eq. (2.2), and the linear fracture energetic criterion [46], expressed in Eq. (2.3). It is important to remind that the subscripts *n* and *s*, referring to tensile (normal) and shear behaviour, correspond to mode I and mode II conditions, respectively.

$$\left\{\frac{\langle t_n \rangle}{t_n^0}\right\}^2 + \left\{\frac{t_s}{t_s^0}\right\}^2 = 1 \tag{2.2}$$

The symbols ⟨ ⟩ are the Macaulay brackets, assuming that a purely compressive stress state does not initiate damage. Therefore, damage initiation in Eq. (2.2) is coupled only between tension and shear.

$$\frac{G_n}{G_n^c} + \frac{G_s}{G_s^c} = 1 \tag{2.3}$$

From the exposed above, it is direct to conclude that the application of CZM requires the knowledge of several adhesive properties, that can be obtained experimentally using the tests mentioned earlier in this document.

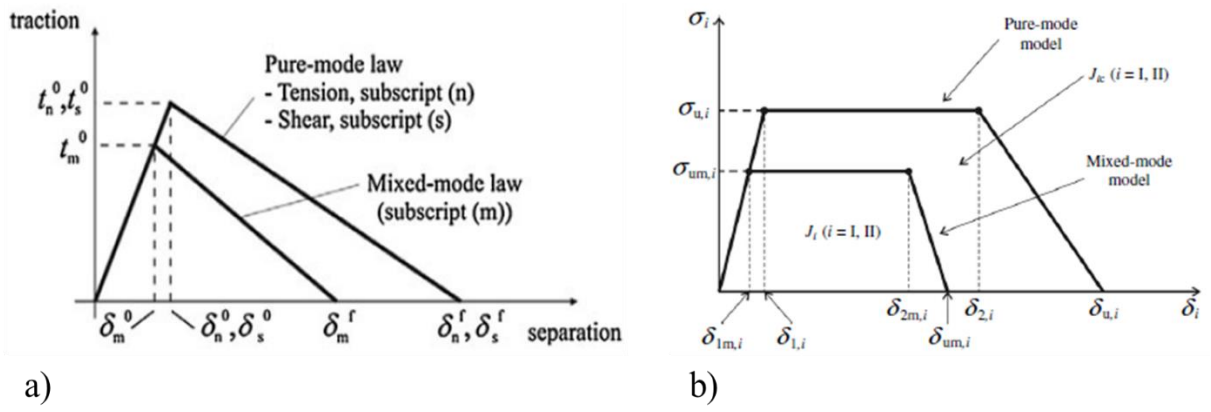

Figure 16 – Traction-separation laws for pure-mode and mixed-mode conditions: a) triangular [47] and b) trapezoidal [44]

2.4 Automotive structures

FE models are a powerful tool for designing adhesively bonded structures, as the models can reduce the number of experimental tests that need to be conducted. SLJs made of aluminium substrates bonded with an epoxy adhesive were tested in [1] and the numerical results showed good accordance to the experimental ones when a quasi-static load was applied. This was not

the case under impact, which was assigned to the lack of property data related with damage initiation and propagation of the studied aluminium alloy. Quasi-static and dynamic numerical analysis of mixed adhesive SLJs for automotive applications were tested in [48]. Besides the difficulty in modelling the plastic behaviour, it was concluded that cohesive numerical models are a viable tool to predict the behaviour of mixed joints. When it comes to real, fully-scaled bonded automotive structures, however, the information available is still limited and few examples can be found regarding a comparison between experimental and numerical results. Therefore, due to the lack of confidence in FE models, experimental analysis is often required to validate the structures and guarantee its agreement with all safety and performance standards, especially those related to impact. Despite offering accurate results about the mechanical behaviour, experimental testing of full-scale automotive components can be very expensive, time consuming and the structure being evaluated inevitably suffers extensive damage.

Golzar et al. [49] manufactured a prototype of a composite body cover structure to replace steel in an automobile model (Figure 17). A FEM study, carried out in Abaqus® (Dassault Systèmes, Suresnes, France), was used to analyse its behaviour under impact and to determine the lay-up's thickness and orientation that would maximize energy absorption. A composite body cover with 1.6 mm thickness was found to have higher energy absorption performance in comparison to steel, while allowing a 42% weight saving. No experimental tests were conducted.

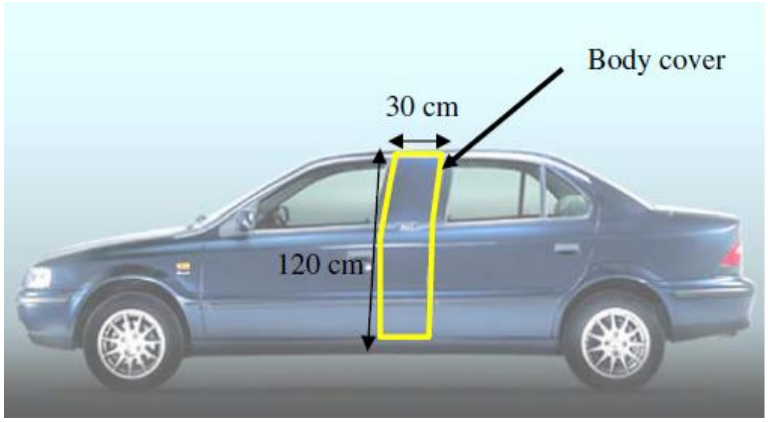

Figure 17 - Body cover analyzed by Golzar et al. [49]

Lahaye et al. [50] focused on the development of an aluminium (AA6016 alloy) bonnet for the Saab 9-3 model in replacement of the steel version. The new prototype allowed a 50% weight reduction and satisfied the performance tests required by Saab®.

The crash behaviour of thin-walled aluminium extrusions, which represent the base of the aluminium space-frame concept, was studied by Langseth et al. [51]. The extrusions were subjected to axial loading conditions and three different configurations were tested, namely

non-filled extrusions and aluminium foam-filled extrusions with and without an epoxy adhesive between the foam and the walls of the extrusion. Results suggested that the presence of the foam filler drastically changes the energy absorption behaviour in comparison to the non-filled extrusions, with the use of adhesive increasing the mass specific energy absorption. The non-linear finite element simulations conducted in the computer code Ls-Dyna® (Livermore Software Technology Corporation, Livermore, USA) over the AA6060 alloy non-filled extrusions (the only numerical simulations presented) were in accordance with the experimental results.

Cheon et al. [52] investigated the use of a glass-fibre-reinforced epoxy composite in alternative to steel in the side-door impact beams of passenger cars. The energy absorption behaviour of the composite beams was found to be worse at static and better at dynamic conditions. The FE results obtained in Abaqus® for static conditions showed good agreement with experimental data. A similar automotive component was analysed by Li et al. [53] exclusively using a numerical approach with the software Ls-Dyna®. The goal was to optimize the design of the beam so that energy absorption could be maximized in a lateral crash accident. The results of the new beam design showed improvements of 18% in the impact energy absorption and 14% in the impact load peak.

Figure 18 - Example of a side-door impact beam, developed by DuPont® [54]

3 Arcan device for impact

As mentioned before, tensile and shear strengths, as well as Young's and shear modulus, are important properties to characterize adhesives' behaviour. Such properties are used to determine the type of adhesive that should be chosen for a certain application and/or to predict the behaviour of bonded joints through numerical models. Of all existent tests to determine these properties, the Arcan test has the advantage of allowing several load combinations (tension, compression and shear) in the adhesive using standard test machines [55].

3.1 Design of the Arcan

The existent Arcan at the beginning of the project (Figure 19) only allowed to perform tests under quasi-static conditions, therefore being necessary its adaptation to obtain the adhesives' properties under impact. The first approach was to design, using the Solidworks® software (Dassault Systèmes, Massachusetts, USA), an easily adaptable structure for impact that could use the same device, as represented in Figure 20, in order to avoid the manufacture of a new one.

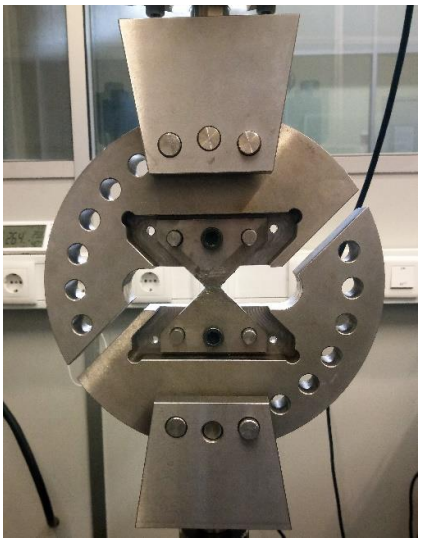

Figure 19 - Configuration of the existent Arcan device, used in static tests

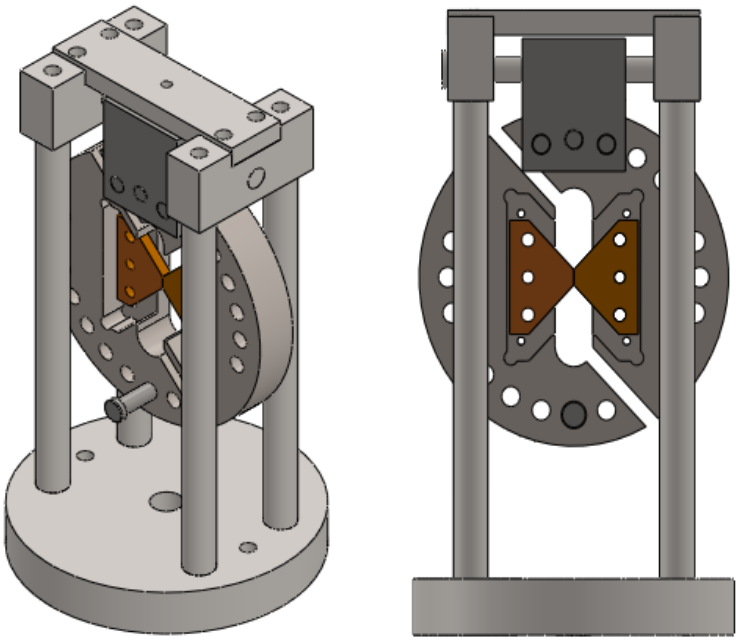

Figure 20 - Initial adaptation of the Arcan for impact tests

This configuration allows the execution of impact shear tests, as an impactor (not represented in Figure 20) is dropped and hits the middle pin, pulling down the left-half of the Arcan and, consequently, loading the adhesive layer that joins the specimen (part coloured in brown). While the right-half of the device is held by the structural support, the left-half must be sustained by the specimen, introducing a stress field in the adhesive at the initial state (prior to impact). The quantification of this stress is of crucial importance in order to guarantee that the weight is not excessively high for the adhesive and that it doesn't cause failure or damage before the test begins. To minimize this stress level, the possibility of decreasing the dimensions of the device for impact conditions was studied, still maintaining its general configuration. The comparison between the old and new Arcan, now assembled with the impactor, is represented in Figure 21. Besides this size reduction, some other changes were made as the two upper components of the structural support were merged. Although the shape of the resulting component is more complex, this solution avoids the use of the upper pin and possible problems related with misalignment.

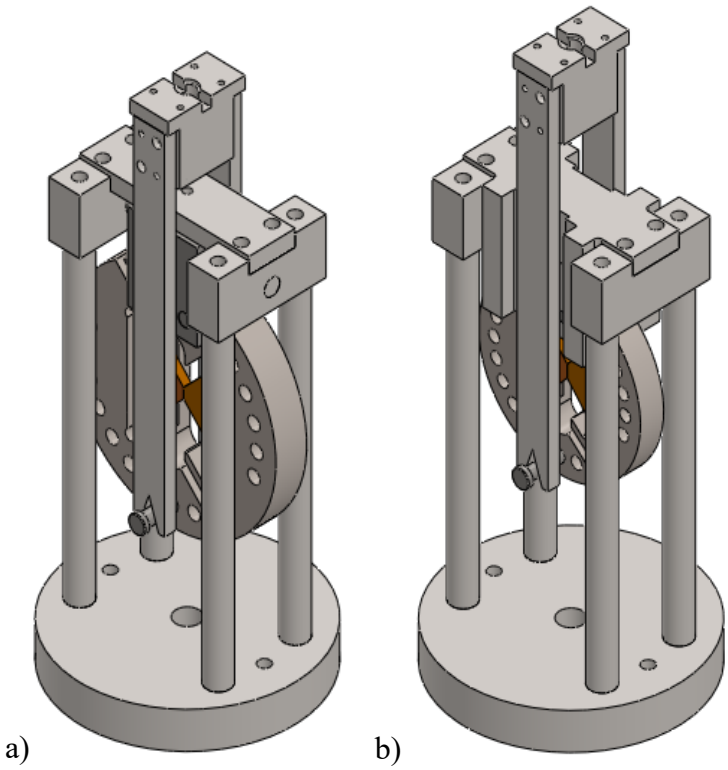

Figure 21 - 3D model of the a) old and b) new Arcan device

The impactor's mass is 8.5 kg and the target velocity during an impact test is 3 m/s. Preliminary numerical studies were conducted in Abaqus® regarding the impact in the standalone pin, which reached the conclusion that the stress level would be excessively high for a single pin. Therefore, the solution found to avoid this problem was to use a lower component, connected to the Arcan through a set of three pins, and which directly receives the impact. This new configuration is shown in Figure 22. The base of the structural support was changed from a circular to a rectangular shape in order to be compatible with other impact testing fixtures that were being developed by other elements of the group. The connection between the specimen and the Arcan is achieved by screws and pins, the latter being used to guarantee the alignment. This configuration allows the testing of specimens with an overlap length up to 50 mm. This device also retains the capability to perform tests under quasi-static conditions, using the assembly shown in Figure 23.

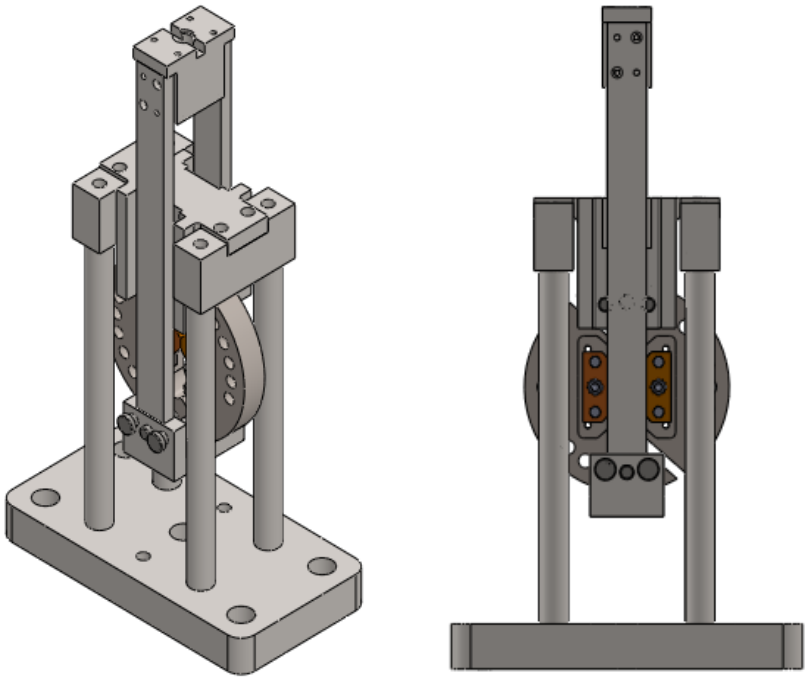

Figure 22 - Final design of the Arcan device to perform impact tests

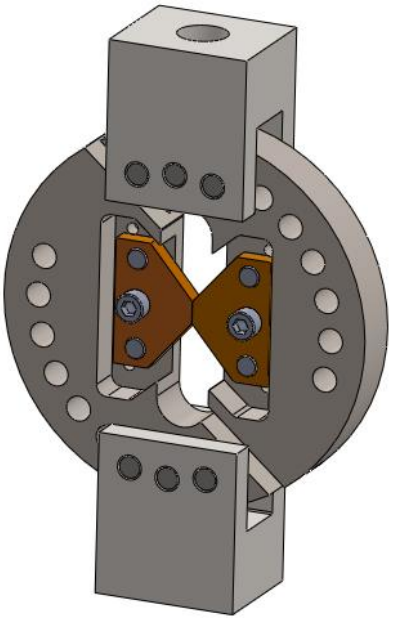

Figure 23 - Configuration of the Arcan for quasi-static tests

3.2 Numerical analysis under impact

A dynamic, explicit simulation was carried out in Abaqus® to verify the integrity of the Arcan device during impact tests. Cohesive (COH3D8) elements were applied to model the adhesive layer (the adhesive AV-138 was used, with the properties of Table 2), while 3D stress (C3D4) elements were selected for the other components. A total of 271981 elements were used. To simulate the impactor, a simplified shape was modelled as a rigid body and discrete

rigid elements (R3D4) were chosen. The mass and velocity of the impactor were applied in reference points (RPs). Since the focus was the behaviour of the left-half of the Arcan and the specimen under impact, the right-side of the Arcan and the structural support were ignored and its effect replaced by an encastre boundary condition at the right-side of the specimen (Figure 24). Additionally, the impactor' shape, the left-half of the Arcan and the inferior component were only permitted to move in the vertical direction. The STATUS and SDEG were requested as outputs to show the degradation of the adhesive during the simulation.

Table 2 - Properties of AV-138 adhesive used in the numerical simulation

Property	***Value***
t_n^0 *(MPa)*	41
t_s^0 *(MPa)*	30.2
E (MPa)	4890
G (MPa)	1560
G_{IC} *(N/mm)*	0.35
G_{IIC} *(N/mm)*	4.91

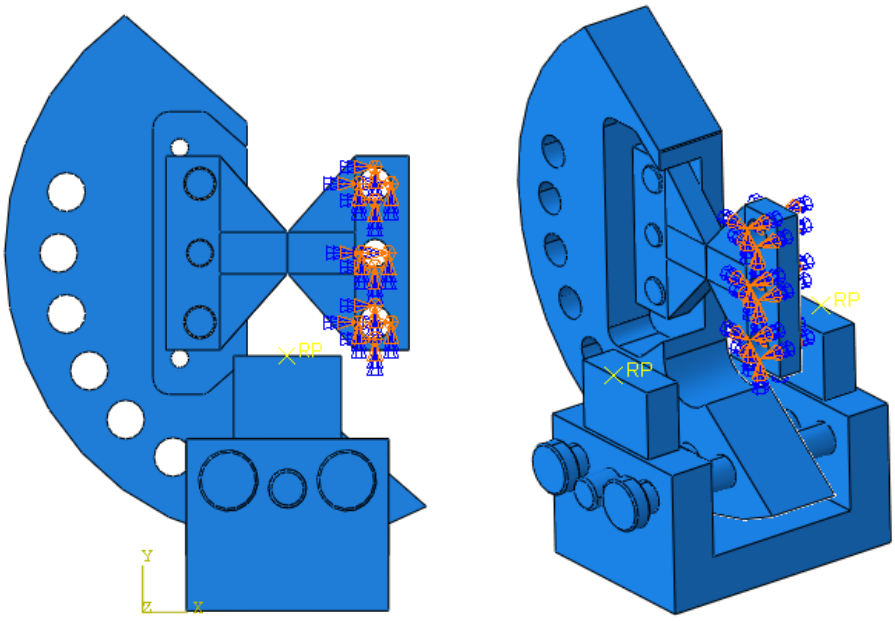

Figure 24 - Encastre boundary condition in the right-side of the specimen

The maximum Von Mises (VM) stress for all the individual components during the dynamic simulation is represented in Figures 25, 26, 27, 28 and 29, using typical steel values of 210 GPa, 7800 kg/m^3 and 0.3 for Young's modulus, density and Poisson's ratio (ν), respectively. Considering the results, a high-strength steel for moulds, with the mechanical properties shown in Table 3, was selected as the material for the Arcan components. The pins

and extractors have standard dimensions and were acquired directly from a supplier. According to literature [56] [57], the steel of the extractors (DIN 1.2344) and pins has a minimum yield stress of about 1280 MPa.

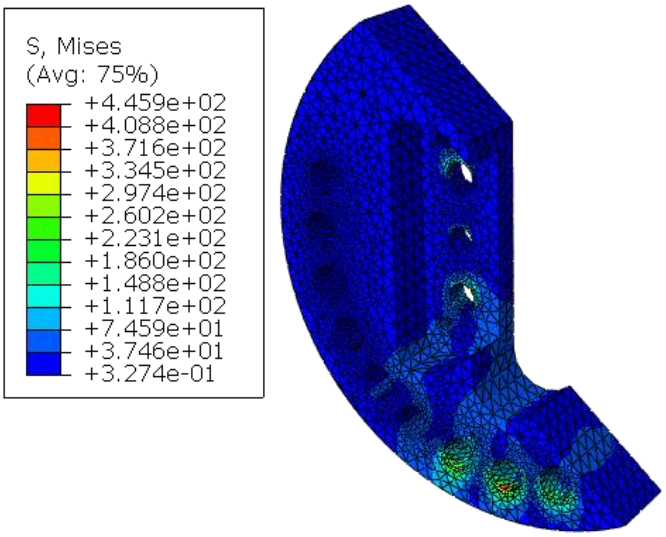

Figure 25 - Maximum VM stress on the half-Arcan

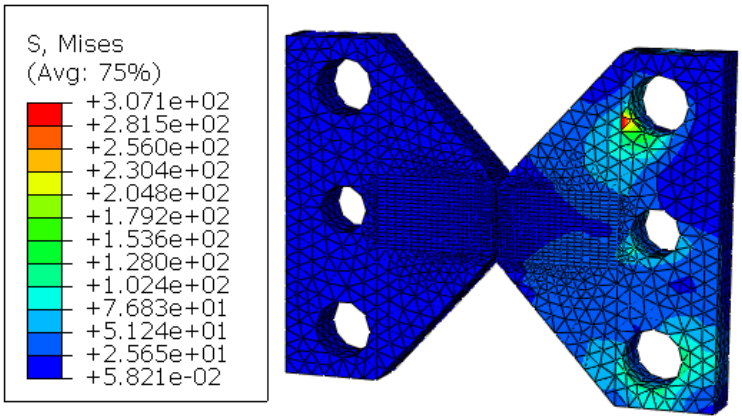

Figure 26 - Maximum VM stress on the steel parts of the specimen

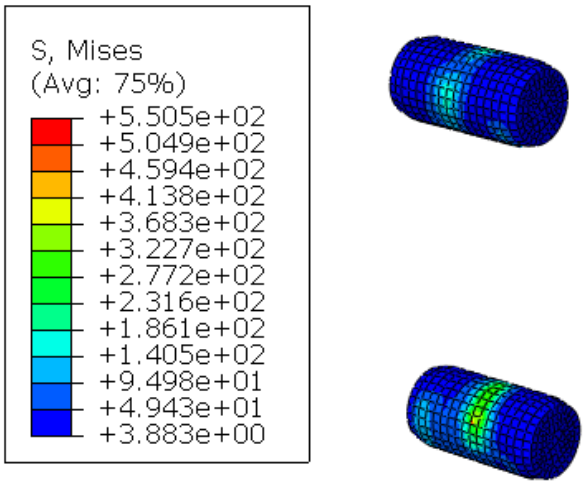

Figure 27 - Maximum VM stress on the pins that connect the specimen to the Arcan

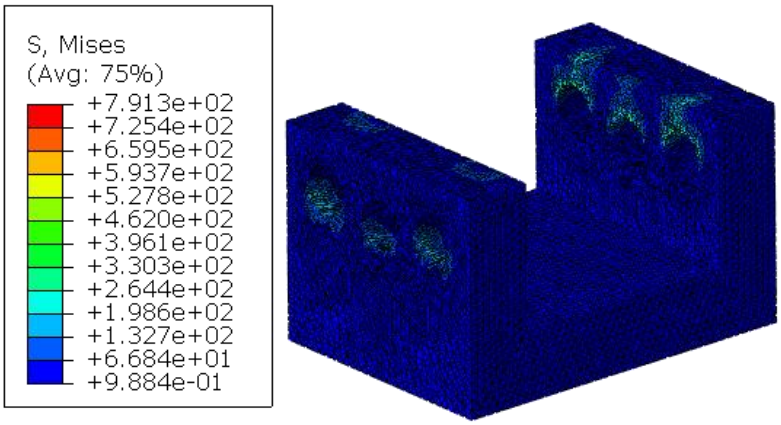

Figure 28 - Maximum VM stress on the inferior component

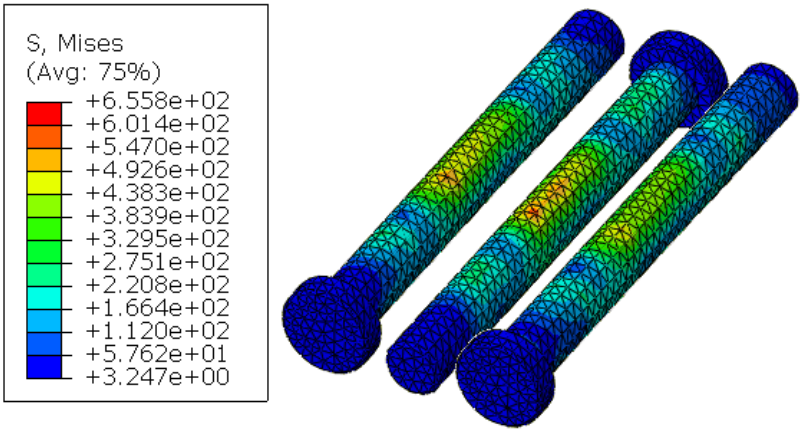

Figure 29 - Maximum VM stress on the inferior extractors

Table 3 - Mechanical properties of PM300 steel at 20 ºC, supplied by Ramada Aços® [58]

Property	***Average Value***
Density (kg/m^3)	7800
E (GPa)	205
v	0.3
Tensile strength (MPa)	1020
Yield strength (MPa)	900
Hardness (HB)	325

Considering the maximum VM stress that each component undergoes and the yield stress of its material, the safety factor (SF) to avoid plastic deformation can be calculated as follows (Eq. (3.1)):

$$SF = \frac{Yield\ stress}{Maximum\ VM\ stress} \tag{3.1}$$

The SF for all components is shown in Table 4.

Table 4 - Safety factors of the Arcan device components under impact

Component	***SF***
Half-Arcan	2.02
Specimen	2.93
Inferior component	1.14
Inferior extractors	1.95
Pins	2.33

3.3 Adhesive's initial stress (due to Arcan's weight)

As mentioned before, it is crucial to know the initial stress level that the adhesive is subjected to prior to impact, due to the own weight of the components that are suspended. The total weight of these components (Figure 30) is about 5.34 kg. To obtain this initial stress, a numerical simulation was carried out in Abaqus® using a static analysis and a 2D simplification. Only the geometry of the specimen was used (Figure 31) and the vertical force (5.34 x 9.81 = 52.4 N) caused by the components was applied in a point (point A) that is equivalent to the center of mass (CM) of the structure. This point has the same horizontal distance from the adhesive as CM, therefore ensuring that the adhesive layer suffers efforts (vertical force and bending moment) equivalent to those caused by CM (see again Figure 30). In the simulation, a static, general step was used and a total of 50 cohesive (COH2D4) and 7408 plane stress (CPS3 and CPS4R) elements were applied to model the adhesive layer, with a bondline (vertical bonding distance in the specimen) of 15 mm, and the steel sides of the specimen, respectively. The right-side of the specimen was fixed once again, as it is connected to the right-side of the Arcan which is, on its turn, assembled to the support structure.

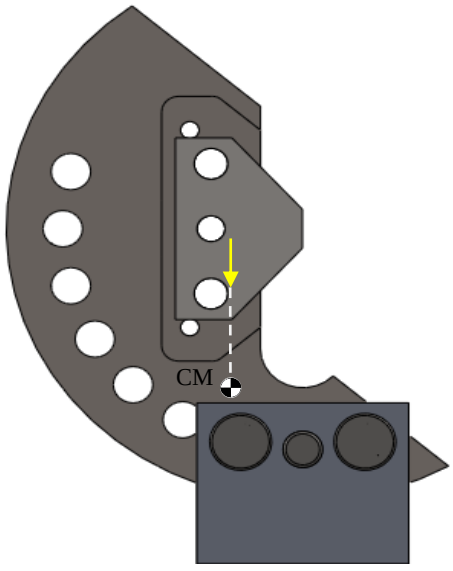

Figure 30 - Suspended structure that the adhesive needs to hold before impact tests

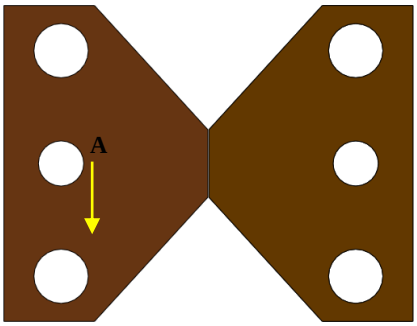

Figure 31 - Schematic of the simulated geometry

The adhesive's initial stress due to the structure's weight is represented in Figure 32, while the stress distribution, in the y-direction (along the bondline) is shown in Figure 33. The y-coordinate in this figure appears normalized. This way, 0 corresponds to the bottom of the bondline (y=0 mm) and 1 corresponds to the top (y=15 mm). The adhesive is under traction at the top of the bondline and under compression at the bottom, being the VM stress distribution symmetric, as expected. The maximum stress occurs at the tops, being its value 3.85 MPa.

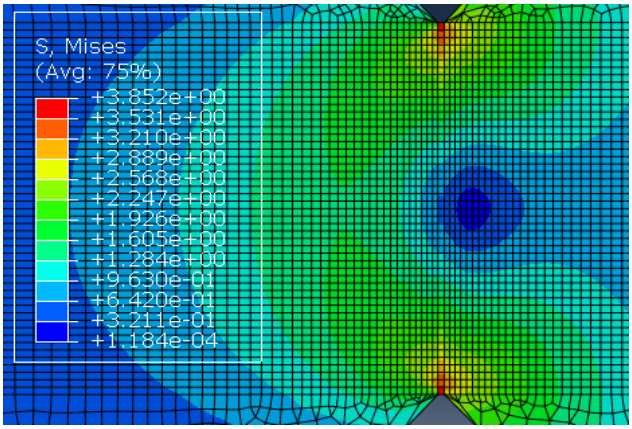

Figure 32 - Adhesive's initial stress

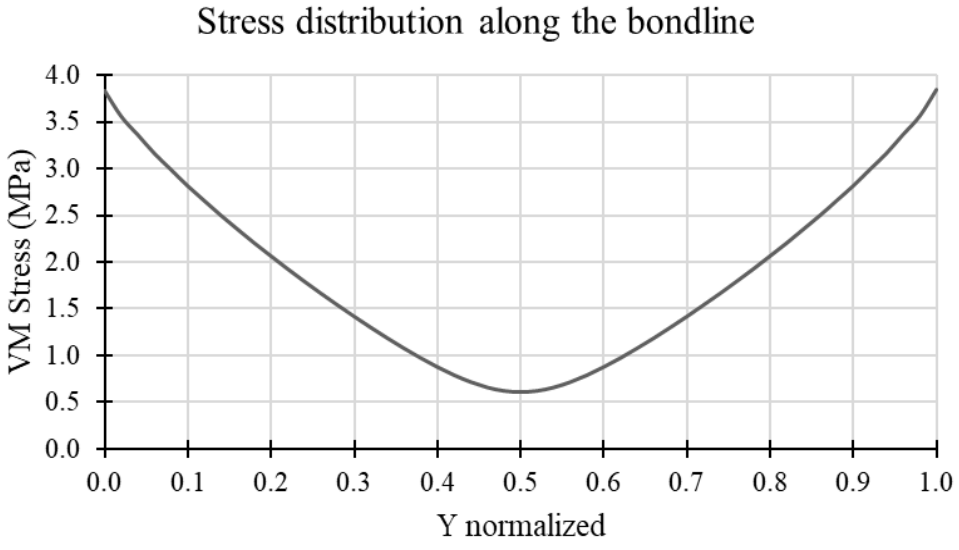

Figure 33 - Stress distribution along the bondline

From the dynamic simulation presented above (section 3.2), it was possible to obtain the evolution (over time) of the stress distribution at the tops of the adhesive layer during impact (Figure 34), being the maximum stress about 70.2 MPa. This value can be compared to the 3.85 MPa that are present in the initial conditions to verify if this last value is acceptable. The stress ratio is 5.5% (3.85/70.2), meaning that the maximum stress in the adhesive caused by the self-weight of the components is 5.5% of the maximum stress that the adhesive undergoes under impact. This value was judged to be acceptable given the design constraints associated with this type of apparatus. If a bondline of 12.5 mm (also common in the tests performed by the group) is used instead, the initial stress in the adhesive increases to 5.45 MPa and the stress ratio to 7.8%.

Finally, it is worth mentioning that, after these steps being completed, all the 2D drawings necessary for manufacturing this device were developed, using AutoCAD® (Autodesk, California, USA), and the materials needed were ordered.

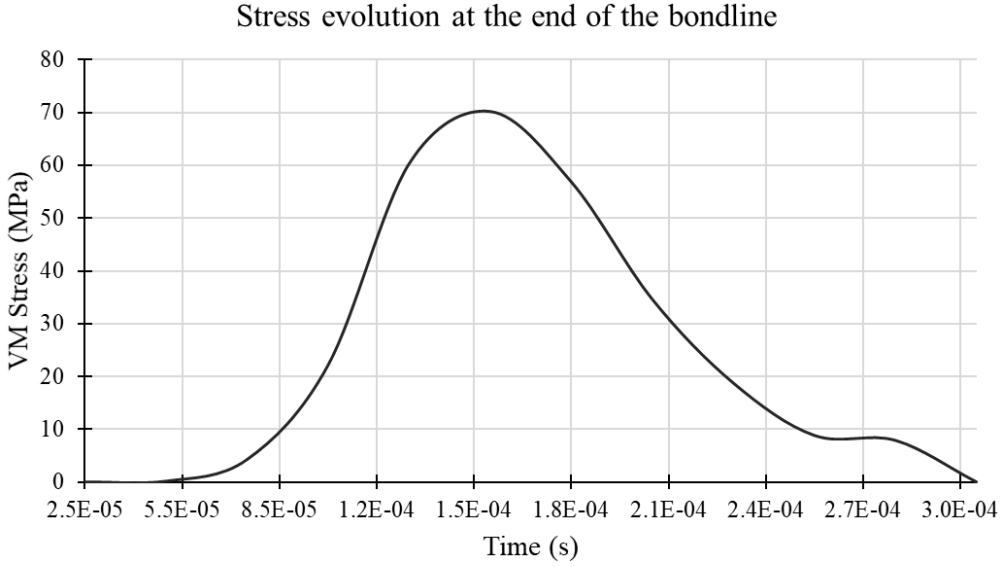

Figure 34 - Stress distribution vs time at the tops of the adhesive layer for a bondline of 15 mm and impact conditions

3.4 Mould for Arcan specimens

The mould that was being used to manufacture the specimens of the existent Arcan (Figure 35) is not compatible with the new specimens. The Arcan device presented above is smaller than the original one, which necessitates the use of smaller specimens. To overcome this problem a new mould, compatible with all kinds of specimens, was designed (Figure 36).

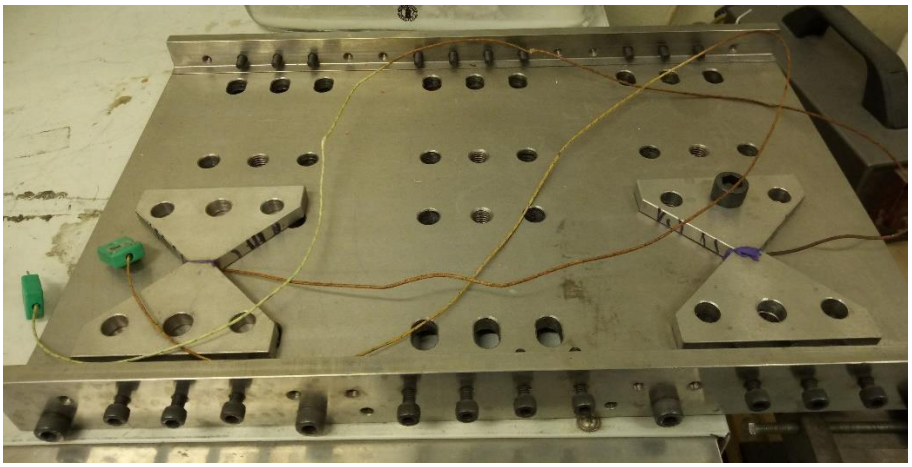

Figure 35 - Existent mould to produce the Arcan specimens

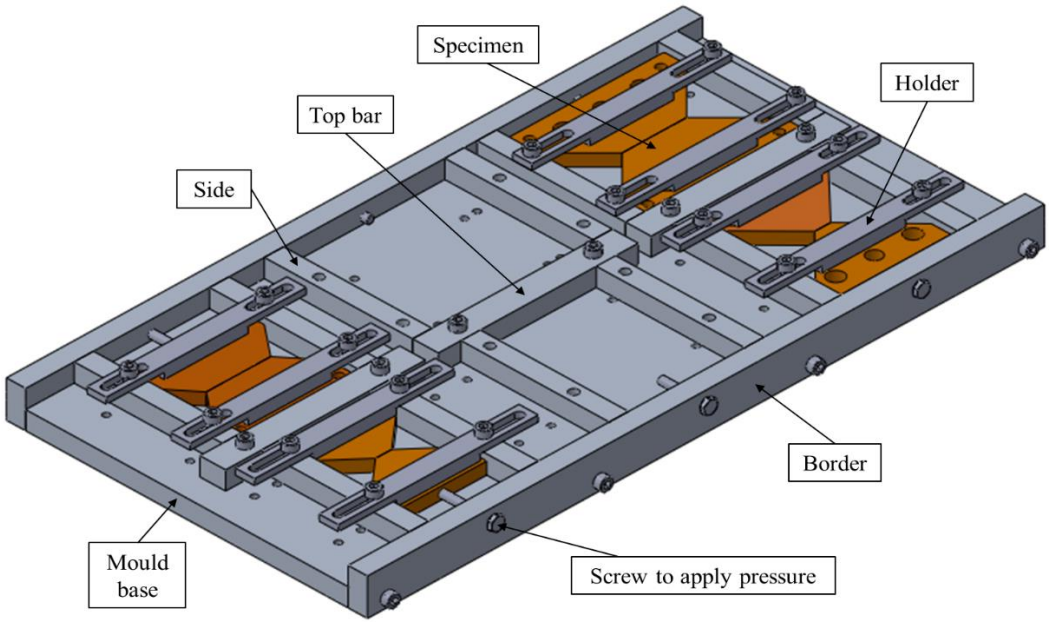

Figure 36 - 3D model of the new mould, designed to be compatible with all specimens

Names were given to the components so that the explanation of the concept could be easier. In this configuration, the mould base, the borders and the top bars are fixed. These last two parts are assembled to the base using a typical screw-threaded hole connection. The side bars are movable to allow the manufacturing of all types of specimens. The specimens should allow testing adhesive layers with bondlines up to 50 mm and thicknesses up to 2 mm. For full scale Arcan, two specimen's sizes were being used (Figure 37), the smallest for smaller bondlines and the biggest for bigger bondlines (again, up to 50 mm). For the newly designed (smaller) Arcan, two specimen's sizes (Figure 38) will be also used, for the same conditions. Although it seems that the side bars should have four different positions (since there are four different specimens), in fact they only need to have three, since two specimens have the same length (90 mm). In the manufacturing process, one of the two halves of the specimen is in

contact with the top bar and the other half is initially free. The pressure needed to produce the adhesive layer is applied by a screw that acts in the free half. When the screw header is in contact with the border, the two halves of the specimen are supposed to be together, which corresponds to an adhesive layer thickness of 0 mm. This way, if a specific layer thickness is desirable, a calibrated tape or washer with that thickness should be inserted between the screw and the edge of the mould wall. Therefore, the thickness can be controlled by adjusting screw's position. The bondline is controlled by the geometry of the specimen itself. The function of the holders is to apply vertical pressure, ensuring that the specimens maintain their position. A total of six specimens can be manufactured at the same time.

All the 2D drawings necessary for the manufacturing of this mould were done as well.

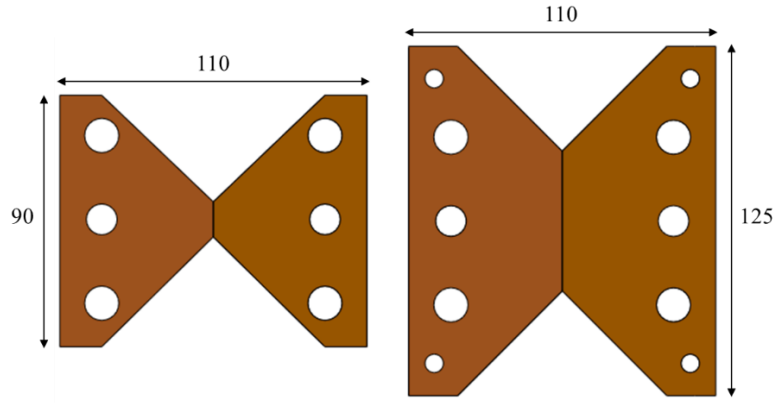

Figure 37 – Dimensions (in mm) of the specimens for the existent Arcan

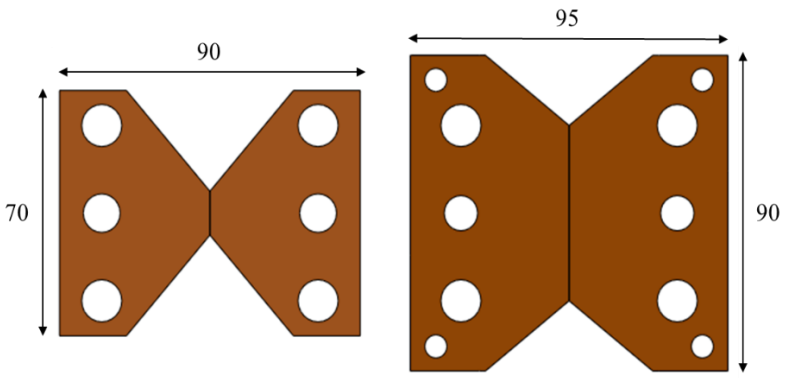

Figure 38 – Dimensions (in mm) of the specimens for the designed/new Arcan

4 Study of aluminium SLJs bonded with a crash-resistant adhesive

Several joint configurations can be applied to bond the adhesive and the adherends, being the choice of the geometry usually associated with design restrictions, so that peel and cleavage stresses can be avoided. The most studied configurations in the literature are single-lap joints (SLJs), double-lap joints (DLJs), scarf joints and stepped-lap joints (Figure 39). Other configurations, not so common, have also been studied such as L and T-shaped joints, stepped-scarf joints, corner joints, strap joints, butt joints and so on. For a certain load, the strength of a joint depends on its geometry and the mechanical properties of both adhesive and adherends [59].

Figure 39 - Joint configurations: a) SLJ, b) DLJ, c) Double scarf joint, d) Double stepped-lap joint (adapted from [59])

To characterize the joint behaviour SLJs are typically used, with an adhesive thickness of 0.2 mm and an overlap (length of the bonded region) of 25 mm. Since the automotive frame tested in this project is supposed to be bonded with an adhesive thickness of about 1.6 mm* (according to the model supplied by Aston Martin Lagonda Limited®), it was decided to test SLJs with a bondline thickness of 0.2 and 1.6 mm. The main goal was to observe the influence

* Due to the complexity of the frame, the adhesive thickness in the supplied model is not constant and exactly 1.6 mm throughout all the structure. This number was chosen as an approximated medium value.

of adhesive thickness in the mechanical response of the joint at RT and different displacement rates, namely quasi-static (1 mm/min), 0.1 m/s and impact (3 m/s) conditions.

The thickness of the aluminium adherends was found by Sawa et al. [60] to influence the strength of a SLJ when subjected to tensile loads, with higher thicknesses leading to higher strengths. In this case, an adherend thickness of 2 mm was used, resulting from a compromise solution between the availability of aluminium sheets in the market and the thickness of the real frame substrates. An overlap of 12.5 mm was selected as previous numerical simulations with 25 mm revealed exclusive failure by plastic deformation of the aluminium substrates due to the high ductility of the adhesive (Figure 41), which is not intended.

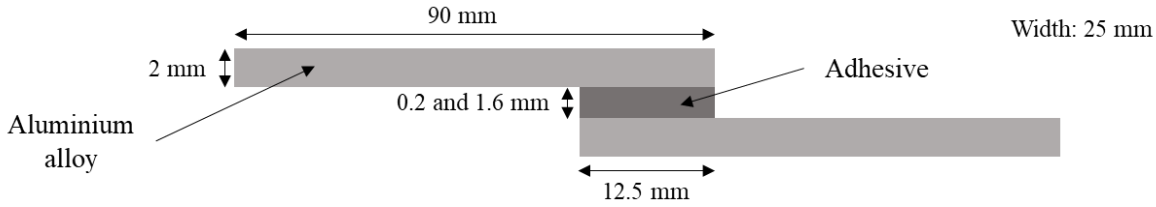

Figure 40 - Schematic of the tested SLJs

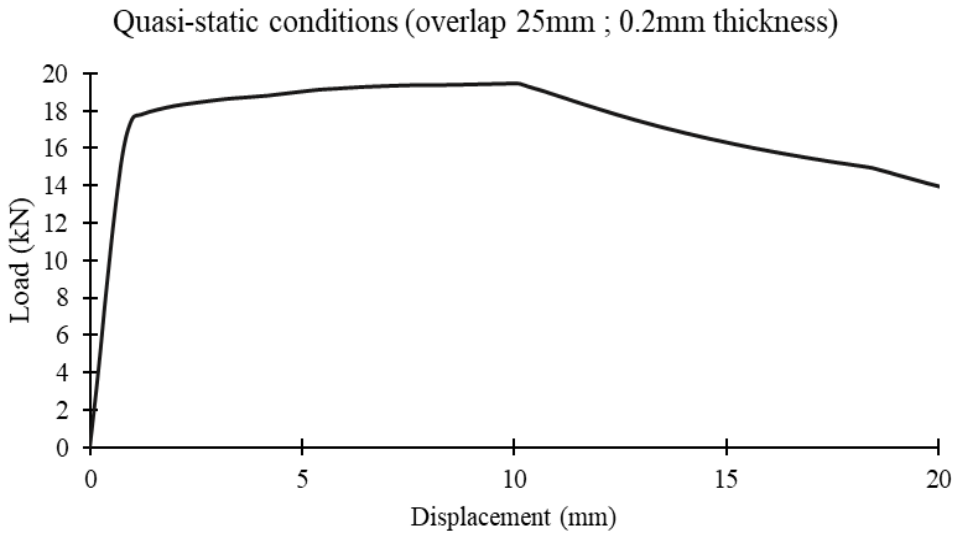

Figure 41 - Load vs displacement curve of a SLJ with an overlap of 25 mm, indicating failure exclusively by plastic deformation of the aluminium substrates

4.1 Materials

4.1.1 Aluminium

The aluminium selected for the adherends was the 6016-T4 alloy, since this is the material of the automotive frame substrates. However, this aluminium alloy is not commonly found in the market, especially in such small quantities required only for testing and not for industrial production. In fact, of the several aluminium suppliers that were contacted, in Europe, North

America and Asia, few of those have it in stock and the ones who do only sell large quantities. Therefore, the 6082-T6 alloy was selected as a replacement, considering its mechanical properties and availability. This alloy is one of the most used within the 6xxx series, being often applied in the manufacturing of automotive parts such as brake housings [61]. According to Aston Martin Lagonda Limited®, the mechanical properties of the 6016-T4 alloy after curing are similar to those of 6016-T6. A comparison between the properties of these three alloys is shown in Table 5.

Table 5 - Mechanical properties of 6016 and 6082 aluminium alloys [62-64]

Property	***6016-T4***	***6016-T6***	***6082-T6***
Density (kg/m^3)	2700	2700	2700
E (GPa)	69	69	69
G (GPa)	26	26	26
v	0.33	0.33	0.33
Tensile strength (MPa)	200	280	310
Yield strength (MPa)	110	210	260
Shear strength (MPa)	130	170	220
Elongation at break (%)	27	11	9.8

The mechanical behaviour of the 6082-T6 alloy was studied by Yibo et al. [65] for quasi-static to moderate strain rates (0.001-100 s^{-1}), showing a slightly increase of yield and tensile strength with strain rate. The yield strength increased 5.4 %, from 306.1 MPa at 0.001 s^{-1} to 322.6 MPa at 100 s^{-1}, while the tensile strength increased 5.5 %, from 364 MPa at 0.001 s^{-1} to 384 MPa at 100 s^{-1}. The stress-strain curves and the strength values for all tested strain rates are presented in Figure 42 and Table 6, respectively. From these results, the 6082-T6 was concluded to present low strain rate sensitivity. This conclusion is in accordance with the information given by Oosterkamp et al. [15] and Chen et al. [16], previously introduced.

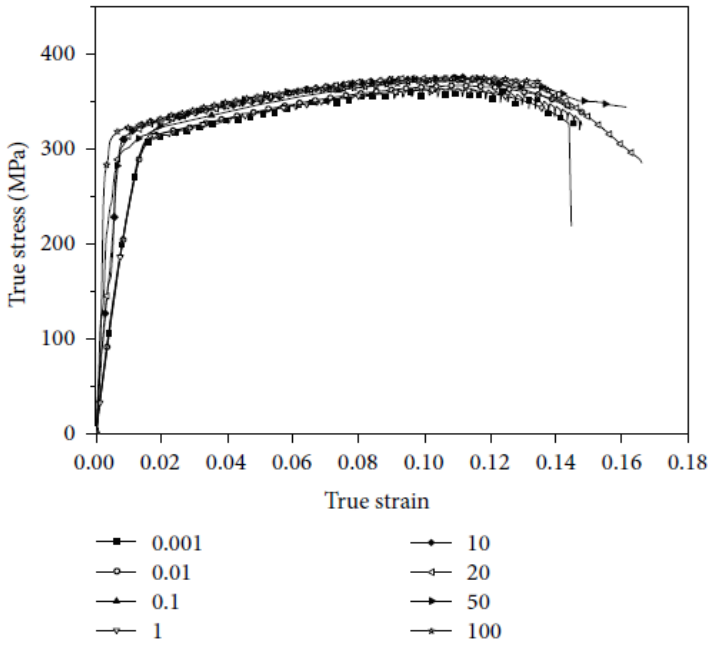

Figure 42 - Stress-strain curves at different strain rates for the 6082-T6 alloy [65]

Table 6 - Yield and tensile strength of 6082-T6 alloy for the tested strain rates (adapted from [65])

Strain rate (s^{-1})	*0.001*	*0.01*	*0.1*	*1*	*10*	*20*	*50*	*100*
Yield strength (MPa)	306.1	309.6	309.2	311.7	313.8	317.0	321.7	322.6
Tensile strength (MPa)	364.0	367.0	372.6	367.8	373.4	374.8	375.5	384.0

The same aluminium alloy, under two heat treatments (O and T6), was also analysed by Torca et al. [61] for strain rates between 0.001 and 0.1 s^{-1} and temperatures between RT and 250 °C. Both heat treatments were selected given their applicability in the automotive industry. T6 refers to components that are solution heat treated and artificially aged. The behaviour of the 6082-T6 alloy for RT is identical for all strain rates, confirming the low sensitivity of this alloy to this parameter. Still, so that the material could be characterized in the best way possible, the information given by Yibo et al. [65] regarding the plastic behaviour of the aluminium at 0.01 s^{-1} was used in the numerical simulations at quasi-static and 0.1 m/s conditions, while the behaviour at 100 s^{-1} was used for impact.

4.1.2 Adhesive

The adhesive used to bond the aluminium adherends is named XNR6852 E-3, supplied by Nagase ChemteX® (Osaka, Japan). This adhesive was previously studied by Machado et al. [2]. Higher tensile strength and Young's modulus were observed with the increase of strain rate and the decrease of temperature. Additionally, an increase of both temperature and strain rate led to an increase in the values of G_{IC} and higher values of shear strength were observed for

higher strain rates. When it comes to the strain at failure, an increase was found with the increase of temperature. Higher strain at failure is expected at higher temperatures since the adhesive becomes more ductile due to the proximity of T_g. For impact conditions at 3 m/s, the same authors observed an almost constant value of strain at failure for all tested temperatures (-30°C, 24°C and 80°C). An increase in the strain rate led to a decrease in the values of strain at failure at high temperatures. When selecting an adhesive for impact conditions, it is important to have high values of strain to failure in order to enhance the energy absorption and increase the damage tolerance.

The mechanical properties of the XNR6852 E-3 at RT and for quasi-static and impact conditions can be found in [1, 2] and are shown in Table 7, being its density 1550 kg/m^3.

Table 7 - Mechanical properties of XNR6852 E-3, at 24 °C, for quasi-static and impact conditions [1, 2]

Property	*E* *(MPa)*	*G* *(MPa)*	t_n^0 *(MPa)*	t_s^0 *(MPa)*	G_{IC} *(N/mm)*	G_{IIC} *(N/mm)*
Quasi-static (1 mm/min)	1873.98	665	48.44	44.9	9.18	51
Impact (3 m/s)	3666.67	603*	71.67	42.9*	13.3*	64.1*

Some of the values presented before for impact conditions were extrapolated by the authors using logarithmic laws, which resulted from experimental data. The same laws were used to determine the properties of the adhesive for a displacement rate of 0.1 m/s. For RT, the tensile strength can be approximated by

$$t_n^0 = 1.9269 \ln(\dot{x}) + 48.208 \quad (4.1)$$

and the Young's modulus by

$$E = -118.9 \ln(\dot{x}) + 2751.4 \quad (4.2)$$

For shear strength we have

$$t_s^0 = 4.6649 \log(\dot{\varepsilon}) + 46.274 \quad (4.3)$$

and for the critical strain energy release rate in mode I

$$G_{IC} = 0.3454 \ln(\dot{x}) + 9.1587 \quad (4.4)$$

where $\dot{x}$ represents the displacement rate (in mm/min), $\dot{\varepsilon}$ is the strain rate (in s^{-1}) and all property values are given in MPa, except G_{IC} which unit is N/mm. For G_{IIC} and G, no laws were presented. Therefore, logarithmic laws were constructed considering the values of these

* Extrapolated values

properties at quasi-static (1 mm/min) and impact conditions (3 m/s = 180000 mm/min) (see again Table 7):

$$G_{IIC} = 1.0826 \ln(\dot{x}) + 51 \quad (4.5)$$

$$G = -5.124 \ln(\dot{x}) + 665 \quad (4.6)$$

with G and G_{IIC} also in MPa and N/mm, respectively. For a displacement rate of 0.1 m/s, the $\dot{x}$ value is 6000 mm/min (0.1x1000x60), $\dot{\varepsilon}$ is 0.83 s^{-1} and, using the previous equations, the properties of the adhesive at 0.1 m/s can be obtained (Table 8). In his work, Machado et al. [2] refers that the strain rate can be obtained by

$$\dot{\varepsilon}(t) = \frac{L(t) - L_0}{L_0} = \frac{v(t)}{L_0} \quad (4.7)$$

where $v(t)$ corresponds to the displacement rate in mm/s and L_0 to the value of length of the specimen in mm. For the adhesive bulk "dogbone" specimens that were tested, the length used to determine the value of the strain rate was 120 mm. Therefore, the value of $\dot{\varepsilon}$ for 0.1 m/s can be calculated as 0.1x1000/120 ≈ 0.83 s^{-1}.

Table 8 – Stipulated mechanical properties of XNR6852 E-3, at 24 °C, for 0.1 m/s condition

Property	*E (MPa)*	*G (MPa)*	t_n^0 *(MPa)*	t_s^0 *(MPa)*	G_{IC} *(N/mm)*	G_{IIC} *(N/mm)*
0.1 m/s	1717.03	620	64.97	45.9	12.2	60.4

4.2 Numerical details

All numerical analyses were conducted using the Abaqus® software package using 2D models with an out-of-plane thickness of 25 mm, corresponding to the width of the SLJs. A comparison between 2D and 3D model results was conducted by Machado et al. [48] when studying the impact behaviour of mixed adhesive SLJs for the automotive industry. For quasi-static conditions the two models showed good accordance, only with the 2D model presenting a slightly higher (1.6 %) failure load, leading to the conclusion that 3D models do not provide significant advantages for this condition. A similar conclusion was drawn from impact modelling, with the difference in this case being less than 1 %. For these reasons, only 2D models were employed in this study to save computational time.

Further details about the numerical simulations and its results are explained in the attached papers.

4.3 Experimental details

Although the papers present the fundamental details regarding the experimental procedures, this section tends to complement that information by performing a step-by-step introduction of the manufacturing process. The same can be resumed in the following phases:

1. Cutting the aluminium substrates in rectangular shapes with dimensions 90x25x2 mm;
2. Drilling the substrates to produce holes with a diameter of 6.5 mm;
3. Anodizing process;
4. Production of the SLJ configuration using an aluminium mould;
5. Curing of the SLJs, by introducing the mould into a hot plate press.

Step 2 is necessary to allow the assembly of the SLJs in the fixture used during the tensile tests.

The use of anodizing is highly recommended in the bonding of aluminium, so that the adhesion between the adhesive and the adherends can be enhanced and the probability of interfacial failure can be reduced. To apply this procedure, the substrates were initially sanded in the region where bonding took place, in order to reduce the superficial roughness and eliminate possible contaminants in the outside layer. In fact, Borsellino et al. [18] concluded that roughness has a negative effect on the wettability of epoxy resins. After this surface cleaning, the substrates were submersed in a solution of sulfuric acid (H_2SO_4), and a power supply was used to introduce electrical current in the bath (Figure 43), leading to the transfer of hydrogen from the cathode to the anode (aluminium substrates), forming an oxide layer that improves adhesion.

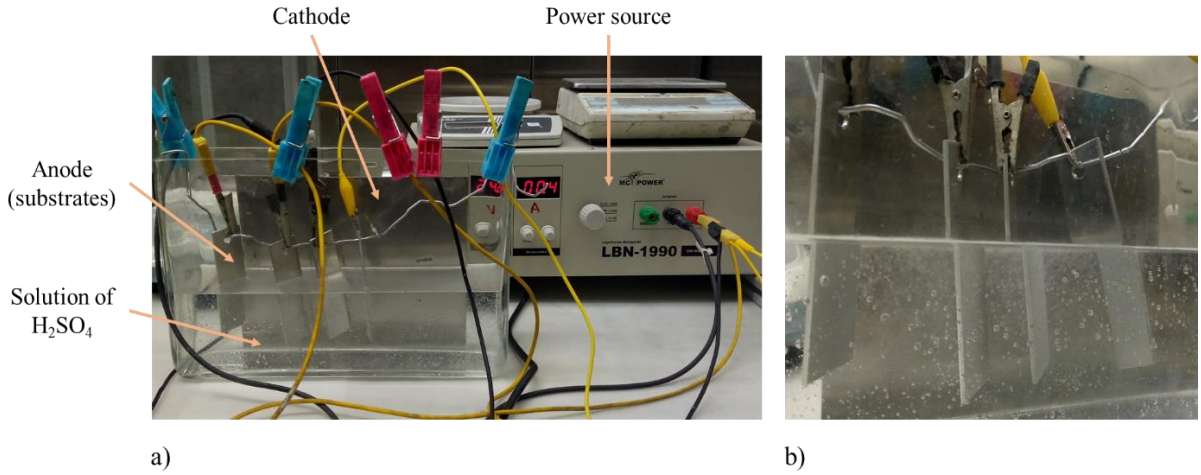

Figure 43 - Anodizing process: a) setup and b) closer look

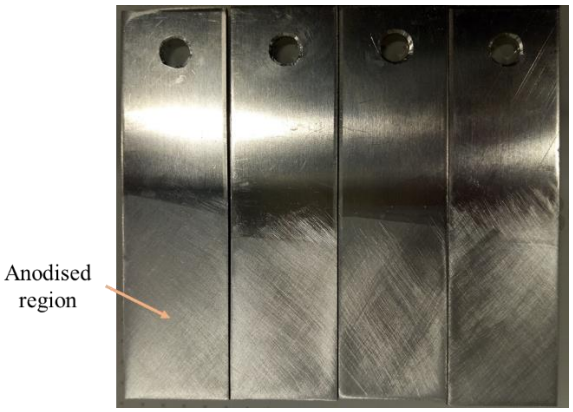

Figure 44 - Aluminium substrates after anodizing

The SLJ configuration was produced using an aluminium mould (Figure 46), so that the difference of thermal expansion coefficients between the mould and the substrates could be minimized. In the beginning of the process, the lower substrates and the spacers, with calibrated tapes on their bottom, were both inserted in the mould. The length of the spacers was 77.5 mm (90 mm of the substrate minus 12.5 mm of the overlap length) and their thickness was 2 mm. This set was then restrained using pins. The next step consisted in placing calibrated tapes and further spacers on the top of the lower substrates, after which the adhesive was applied on their surface. A thin layer of adhesive was also introduced in the surface of the upper substrates to improve adhesion. Finally, the upper substrates were assembled in the mould, placed on the top of the first spacers. After this process, an overlap length of 12.5 mm was achieved, and the thickness of the calibrated tapes controls the thickness of the adhesive layer. This way, calibrated tapes with a thickness of 0.2 and 1.6 mm were used in the production of SLJs with an adhesive thickness of 0.2 and 1.6 mm, respectively. Adjustment screws allowed to fine tune the position of the joints, ensuring their correct alignment. Figure 45 shows a schematic of the side view of the configuration, which can be useful to better understand the explanation presented above.

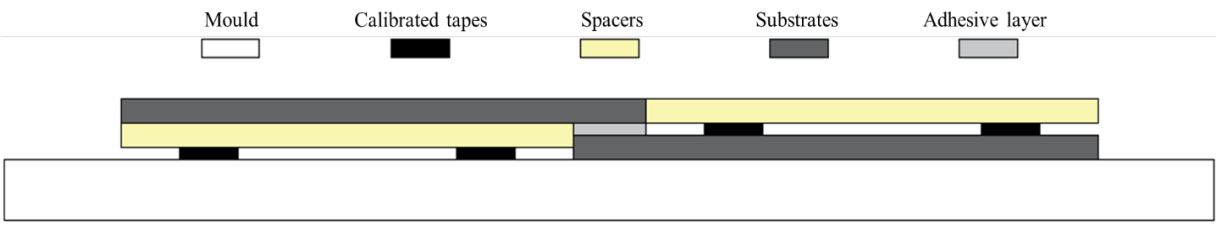

Figure 45 - Schematic of the SLJ configuration in the mould

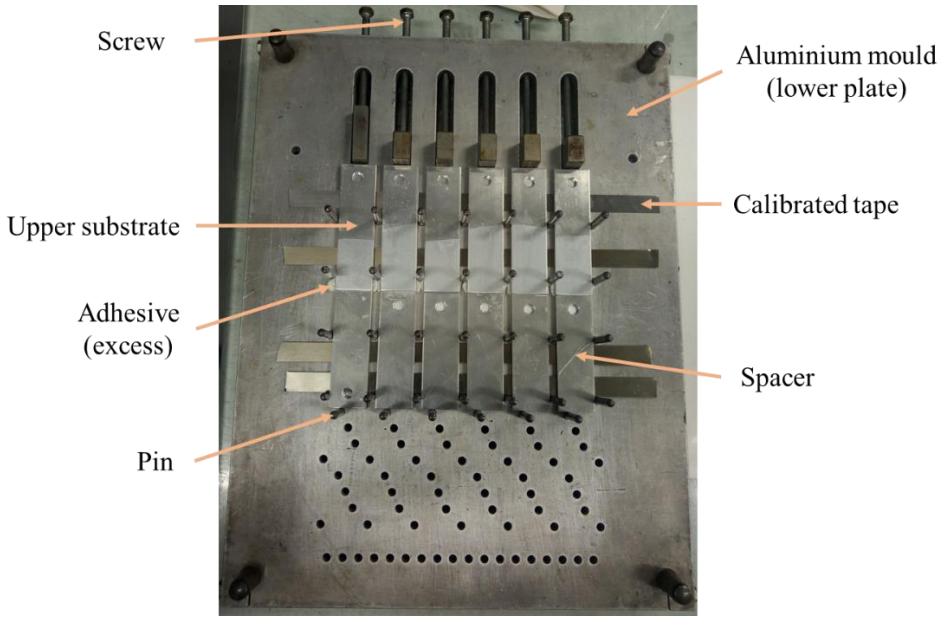

Figure 46 - Manufacturing of SLJs using a mould

To complete the manufacturing process, the mould was introduced in a hot plate press (Figure 47) under high pressure and temperature conditions, allowing to fulfil the curing cycle of the adhesive which requires 4 hours at 165 °C.

Figure 47 – Hot plate press used to cure the adhesive layer

An INSTRON® universal testing machine, model 3367 (Norwood, Massachusetts, USA), Figure 48 a), with a loading capacity of 30 kN was used for the quasi-static tests , while for the 0.1 m/s condition an INSTRON® 8801 servo hydraulic testing machine (Figure 48 b)) with a capacity of 100 kN was used. The impact tests were performed with an in-house developed drop-weight testing machine (Figure 49).

Figure 48 - Universal machines used to perform tests under a) quasi-static and b) 0.1 m/s conditions

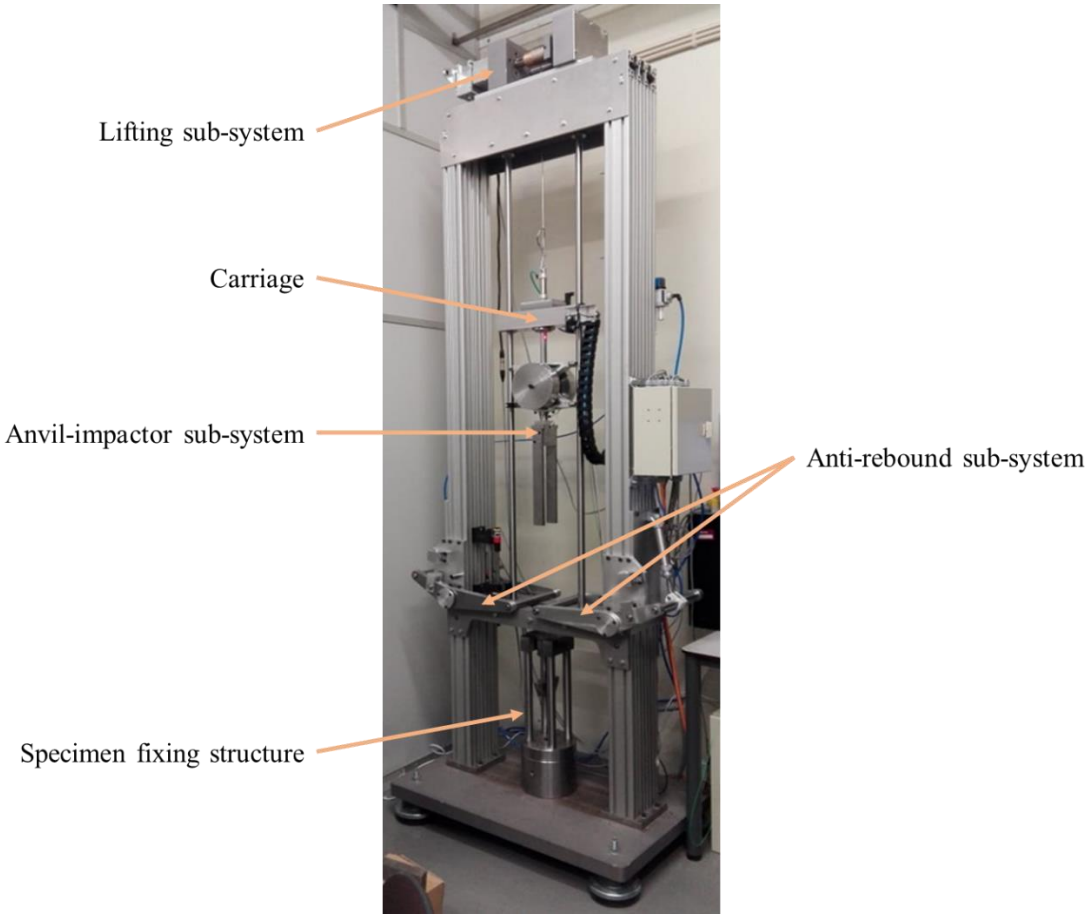

Figure 49 - Drop-weight machine used to perform impact tests

5 Analysis of an adhesively bonded automotive structure

The core of the present work is to numerically and experimentally study the mechanical behaviour of a component scale, adhesively bonded automotive frame, showing the applicability of structural adhesives to "real-life" automotive structures. The analysis of this component is of extreme importance due to its role on the safety of the passengers during impact and the inexistence of a middle vertical support. In fact, as shown in Figure 50, this *front header* (designation given by Aston Martin Lagonda Limited® for this component) is only supported at its ends in the body structure of the vehicle. The tests will be carried out at RT and for two different displacement rates, corresponding to quasi-static (1 mm/min) and impact conditions (3 m/s).

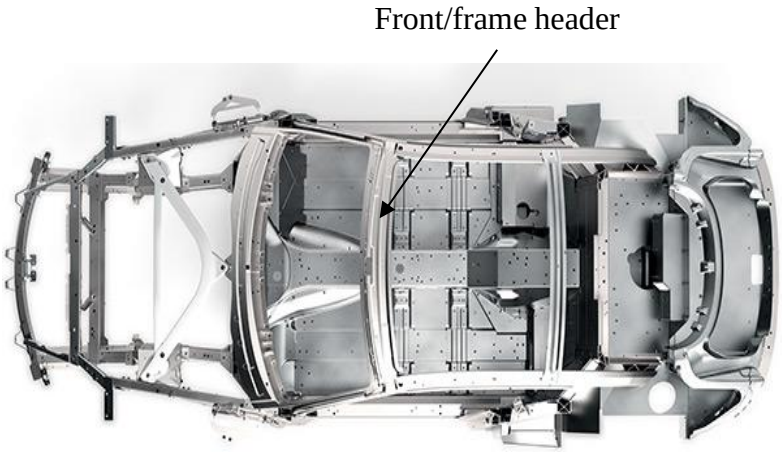

Figure 50 – Front header in the body structure of an Aston Martin's DB-11 model [66]

Each header is composed of two aluminium substrates, supplied by Aston Martin Lagonda Limited® and belonging to the DB-11 model, that are designed to be bonded with a crash-resistant epoxy adhesive. A 3D model of the frame (Figure 52) was also provided in the computer code Hypermesh® (Altair Engineering, Michigan, USA), so that a numerical analysis could be performed.

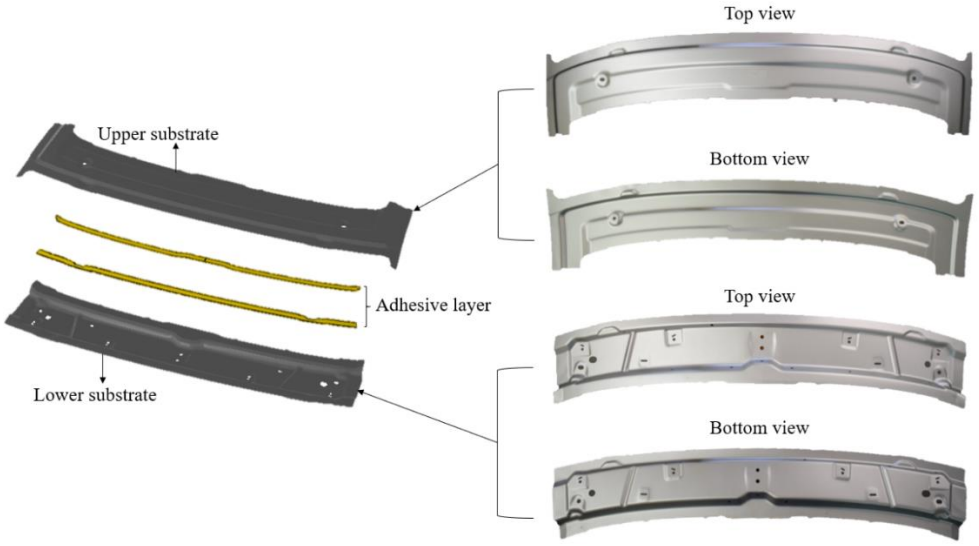

Figure 51 - Substrates of the automotive front header

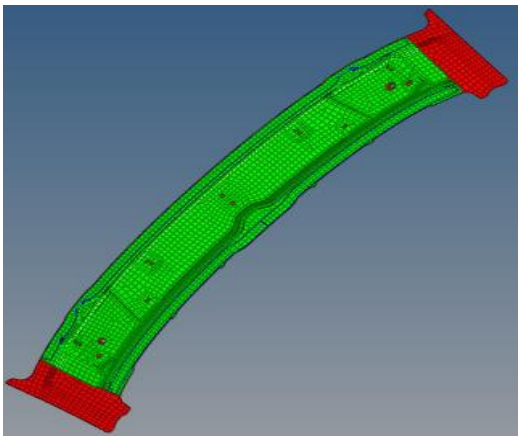

Figure 52 - 3D model of the component in Hypermesh® (supplied by Aston Martin Lagonda Limited®)

5.1 Structural support

The tests under quasi-static conditions were carried out in a INSTRON® 8801 universal testing machine (see again Figure 48 b)), equipped with a 100 kN capacity load cell, while the impact tests were made using the drop-weight testing machine presented before (see again Figure 49), with a capacity up to 50 kg for the dropping mass and 5 m/s for the impact velocity.

In order to mount the specimen in the test equipments presented above, a new support fixture was designed. The design was guided by the intention of having a structure compatible with both machines, could be quickly assembled and disassembled and reusable. Therefore, an initial aluminium profile-based support was designed (Figure 53) and industrial clamps were considered to fix component's ends, representing the real service conditions in an automobile.

Steel parts were drawn to connect the clamps to the profiles and the structure to the machines*. The restraints of the header could be easily ajusted in the three directions, since the vertical aluminium profiles could be moved in the x-direction, the openings in the component that connects the clamps to the profiles allow movement of the clamps in the z-direction, and the configuration of the clamps itself allow some adjustment in the y-direction. In addition, T-shaped aluminium plates were added to the structure in order to increase its torsional stiffness during the tests.

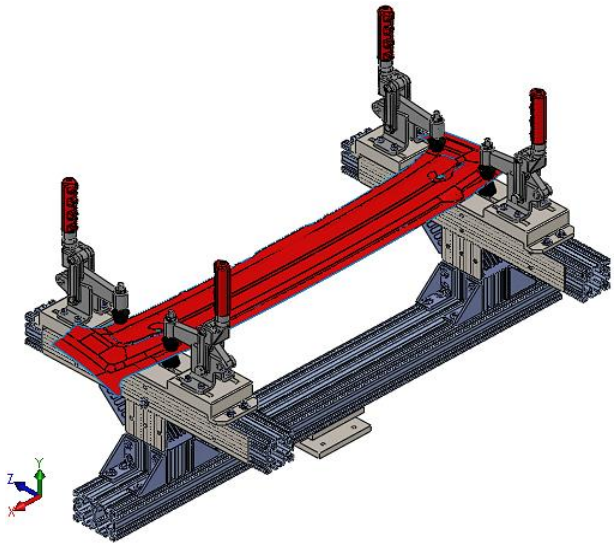

Figure 53 - Designed structural support with clamps being used to fix the automotive front header

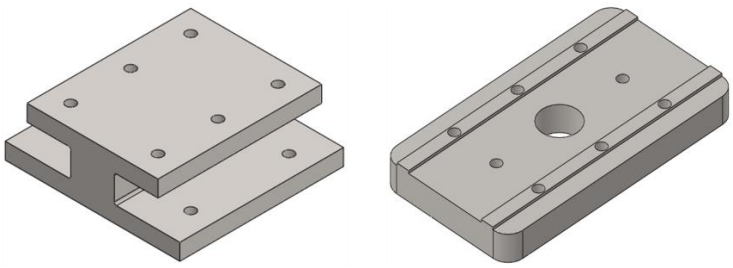

a) b)

Figure 54 - Steel parts that allow the connection of the structural support with a) the drop-weight and b) universal testing machines

Once the initial design of the structure was complete and the material acquisition process was started, it was observed that the clamps needed to fix the header were too expensive in the context of this project. Therefore, some modifications were made regarding the fixation of the component and the solution of Figure 55 was used instead. A typical connection screw-nut was

* The structure in Figure 53 is adapted for impact tests, where the bottom steel part connects the structure to the floor of the impact machine (shown in Figure 49). The structure for quasi-static tests is the same, except for this steel part which is different to ensure the connection to the machine in Figure 48 b).

selected to overcome this problem, with layers of rubber being applied to avoid damage to the front header. This simpler solution avoids the need of expensive clamps and clamping bolts and the manufacturing of the steel parts to connect the clamps with the profiles, although it requires the drilling of the component. In this new approach, the remaining structure of the fixture remains unchanged.

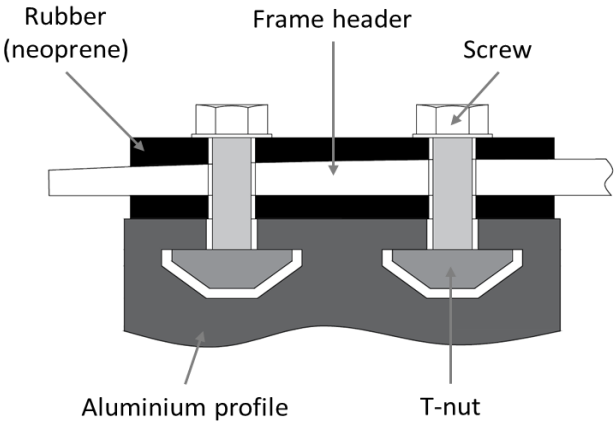

Figure 55 - Schematic of the new approach to fix the geometry of the automotive component

5.2 Impactor

The impactor is the tool that will make contact with the specimen at the desired testing speed, and its design is common to both test speeds (Figure 56). During impact conditions, the impactor is rigidly connected to the anvil of the drop weight impact testing machine. This connection includes a component equipped with a piezoelectric load cell, which is used to record the force acting upon the impactor. For use under quasi-static conditions, a threaded hole was manufactured on the top of the impactor, allowing a direct fit of the impactor to the servo-hydraulic testing machine. The shape of the contact surface of the impactor was chosen to be rounded so that the contact could be done through a surface and not a single line. In fact, as the impactor moves down, the front header tends to bend around the surface of the impactor, distributing the impact pressure. This was performed to better simulate a collision with a round object.

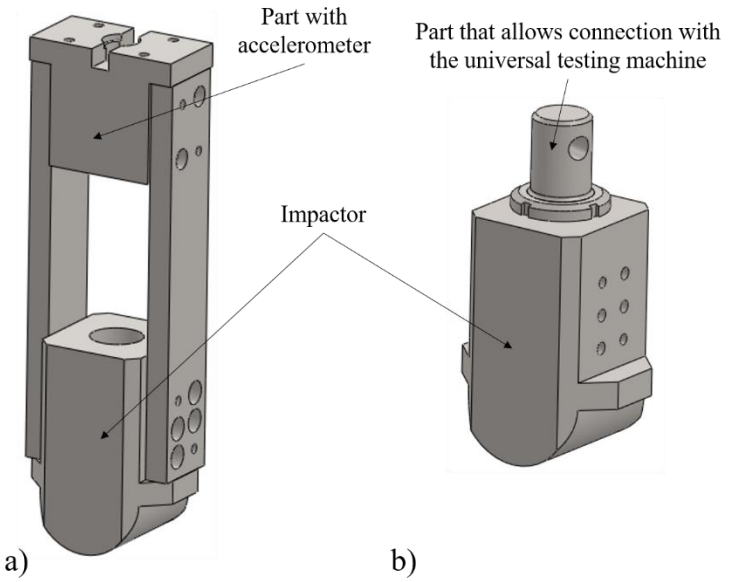

Figure 56 - Impactor's configuration for a) impact and b) quasi-static tests

5.3 Materials

5.3.1 Aluminium

The aluminium substrates used are manufactured by stamping sheets of 6016-T4 aluminium alloy, commonly used in the automotive industry. For this aluminium alloy, in the heat treated and naturally aged state (T4), Simões et al. [67] studied the influence of temperature, strain rate and aging on the mechanical properties. Three values of strain rate ($2x10^{-4}$, $2x10^{-3}$ and $2x10^{-2}$ s^{-1}) were tested for two different temperatures (20 and 200°C) and it was shown that the strain rate sensitivity increases with the increase of temperature (Figure 57). For RT, the results show that 6016-T4 is not sensitive to strain rate, which is in accordance to the conclusions also drawn in Chapter 4 for the 6082-T6 alloy.

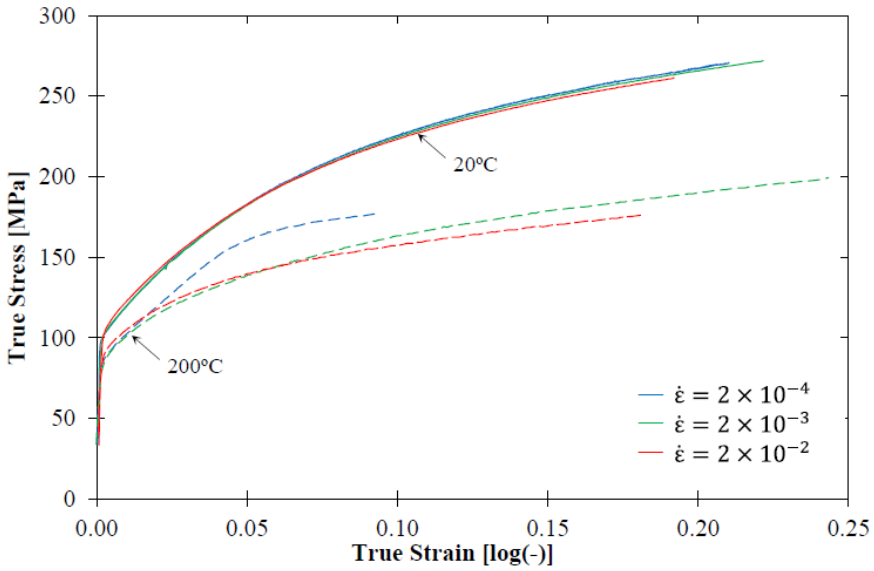

Figure 57 - Influence of strain-rate on stress-strain curves of 6016-T4 alloy, for two different temperatures [67]

As previously stated, the properties of 6016-T4 become similar to those of 6016-T6 alloy after adhesive's curing. The information regarding the plastic behaviour of this alloy was provided by Aston Martin Lagonda Limited® and is represented in Figure 58. Its mechanical properties were also presented in Chapter 4 and were considered constant for all tested conditions, due to the strain rate insensitivity evidenced by the aluminium alloys.

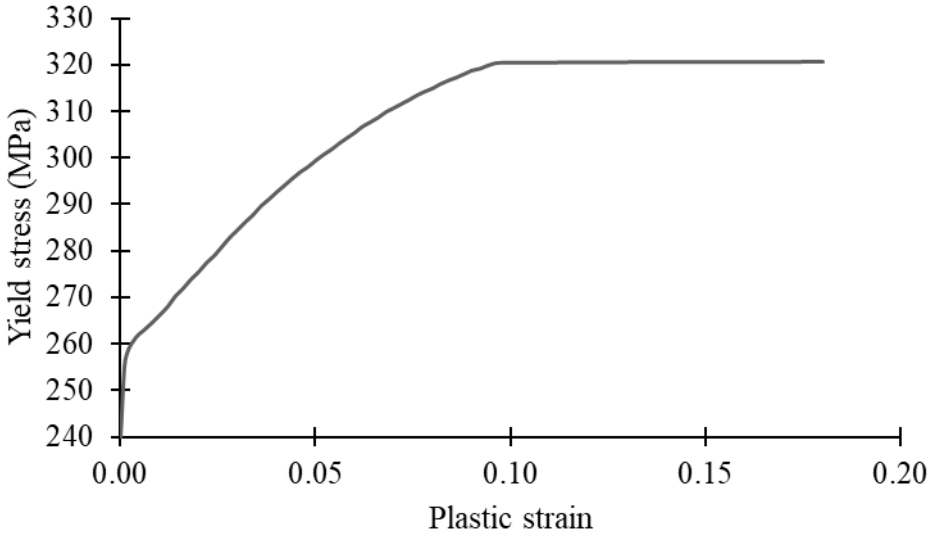

Figure 58 - Plastic behaviour of the 6016-T6 aluminium alloy

5.3.2 Adhesives

The initial adhesive selected for joining the substrates was a ductile, crash-resistant epoxy system, namely XNR6852 E-3 (Table 9), which mechanical properties were introduced in Chapter 4 for quasi-static and impact conditions.

Table 9 - General characteristics of XNR6852 E-3 adhesive

Type of adhesive	Epoxy
Physical form	One-component system
Cure cycle	4h at 165°C
T_g	132 ± 4.51°C

At a more advanced stage of the project, after the results of the specimens bonded with the epoxy adhesive were treated and analysed, a high-performance structural polyurethane was also considered to bond the automotive front header. This adhesive, with the reference SikaForce®-7818 L7, was supplied by Sika® and its general properties and characteristics, given by the manufacturer, are shown in Table 10.

Table 10 - General properties and characteristics of the polyurethane used to bond the automotive structure

Type of adhesive	Polyurethane
Physical form	Two-component system
Cure	Chemical reaction of the two components at RT
T_g ***(°C)***	45
Density [kg/m^3]	1230
Tensile strength [MPa]	35
Young's modulus [MPa]	2500
Tensile lap-shear strength [MPa]	20
Elongation at break [%]	2.5

5.4 Numerical analysis

The numerical simulations of the automotive structure were carried out in the Abaqus® software FE package, using CZM in the adhesive layer. The details regarding the simulations at quasi-static and impact conditions are presented in papers 1 and 2, respectively.

5.5 Experimental details

Before manufacturing the front header joints, some preliminary tests were performed to ensure that the adhesive layer geometry in the experimental model would match that of the supplied 3D model. The geometry of the front header is complex and one of the first concerns was to define how the adhesive would be applied so that the adhesive layer dimensions could be satisfied. To achieve this goal, a simply experimental test was done to verify the adhesive distribution on the joint. Two acrylic plates (Figure 59) were cut, cleaned and degreased.

Calibrated metallic tapes were applied between them, to guarantee a minimum distance between plates of 1.6 mm, approximately the thickness of the adhesive in the model. Two tapes with a calibrated thickness of 0.8 mm were used in each end.

The cross-section of the adhesive layer in the model is about 1.6x17 mm. It is important to take into account that these are approximate values, since these dimensions will necessarily exhibit slight variations throughout the length of this relatively long component. During the manufacture process of this type of component, the adhesive is typically applied using an applicator gun which forces the adhesive to flow through a circular nozzle, creating an adhesive bead with a roughly circular cross section. To find the diameter that this nozzle should have, a simple analysis was done, based in the areas of both adhesive string and nozzle:

$$1.6 \times 17 = \pi \times r^2$$
$$\therefore r \approx 3\ mm \tag{5.1}$$

Therefore, to obtain an adhesive layer which matches the numerical model, a nozzle with a diameter of 6 mm was produced. After the application of the adhesive in the bottom plate, the INSTRON® universal testing machine (Norwood, Massachusetts, USA) was used to gradually press the two plates together. A displacement rate of 1 mm/min was imposed to the machine and a video camera was used to record the evolution of the test, being the initial and final moments of the same represented in Figure 60. Good results were achieved, as the adhesive distribution was approximately constant, and the dimensions of the string were similar to what was observed in the model.

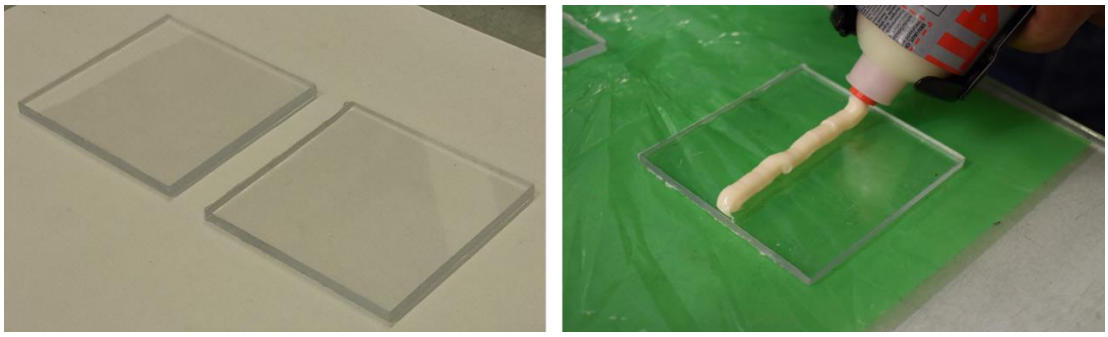

Figure 59 - Acrylic plates used in the test (left) and application of the adhesive (right)

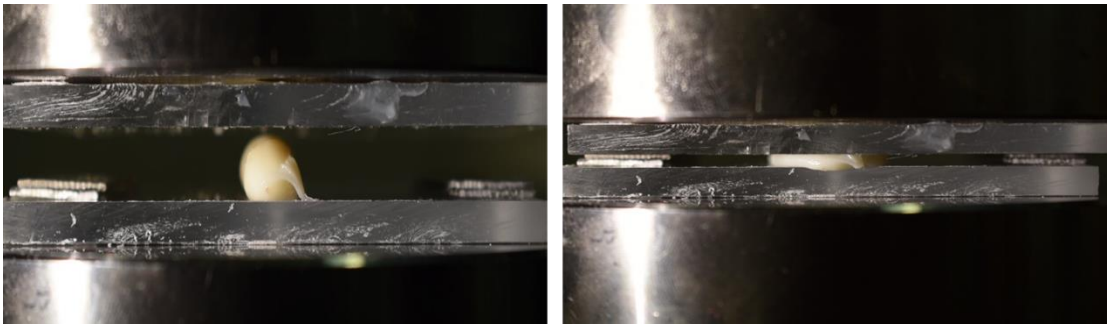

Figure 60 – Adhesive's shape before (left) and after (right) the test

Another concern about the manufacturing of the joints was related to the cure of the epoxy adhesive, namely ensuring that the target curing temperature was reached. The manufacturer recommends a cure cycle of 4h at 165 °C and, due to the dimensions of the front header, the cure of the adhesive had to be carried out in the oven shown in Figure 61. The temperature displayed by the controller of this oven does not accurately represents the temperature of the adhesive layer, as it actually records the temperature of the air as it passes through a recirculating fan. Therefore, a thermocouple, inserted between two aluminum substrates, was used to read a temperature representative of that of the adhesive layer, allowing a comparison with the temperature displayed. The controller temperature was set to 210 °C and data was collected every minute, for a total of 135 record points, allowing the construction of the curves shown in Figure 62.

Figure 61 - Oven used to manufacture the front header joints

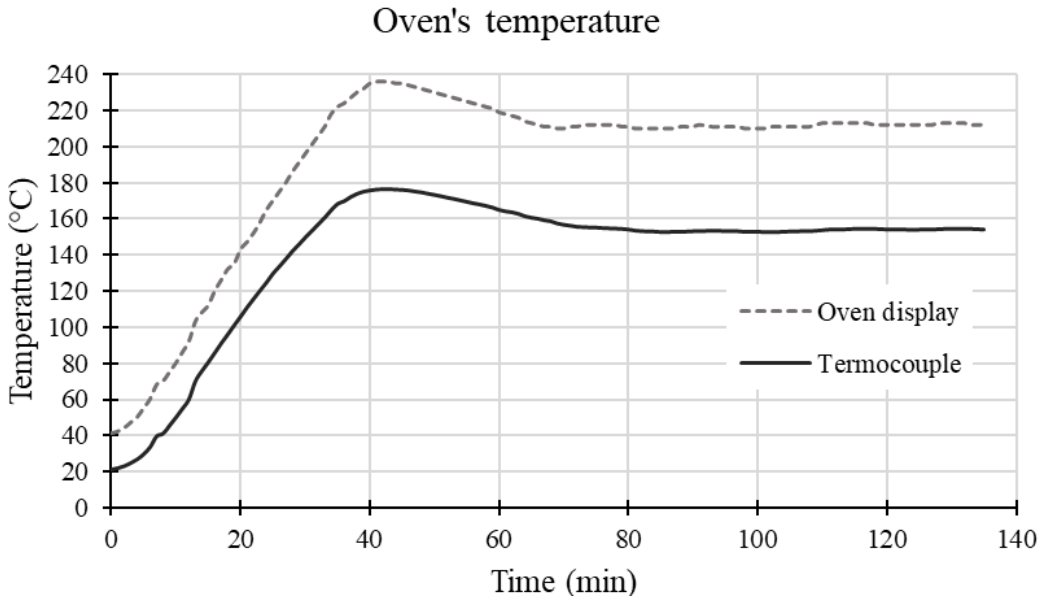

Figure 62 - Evolution of the temperature inside and measured by the oven, for a set temperature of 210 °C

It can be concluded that the difference between the displayed and the real value is high, as a set temperature of 210 °C will represent a temperature of around 154 °C in the adhesive layer, which is close to the desired 165 °C. In these conditions, the oven takes about 70 minutes to reach a stable temperature and the real overshoot (measured by the thermocouple) is acceptable. Besides this inconvenient, the most important factor to retain is that the oven is indeed capable to maintain a stable temperature and therefore can be used to cure the epoxy layers on the automotive front header. The complete cure of the adhesive can be reached by increasing a bit the set temperature or by using this temperature for a longer time.

This being said, further and complete details about the manufacturing process of the joints are explained in the papers and, therefore, will not be presented in this section.

6 Conclusions

The present work focused on the study of a real-scale, adhesively bonded automotive structure, designated as *front header*, belonging to the Aston Martin's DB 11 model. This component can play a significant role in the passengers' safety during a crash situation, due to its location and how it is connected to the other components of the body structure of the car. Experimental tests on this structure were performed at RT and for different displacement rates, namely quasi-static (1 mm/min) and impact (3 m/s) conditions. When epoxy-bonded, the experimental data revealed that the load capacity and energy absorption capabilities of the structure are low for both tested conditions. This can be assigned to the premature failure of the component caused by stress concentration around the middle holes, which lead to the initiation and propagation of a crack in the lower substrate. Considering these results, another adhesive, namely a high-performance structural polyurethane, was also used to bond the structure. For both loading conditions, the polyurethane-bonded specimens revealed better results regarding the failure load and the absorbed energy. Such observations can be assigned to the higher flexibility of the polyurethane system in comparison to the epoxy, which allows the absorption of higher amounts of energy and less transmission to the lower substrate, avoiding its fracture. Therefore, it is possible to conclude that the type of adhesive influences the response of the automotive joint, but in neither case the failure (when existed) occurred in the adhesive layers. Based on these results, the adhesives applied to bond the structure can be concluded not to compromise its integrity, which validates the application of adhesive systems in real structures and encourages further investigation. The numerical models for the epoxy-bonded structure showed good agreement with the experimental tests, which allows to conclude that FE models combined with CZM in the adhesive are a powerful and trustworthy tool to predict the behaviour of real structures under different loading conditions, avoiding some experimental procedures that can be highly time-consuming, require specific equipment and lead to material waste.

To support the study of the front header, tests were performed on SLJs with aluminium substrates bonded with the same crash-resistant epoxy adhesive. From these tests several conclusions can be reached regarding the influence of the displacement rate and adhesive thickness on the failure load. An increase of the displacement rate was found to lead to an increase in the failure load of the joint, as the best results were obtained for impact conditions and the worst for quasi-static. Additionally, it was also experimentally demonstrated that thicker adhesive layers have a negative effect on the load capacity of the SLJs at both quasi-static and impact conditions, as results for 1.6 mm were worse than those for 0.2 mm. Also for this case, the conducted numerical simulations were found to accurately predict the experimental failure load, suggesting once again that they can be a good alternative to the physical tests.

Finally, the design of a new Arcan device for impact conditions was successfully completed. Once manufactured, this device will be of extreme importance for the characterization of the mechanical behaviour of structural adhesives under impact, as its configuration allows to determine the strength and stiffness of the adhesives for any given loading mode, from mode I, to mode II and various mixed modes in between. Therefore, the use of extrapolation laws for impact, like those presented in this document, will not be necessary and it will be possible to more accurately define the mixed mode behaviour of adhesives under impact, allowing the use of this data to create more powerful cohesive laws.

7 Future work

After the completion of this project, several steps can be done to improve the understanding of adhesive systems and its application to real structures, namely:

1. Arcan device:
    - After the design stage and all the 2D drawings completed, the manufacturing of the Arcan and its validation are required;
    - The mould to produce the Arcan specimens needs also to be manufactured and implemented;
2. SLJs:
    - Due to some difficulties found in modelling SLJs for a thickness of 1.6 mm, further studies with larger thicknesses should be conducted in order to understand if the observed failure mechanisms remain the same and if the trapezoidal law is more suited than the triangular one for these cases, under quasi-static conditions. If yes, it would be interesting to know from which thickness forward the trapezoidal law becomes more suited for failure load prediction;
    - Besides aluminium, other materials such as carbon fibre reinforced plastics are being increasingly applied in the automotive industry with the goal of weight reduction in mind. Therefore, the study of SLJs with carbon and glass fibres substrates would be a good complement for this work, and a comparison with the results obtained for aluminium could be made. This would allow to understand if the weight reduction allowed by the composite systems is followed by a decrease in the load capacity of the joints or not;
3. Automotive front header:
    - The lack of information regarding the aluminium alloy used as substrates, AA6016-T6, caused some difficulties in the numerical modelling of the automotive structure. In fact, only the plastic behaviour was given, and the

correct modelling of the component requires the use of a damage criterion (like the ductile damage or the Johnson-Cook criteria), which parameters are not fully known. Additionally, this specific alloy is not commonly studied in the literature, which made the definition of these parameters even more difficult. Therefore, a complete characterization of this alloy could be performed in order to enhance the failure load and displacement at failure prediction of the structure;

- The polyurethane adhesive used to bond the automotive component could be mechanically characterized using the tests applied to the crash-resistant epoxy. This information would allow the analysis of the polyurethane-bonded structure in a FEM software and the numerical results for the two types of adhesive could be compared;
- Although the typical service temperature of a vehicle is about 25 °C, some exceptions can occur. Extreme temperatures can be verified during hot or cold seasons in Europe or in other regions of the globe. The response of this component under negative and high temperatures would also be interesting to analyse and compare with the response at RT;
- Finally, to ensure that the adhesive is able to perform consistently throughout the service life of the vehicle, a fatigue analysis of the automotive front header could be performed.

References

1. Nunes, P.D.P., *Impact strength of dissimilar joints for the automotive industry*, in *Mechanical Engineering*. 2018, Faculty of Engineering of University of Porto.
2. J. J. M. Machado, A.H., P. D. P. Nunes, E. A. S. Marques, R. J. C. Carbas, C. Sato, L. F. M. da Silva, *Strain rate dependence of a crash resistant adhesive as a function of temperature for the automotive industry*. 2018.
3. Barnes, T.A. and I.R. Pashby, *Joining techniques for aluminium spaceframes used in automobiles: Part II — adhesive bonding and mechanical fasteners.* Journal of Materials Processing Technology, 2000. **99**(1): p. 72-79.
4. Brooks, R., S.M. Shanmuga Ramanan, and S. Arun, *Composites in Automotive Applications: Design*, in *Reference Module in Materials Science and Materials Engineering*. 2017, Elsevier.
5. Beardmore, P. and C.F. Johnson, *The potential for composites in structural automotive applications.* Composites Science and Technology, 1986. **26**(4): p. 251-281.
6. Thornton, P. and R. Jeryan, *Crash energy management in composite automotive structures.* International Journal of Impact Engineering, 1988. **7**(2): p. 167-180.
7. C England, J., et al., *Design of Automotive Metal and Composite Chassis Structures.* Recent Patents on Mechanical Engineering, 2010. **3**(3): p. 211-225.
8. Khan, A.S. and H. Liu, *Variable strain rate sensitivity in an aluminum alloy: Response and constitutive modeling.* International Journal of Plasticity, 2012. **36**: p. 1-14.
9. Miller, W.S., et al., *Recent development in aluminium alloys for the automotive industry.* Materials Science and Engineering: A, 2000. **280**(1): p. 37-49.
10. Tisza, M. and I. Czinege, *Comparative study of the application of steels and aluminium in lightweight production of automotive parts.* International Journal of Lightweight Materials and Manufacture, 2018. **1**(4): p. 229-238.
11. Hirsch, J., *Recent development in aluminium for automotive applications.* Transactions of Nonferrous Metals Society of China, 2014. **24**(7): p. 1995-2002.
12. MediaCenter, A. *The Audi Q8: the new top model of the Q family*. 2018 [cited 2019 February 29th]; Available from: www.audi-mediacenter.com/en/the-audi-q8-the-new-top-model-of-the-q-family-10412/body-10419.
13. Hirsch, J., *Aluminium Alloys for Automotive Application*. Vol. 242. 1997. 33-50.

14. Smerd, R., et al., *High strain rate tensile testing of automotive aluminum alloy sheet.* International Journal of Impact Engineering, 2005. **32**(1): p. 541-560.

15. Oosterkamp, L.D., A. Ivankovic, and G. Venizelos, *High strain rate properties of selected aluminium alloys.* Materials Science and Engineering: A, 2000. **278**(1-2): p. 225-235.

16. Chen, Y., et al., *Stress–strain behaviour of aluminium alloys at a wide range of strain rates.* International Journal of Solids and Structures, 2009. **46**(21): p. 3825-3835.

17. Galvez, P., et al., *Study of the behaviour of adhesive joints of steel with CFRP for its application in bus structures.* Composites Part B: Engineering, 2017. **129**: p. 41-46.

18. Borsellino, C., G. Di Bella, and V. Ruisi, *Adhesive joining of aluminium AA6082: The effects of resin and surface treatment.* International Journal of Adhesion and Adhesives, 2009. **29**(1): p. 36-44.

19. Costa, A.P.d., et al., *A Review of Welding Technologies for Thermoplastic Composites in Aerospace Applications.* Journal of Aerospace Technology and Management, 2012. **4**: p. 255-265.

20. Kinloch, A., *Adhesion And Adhesives: Science And Technology*. 1987.

21. Silva, L.F.M., A. Öchsner, and R. Adams, *Handbook of Adhesion Technology*. 2011. p. 1-7.

22. Grujicic, M., et al., *An overview of the polymer-to-metal direct-adhesion hybrid technologies for load-bearing automotive components.* Journal of Materials Processing Technology, 2008. **197**(1-3): p. 363-373.

23. Machado, J.J.M., E.A.S. Marques, and L.F.M. da Silva, *Adhesives and adhesive joints under impact loadings: An overview.* The Journal of Adhesion, 2018. **94**(6): p. 421-452.

24. Banea, M.D., et al., *Effects of Temperature and Loading Rate on the Mechanical Properties of a High Temperature Epoxy Adhesive.* Journal of Adhesion Science and Technology, 2011. **25**(18): p. 2461-2474.

25. Lees, W., *Adhesives in engineering design*. 1984: Springer.

26. Mata, R.A., *Impact of adhesive joints for the automotive industry at low and high temperatures*, in *Mechanical Engineering*. 2014, Faculty of Engineering of University of Porto.

27. Hill, J., *Adhesively Bonded Structural Composites for Aston Martin Vehicles.* Ford Motor Company Research and Advanced Engineering, 2003.

28. *Vanquish & Vanquish S.* 2018 [cited 2019 18 april]; Available from: https://www2.astonmartin.com/heritage/past-models/vanquish.

29. Saldanha, D.F.S., et al., *Mechanical characterization of a high elongation and high toughness epoxy adhesive.* International Journal of Adhesion and Adhesives, 2013. **47**: p. 91-98.

30. Silva, M.R.G., E.A.S. Marques, and L.F.M.d. Silva, *Behaviour under Impact of Mixed Adhesive Joints for the Automotive Industry.* Latin American Journal of Solids and Structures, 2016. **13**: p. 835-853.

31. Adams, R.D., *Adhesive bonding: science, technology and applications*. 2005: Elsevier.

32. Feraboli, P. and A. Masini, *Development of carbon/epoxy structural components for a high performance vehicle.* Composites Part B: Engineering, 2004. **35**(4): p. 323-330.

33. Araújo, H.A.M., *Impact and damping behaviour of composite adhesive joints*, in *Mechanical Engineering*. 2016, Faculty of Engineering of University of Porto.

34. Griffith, A.A., *VI. The phenomena of rupture and flow in solids.* Philosophical transactions of the royal society of london. Series A, containing papers of a mathematical or physical character, 1921. **221**(582-593): p. 163-198.

35. Ripling, E.J., S. Mostovoy, and H.T. Corten, *Fracture Mechanics: A Tool for Evaluating Structural Adhesives.* The Journal of Adhesion, 1971. **3**(2): p. 107-123.

36. Bezemer, A.A., C.B. Guyt, and A. Vlot, *New impact specimen for adhesives: optimization of high-speed-loaded adhesive joints.* International Journal of Adhesion and Adhesives, 1998. **18**(4): p. 255-260.

37. Adams, R.D., et al., *Structural adhesive joints in engineering*. 1997: Springer Science & Business Media.

38. da Silva, L.F.M. and R.D. Adams, *Adhesive joints at high and low temperatures using similar and dissimilar adherends and dual adhesives.* International Journal of Adhesion and Adhesives, 2007. **27**(3): p. 216-226.

39. Silva, M.R.G., *Impact of mixed adhesive joints for the automotive industry*, in *Mechanical Engineering*. 2015, Faculty of Engineering of University of Porto.

40. Banea, M. and L.F.M. Silva, *Mechanical Characterization of Flexible Adhesives*. Vol. 85. 2009. 261-285.

41. Campilho, R.D.S.G., et al., *Modelling adhesive joints with cohesive zone models: effect of the cohesive law shape of the adhesive layer.* International Journal of Adhesion and Adhesives, 2013. **44**: p. 48-56.

42. Elices, M., et al., *The cohesive zone model: advantages, limitations and challenges.* Engineering Fracture Mechanics, 2002. **69**(2): p. 137-163.

43. Hillerborg, A., M. Modéer, and P.-E. Petersson, *Analysis of crack formation and crack growth in concrete by means of fracture mechanics and finite elements.* Cement and concrete research, 1976. **6**(6): p. 773-781.

44. Campilho, R.D., M. De Moura, and J. Domingues, *Using a cohesive damage model to predict the tensile behaviour of CFRP single-strap repairs.* International Journal of Solids and Structures, 2008. **45**(5): p. 1497-1512.

45. Khoramishad, H., et al., *Predicting fatigue damage in adhesively bonded joints using a cohesive zone model.* International Journal of fatigue, 2010. **32**(7): p. 1146-1158.

46. Machado, J., et al., *Numerical study of the behaviour of composite mixed adhesive joints under impact strength for the automotive industry.* Composite Structures, 2018. **185**: p. 373-380.

47. Da Silva, L.F. and R.D. Campilho, *Advances in numerical modelling of adhesive joints*, in *Advances in numerical modeling of adhesive joints*. 2012, Springer. p. 1-93.

48. Machado, J.J.M., et al., *Numerical study of impact behaviour of mixed adhesive single lap joints for the automotive industry.* International Journal of Adhesion and Adhesives, 2018. **84**: p. 92-100.

49. Golzar, M. and M. Poorzeinolabedin, *Prototype fabrication of a composite automobile body based on integrated structure.* The International Journal of Advanced Manufacturing Technology, 2010. **49**(9-12): p. 1037-1045.

50. Lahaye, C., et al., *Development of an aluminium prototype bonnet for Saab 9-3*. 1998, SAE Technical Paper.

51. Langseth, M., O.S. Hopperstad, and A.G. Hanssen, *Crash behaviour of thin-walled aluminium members.* Thin-Walled Structures, 1998. **32**(1): p. 127-150.

52. Cheon, S.S., D.G. Lee, and K.S. Jeong, *Composite side-door impact beams for passenger cars.* Composite Structures, 1997. **38**(1): p. 229-239.

53. Li, Q.F., et al., *Optimum Design and Numerical Simulation of Automotive Front Side-Door Impact Beam.* Key Engineering Materials, 2011. **452-453**: p. 169-172.

54. Winter, D., *DuPont Develops Plastic Side-Impact Door Beam*, in *WardsAuto*. 2013: www.wardsauto.com.

55. Cognard, J.Y., et al., *Analysis of the nonlinear behavior of adhesives in bonded assemblies—Comparison of TAST and Arcan tests.* International Journal of Adhesion and Adhesives, 2008. **28**(8): p. 393-404.

56. Uddeholm, *Uddeholm Orvar Supreme*, R. Aços, Editor. 2013, Ramada Aços: https://www.ramada.pt/en/products/steels/steel-working-tools-hot-work/mg50-.html.

57. steel, O. *H13 Tool Steel | 1.2344*. 2019 [cited 2019 22 april]; Available from: http://www.astmsteel.com/product/h13-tool-steel-x40crmov5-1-skd61-hot-work-steel/.

58. Uddeholm, *Uddeholm Impax Supreme*, R. Aços, Editor. 2011, Ramada Aços: https://www.ramada.pt/pt/produtos/acos/aa-os-de-construa-ao-ligados/pm300-.html.

59. Banea, M.D. and L.F.M. da Silva, *Adhesively bonded joints in composite materials: An overview.* Proceedings of the Institution of Mechanical Engineers, Part L: Journal of Materials: Design and Applications, 2009. **223**(1): p. 1-18.

60. Sawa, T. and H. Suga. *Behaviors of single-lap adhesive joints subjected to static and impact loads*. in *International Conference on Experimental Mechanics: Advances and Applications*. 1997. International Society for Optics and Photonics.

61. Torca, I., et al., *Tensile Behaviour of 6082 Aluminium Alloy Sheet under Different Conditions of Heat Treatment, Temperature and Strain Rate*. Vol. 423. 2009. 105-112.

62. MakeItFrom. *6016-T4 Aluminium*. 2018 [cited 2019 1 april].

63. MakeItFrom. *6016-T6 Aluminium*. 2018 [cited 2019 2 april].

64. Polylanema, *AW 6082*, P. Lda., Editor. 2019: www.polylanema.pt.

65. Yibo, P., et al., *Dynamic Mechanical Behaviors of 6082-T6 Aluminum Alloy.* Advances in Mechanical Engineering, 2013. **5**: p. 878016.

66. Lagonda, A.M., *Centenary 90's to present*, in *AM Magazine*. Aston Martin Lagonda: http://cdn.astonmartin.com/magazine/issue-23/centenary-90s.html.

67. Simoes, V., et al. *Influence of temperature, strain-rate and aging on the mechanical behaviour of an Al-Mg-Si alloy*. in *Congrès français de mécanique*. 2015. AFM, Association Française de Mécanique.

Appendix A: Paper 1

Experimental and numerical study of the quasi-static response of an adhesively bonded automotive structure

N.D.D. Silva[1], J.J.M. Machado[1], E.A.S. Marques[1], M. Parente[2], L.F.M. da Silva[2,*]

[1]Instituto de Ciência e Inovação em Engenharia Mecânica e Engenharia Industrial (INEGI), Rua Dr. Roberto Frias, 4200-465 Porto, Portugal

[2]Departamento de Engenharia Mecânica, Faculdade de Engenharia (FEUP), Universidade do Porto, Rua Dr. Roberto Frias, 4200-465 Porto, Portugal

Abstract

The constant demand for fuel saving in the automotive industry requires the design of lighter structures, which encourage the application of low-density materials together with structural adhesives to bond the automotive frames. Still, it is fundamental to ensure that weight reduction does not compromise mechanical resistance, making it possible to obtain lighter yet strong structures, able to fulfil the requirements of this sector. The aim of this work is to analyse the quasi-static behaviour of a component-scale automotive frame bonded with a crash-resistant epoxy adhesive, representative of the use of adhesives in real-life automotive structures. The tests were performed at room temperature (24 ºC), characteristic of normal service conditions. A numerical simulation of the structure was also conducted, allowing the comparison of the finite element model predictions with the experimental data. The results showed that the adhesive did not compromise the integrity of the automotive structure, as the failure was caused by fracture in the lower aluminium substrate. The numerical analysis revealed good accuracy in the failure load prediction of the joint. Considering the experimental observations, a more flexible polyurethane adhesive was considered to join the component, avoiding the previous fracture.

Keywords

High-performance crash-resistant adhesive; Adhesively bonded automotive structure; Quasi-static; Displacement rate; Single lap joints

[*] Corresponding author. Tel.: +351 22 508 17 06; fax: +351 22 508 14 45. *E-mail address:* lucas@fe.up.pt (L.F.M. da Silva)

1. Introduction

Reduction in both fuel consumption and CO_2 emissions is one of the most challenging concerns for automotive manufacturers. A solution to achieve this goal is the manufacture of lighter structures, encouraging the use of materials such as aluminium and composites in opposition to traditional steel in the body structure of vehicles [1]. Despite the excellent strength and stiffness to weight ratios of composites, their use in high volume structural automotive applications is still limited, mainly due to high material and manufacturing process costs as well as some uncertainty related to its functionality and long term durability [2, 3]. On the other hand, aluminium is a well-studied material and its low density in comparison to steel, associated to high corrosion resistance and good formability [4, 5], makes it attractive for body frame construction.

These lightweight concepts are also leading to innovations and new paradigms in the field of joining techniques. Fasteners and rivets represent a common solution in worldwide applications, but imply discontinuity of the materials, increase in total weight and local stress concentration that reduces structures' integrity [6]. Welding processes often cause heat distortions and residual stresses in the heat affected zone (HAZ), leading to deterioration of material properties [7]. Premature failure due to corrosion is another frequent problem, demanding more regular inspections [8]. Furthermore, it is difficult to weld aluminium properly as it tends to react with oxygen, forming an oxide layer in the surface that, although protecting against corrosion, has a higher melting point than aluminium [9]. Welding composites is also difficult and a matter of intense research, as existing processes and technologies cannot be directly transferred to these materials [10]. For these reasons, the automotive industry (as well as others like the aerospace and naval sectors) have searched for alternative joining methods and increased the use of adhesive bonding. This technique allows the manufacture of structures that would be impossible otherwise and is readily automated [9], leading to an equal stress distribution along the bonded length and reduction of stress concentrations [11], thus enhancing fatigue resistance [9, 12]. Additionally, the use of adhesives leads to a reduction of noise and vibrations [1, 9], improved damage tolerance and lower fabrication costs [13].

Adhesives, which are usually polymeric materials, are known to be highly sensitive to strain rate [12-14]. Several studies were conducted in the last decade about the effect of this parameter on the properties of the adhesives. For instance, Banea et al. [13] investigated the effect of test speed on the tensile properties of an epoxy and concluded

that both ultimate tensile stress and Young's modulus increased with strain rate. Machado et al. [12] tested a crash-resistant epoxy adhesive at different strain rates and similar conclusions were drawn. Of all types of adhesives, epoxies are one of the most used in automotive structural applications due to their high strength [15]. Borsellino et al. [9] analysed the joint resistance of an aluminium alloy sheet with several adhesives (orthophtalic polyester, vinylester and epoxy resins) and concluded that the epoxy resin joint was the most resistant, due to the intrinsic strength of the adhesive, the enhanced stability of aluminium oxide in alkaline environment and the effect of mixing with catalyst. Besides epoxy systems, the use of structural polyurethanes in the automotive industry is also common, mainly due to their high durability, good fatigue behaviour and peel strength [16].

Despite offering accurate results, experimental testing is not always desired, as it often requires time-consuming manufacturing processes, material spending and specific testing equipments and procedures. Therefore, numerical simulation through finite element (FE) models has become a powerful tool for design, as it allows a reduction in the number of experimental tests that must be conducted. When designing bonded joints, a damage mechanics approach based in cohesive zone modelling (CZM) has been widely used in the strength prediction of adhesive joints, using energy-based principles to model damage growth [17]. The validation of the FE models with experimental data is necessary in a first stage, so that model calibration can be performed and reliable results achieved. Numerical modelling using CZM has already been extensively applied in the prediction of the mechanical behaviour of adhesive joints with simple configurations, such as single lap joints (SLJs). Mixed adhesive SLJs under quasi-static conditions were numerically analysed by Machado et al. [18] and the results were compared to the experimental data obtained in a previous work. Cohesive numerical models were concluded to be a viable tool to predict the behaviour of mixed joints. A numerical approach was also used in [17] with the goal of predicting the behaviour of adhesive corner joints, previously tested in [19]. The FE analysis was considered to present a good agreement with the data obtained in the experiments, showing that cohesive damage models provide good results for these configurations. However, for the static response of real, full-scale automotive structures, the information available is still limited and few examples can be found where comparisons are made between experimental and numerical results. Lahaye et al. [20] focused on the development of an aluminium bonnet for the Saab 9-3 model in replacement of the steel version. The new prototype underwent a series of tests to evaluate

its performance during the lifetime of a vehicle and allowed a 50% weight reduction while satisfying the performance tests required by Saab®. Cheon et al. [21] investigated the use of a glass-fibre-reinforced epoxy composite in alternative to steel in the side-door impact beams of passenger cars. The energy absorption behaviour of the composite beams was found to be worse when the beams were subjected to static conditions. The FE results obtained in ABAQUS® showed good agreement with experimental data.

The present work aims to experimentally analyse the mechanical behaviour of a real, adhesively bonded automotive structure under quasi-static (1 mm/min) conditions. Using the data collected in previous works [12, 22], the mechanical properties of the epoxy system will allow the definition of cohesive laws that can be applied to predict the behaviour of the joint through a finite element method (FEM) simulation using CZM in the adhesive. The numerical results can then be compared to the experimental data obtained at room temperature (RT) to validate the model. Since the adhesive layer thickness used to bond the automotive structure is considerably high (1.6 mm), the quasi-static (1 mm/min) and 0.1 m/s response of SLJs bonded with different thicknesses of the same adhesive is also studied, so that the influence of this parameter in the behaviour of the joint can be properly evaluated. As a complement, a polyurethane adhesive was also used to bond the automotive structure under the same loading conditions.

2. Experimental details

2.1. SLJ

2.1.1. Material and properties

The SLJ specimens used in the present work were manufactured with aluminium substrates, bonded with a highly ductile, crash-resistant epoxy adhesive, with the reference XNR6852 E-3, supplied by Nagase ChemteX®.

2.1.1.1. Aluminium

Since the substrates of the automotive structure are made of the AA6016-T4 aluminium alloy, the research plan for SLJ tests entailed use the same material. However, this was not possible because the aluminium manufacturers that were contacted only provide the AA6016-T4 alloy in large quantities, compatible with industrial production

but not with scientific research. Furthermore, the storage of this alloy is not common in T4 (naturally aged) temper, as prolonged exposure to environmental agents leads to the deterioration of this heat treatment. For these reasons, the AA6082-T6 alloy was selected for this step instead due to its similar mechanical properties, shown in Table 1, and greater availability in the market.

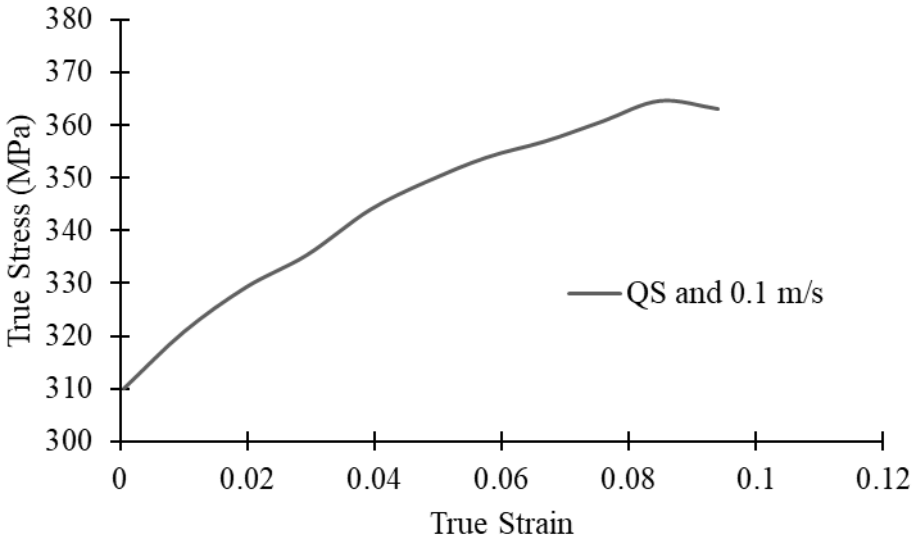

Fig. 1. Plastic behaviour of AA6082-T6 for the tested conditions (adapted from [23]).

The influence of strain rate on the mechanical properties of this alloy was studied by several authors [23-26], all reporting that AA6082-T6 presents low strain rate sensitivity at RT. Its plastic behaviour was adapted from [23] and is represented in Fig. 1.

Table 1. General mechanical properties of the AA6082-T6 aluminium alloy.

Properties	
Density, ρ [kg/m^3]	2700
Young's modulus, E [MPa]	69000
Shear modulus, G [MPa]	26000
Poisson's ratio, ν	0.33
Tensile strength, σ_n [MPa]	360
Yield strength, σ_y [MPa]	310
Shear strength, τ [MPa]	220
Elongation at break, ε [%]	9.8

2.1.1.2. Adhesive

The adhesive chosen to bond the aluminium substrates in the SLJs is the same that was initially applied in the automotive structure, namely a crash-resistant epoxy system.

The mechanical properties of this adhesive at RT have already been obtained in previous works for quasi-static (1 mm/min) conditions. The tensile strength and Young's modulus were determined by Machado et al. [12] performing tensile tests over bulk specimens. DCB specimens tested at 1, 10 and 100 mm/min allowed the assessment of the critical strain energy release rate in mode I (G_{IC}). The remaining properties of the adhesive, as the critical strain energy release rate in mode II (G_{IIC}) and the shear strength and modulus, were studied by Araújo et al. [22].

The properties of XNR6852 E-3 for a displacement rate of 0.1 m/s were found using the logarithmic laws proposed in [12]. These laws are generically given by Eq. (1).

$$\text{Property to determine} = A\ln(x) + B \tag{1}$$

where A and B are constants obtained from experimental data. When determining tensile strength, Young's modulus and G_{IC}, the value of x should be the displacement rate, in mm/min, while for shear strength the x variable stands for the strain rate, in s^{-1}. A displacement rate of 0.1 m/s is equivalent to 6000 mm/min and the conversion to strain rate can be achieved by using Eq. (2).

$$\dot{\varepsilon}(t) = \left(\frac{L(t) - L_0}{L_0}\right) = \frac{v(t)}{L_0} \tag{2}$$

where $v(t)$ corresponds to the displacement rate, in mm/s, and L_0 to the value of length of the adhesive bulk tensile specimen used to determine the shear properties, which acquired the value of 120 mm. Therefore, a displacement rate of 0.1 m/s leads to a strain rate of 0.83 s^{-1}. Logarithmic laws were not proposed for the shear modulus and G_{IIC} in [12]. For these parameters, similar laws were constructed using the values at 1 mm/min (quasi-static) and 180000 mm/min (3 m/s, impact condition), the last presented as well in [22]. The properties at 0.1 m/s were then calculated using the same procedure. Table 2 summarizes the properties of the adhesive for quasi-static and 0.1 m/s conditions. The glass transition temperature, T_g, was also determined to be 132 ± 4.51°C [12] and its density 1550 kg/m^3.

Table 2. Mechanical properties of XNR6852 E-3 adhesive for quasi-static and 0.1 m/s loadings.

Properties	**QS (1 mm/min)**	**0.1 m/s**
Cohesive tensile strength, t_n^0 [MPa]	48	65
Young's modulus, E [MPa]	1874	1717
Cohesive shear strength, t_s^0 [MPa]	45	46
Shear modulus, G [MPa]	665	620
Critical strain energy release rate in mode I, G_{IC} [N/mm]	9.2	12.2
Critical strain energy release rate in mode II, G_{IIC} [N/mm]	51	60

2.1.2. Fabrication and testing

The SLJs specimens used aluminium adherends with a thickness of 2 mm, as this value is close to the substrates thickness in the automotive structure. Due to the high ductility of the adhesive, an overlap length of 12.5 mm was chosen in an effort to ensure that failure was ruled only by the adhesive's behaviour and not by the plasticity of aluminium. Two adhesive layer thicknesses were tested, namely 0.2 and 1.6 mm, allowing to analyse the influence of this parameter on the failure load. The last is the approximate thickness of the adhesive in the automotive frame, while the first is well known as a typical optimum thickness that provides the highest static strength in most joint configurations. However, in many practical applications, including in the automotive industry, non-optimal configurations are often used, as very thin layers are difficult to manufacture and control in a typical production line [27]. At least three specimens (which dimensions are shown in Fig. 2) were tested for each configuration and loading condition.

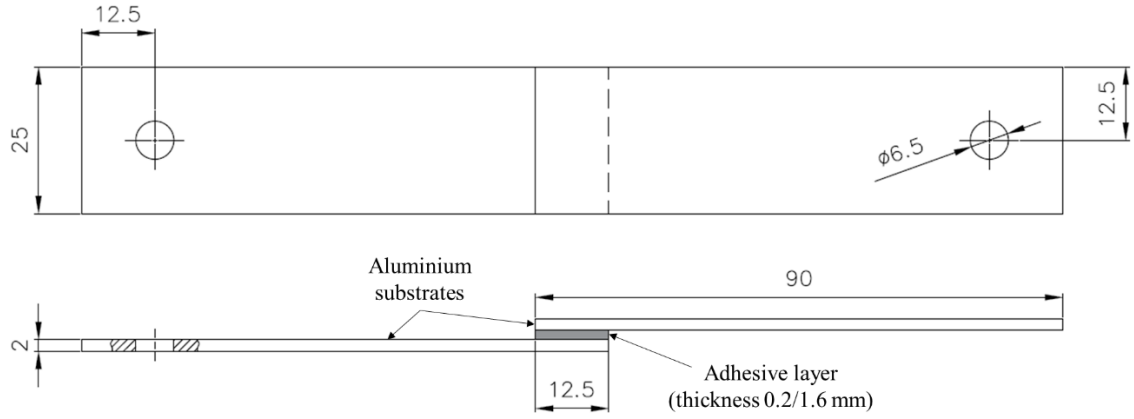

Fig. 2. Configuration and dimensions of the tested SLJs.

The first step in the fabrication of the SLJs was to drill and anodise the adherends using phosphoric acid anodizing. This superficial treatment is recommended for adhesive joints with aluminium substrates, creating a surface which offers a good level of adhesion and avoids interfacial failure. The joints were manufactured using an aluminium mould, with pins being used to ensure the correct alignment of the joint. Spacers with a length of 77.5 mm were inserted in the mould assembly, ensuring that the desired overlap length is attained. Aluminium was chosen as the mould material to avoid large differentials in thermal expansion between the mould and the joints. For a bond thickness of 0.2 mm, the adhesive was manually spread with a spatula, while a pressure gun was used for a thickness of 1.6 mm so that voids in the adhesive layer could be avoided. The manufacturing process was completed by placing the mould in a hot plate press, under pressure and temperature, allowing the fulfilment of the curing cycle of this epoxy system, defined by the manufacturer as 4h at 165 °C.

The quasi-static tests of the joints were performed in an INSTRON® universal testing machine, model 3367 (Norwood, Massachusetts, USA), with a loading capacity of 30 kN. The tests were performed at a constant cross-head displacement rate of 1 mm/min. For 0.1 m/s condition, a Material Test System® 8801 servo-hydraulic testing machine with a capacity of 100 kN was used. This machine was necessary to perform tests at this condition as the first equipment, which uses electrical drive, does not have capacity to apply such a large displacement rate.

2.2. Automotive structure (front header)

Fig. 3 shows the analysed automotive component in the body structure of the vehicle.

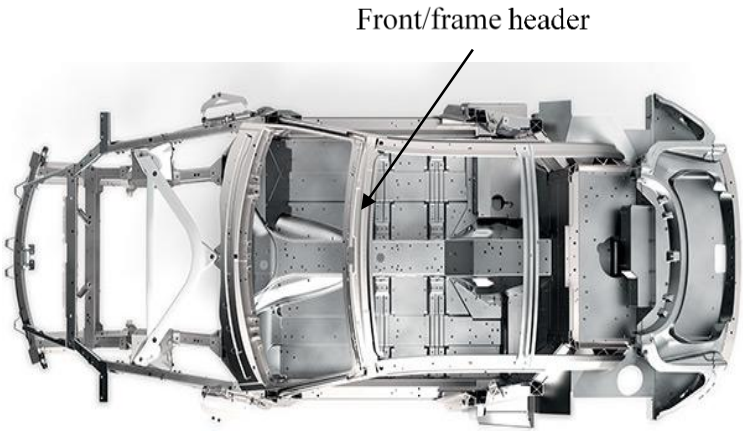

Fig. 3. Location of the front header in the structure of the Aston Martin's DB11 model.

2.2.1. Material and properties

2.2.1.1. Aluminium

The automotive structure, often called front header of a vehicle, uses AA6016-T4 alloy substrates, and were supplied in an already anodised state. After being submitted to the curing cycle of the adhesive, the properties of this alloy become similar to those of the AA6016-T6. The mechanical properties of both alloys are shown in Table 3, while the plastic behaviour of the substrates after curing is represented in Fig. 4.

Table 3. General mechanical properties of the AA6016-T4 and AA6016-T6 alloys.

Properties	**AA6016-T4**	**AA6016-T6**
Density, ρ [kg/m^3]	2700	2700
Young's modulus, E [MPa]	69000	69000
Shear modulus, G [MPa]	26000	26000
Poisson's ratio, ν	0.33	0.33
Tensile strength, σ_n [MPa]	200	280
Yield strength, σ_y [MPa]	110	210
Shear strength, τ [MPa]	130	170
Elongation at break, ε [%]	27	11

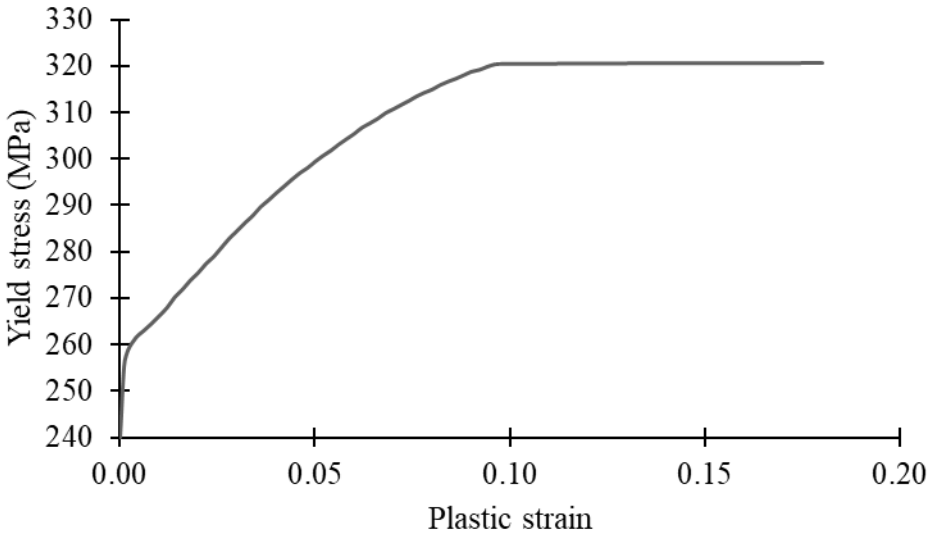

Fig. 4. Plastic behaviour of the AA6016-T6 aluminium alloy, used in the substrates of the automotive structure.

2.2.1.2. Adhesive

The lower and upper substrates of the structure were initially bonded with the XNR6852 E-3 adhesive, which properties at quasi-static conditions were already described in Table 2.

2.2.2. Fabrication and testing

Before the actual bonding procedure was carried out, the lower and upper substrates were cleaned with isopropanol alcohol in order to clean and degrease the surfaces and ensure a good adhesion. The adhesive bead was adjusted to ensure that the final adhesive layer was approximately 17 mm wide and 1.6 mm thick, with constant dimensions throughout all the bondline. To guarantee this thickness, a total of 14 spacers consisting of overlapped calibrated tape layers were assembled in the edges of the lower substrate, in order to minimize the interference with the adhesive bead. The XNR6852 E-3 was applied at both sides of the lower substrate using an applicator gun (approximately 70 g of adhesive were deposited for each specimen) and the upper substrate was then assembled on its top. Clamps were positioned in the spacers' locations to fix the substrates together and apply pressure along the bondlines. Finally, the structure was placed in an oven to perform the curing cycle of the adhesive and any excess was removed from the joint after this process. The steps of the manufacturing procedure are resumed in Fig. 5.

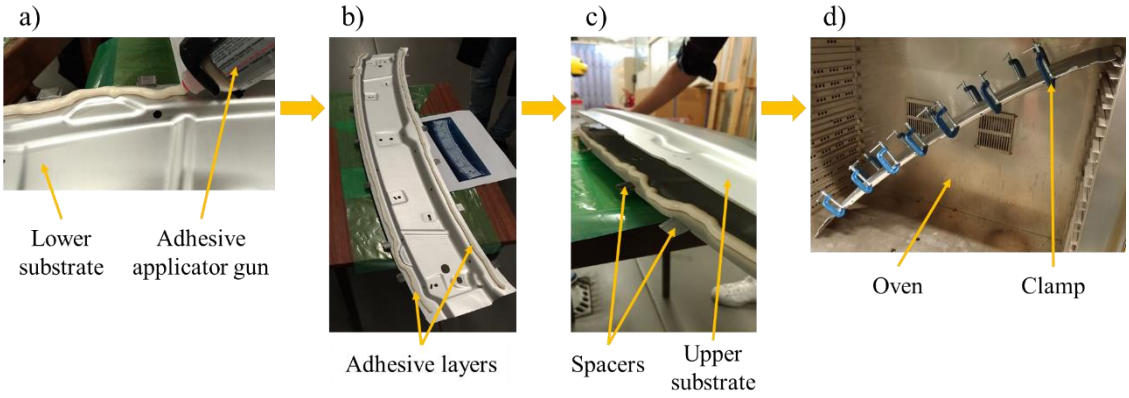

Fig. 5. Manufacturing sequence of the "front header": a) adhesive application; b) adhesive layers on the lower substrate; c) assembling of the upper substrate; d) introduction in the oven of the clamped structure to perform the curing cycle.

The tests were performed in a Material Test System® 8801 servo-hydraulic testing machine with a capacity of 100 kN, with a constant cross-head displacement rate of 1 mm/min being applied. The contact with the structure was made by an "impactor",

designed with a round bottom shape to apply the load uniformly throughout the contact area. A total of eight screw-nut connections were used to fix the automotive structure on its ends. The applied load and vertical displacement, necessary to construct the load-displacement curves, were directly measured by the machine. The assembly of the test is shown in Fig. 6 and two specimens were tested.

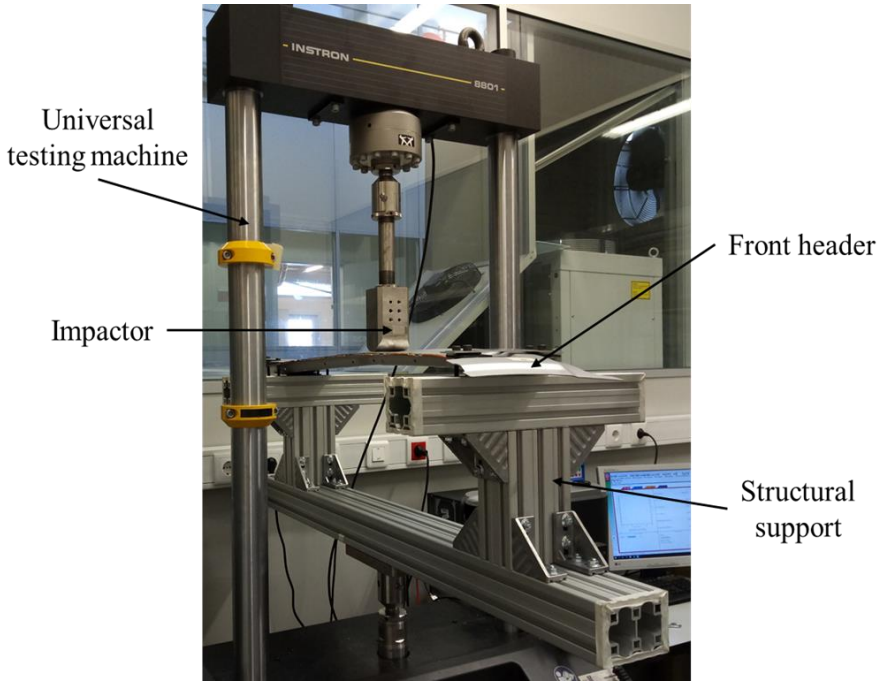

Fig. 6. Configuration of the performed tests under quasi-static conditions.

3. Numerical details

As mentioned before, numerical modelling using CZM is a powerful and accurate tool for failure load prediction of adhesive joints. This technique, originally applied by Hillerborg [28], is able to model the fracture process through the combination of concepts from elasticity and classical fracture mechanics. Cohesive elements, which make use of strength and energetic parameters, are used to simulate crack growth and traction-separation laws are responsible for establishing a relation between stresses and displacements along the process [22]. The most commonly used laws in adhesive bonding are the triangular, trapezoidal and exponential laws and, within these three, the triangular shape (Fig. 7) is often the first choice due to its simplicity, standard implementation in FEM packages as ABAQUS® and lowered susceptibility to convergence problems [29]. The application of these laws requires the knowledge of several adhesive properties and

can be constructed for tensile (mode I) and shear (mode II) loading conditions. When the law is built for mode I, the cohesive tensile strength (σ_n), the Young's modulus (E) and the critical strain energy release rate in mode I (G_{IC}) are needed, while the cohesive shear strength (τ_s), the shear modulus (G) and the critical strain energy release rate in mode II (G_{IIC}) are required for mode II.

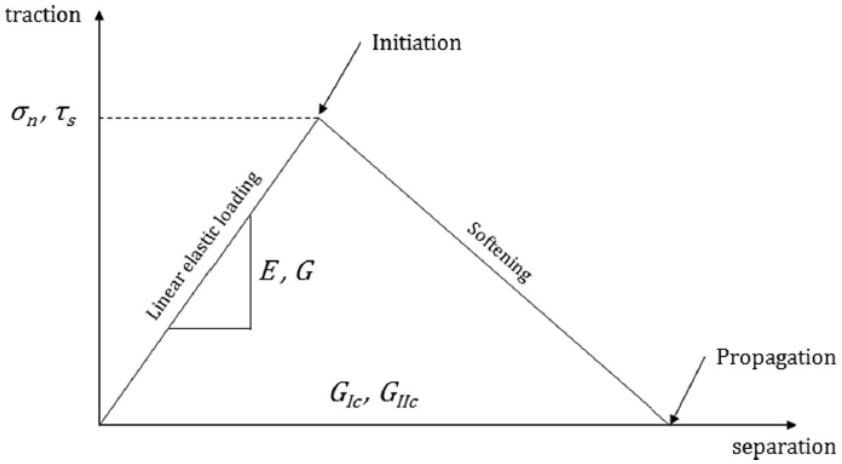

Fig. 7. Triangular traction-separation law for mode I, mode II [22].

3.1. SLJ

3.1.1. Quasi-static modelling

All FE analysis were conducted with the ABAQUS® software package, with two-dimensional (2D) meshes being used to model the SLJs due to its simple geometry. For an adhesive thickness of 0.2 mm, 4-node bilinear plain strain quadrilateral elements (CPE4 in ABAQUS® nomenclature) were assigned to the aluminium adherends, while a unique layer of 4-node two-dimensional cohesive elements (COH2D4 in ABAQUS® nomenclature) was used in the adhesive region. In the case of the SLJs with an adhesive thickness of 1.6 mm, the only difference was located on the bonded area, which was modelled using intercalated layers of plain strain and cohesive elements (Fig. 8). Within this region, the elastic properties of the adhesive were attributed to the plain strain elements. This new design was considered for the higher adhesive thickness as it reproduces the failure mechanism more accurately, leading to better results in the failure load prediction of the joints. For both thicknesses, the cohesive elements were modelled through a triangular law (Fig. 10a), built with the quasi-static properties mentioned before (Table 2). A mesh refinement was made in the most stressed areas, namely the overlap

region, using the bias functionality (Fig. 9). This technique allows a good compromise between accuracy in the results and computational time. A static, general step was chosen to solve the model and as boundary conditions, one end of the joint was prevented to move in the two in-plane directions, while on the other end of the specimen, an horizontal displacement was directly imposed, with a restriction in vertical movement being made, simulating the displacement imposed by the universal testing machine (Fig. 11). Finally, the SDEG parameter (that allows to check the degradation of the cohesive elements representing the adhesive), the reaction forces on the bi-restrained end and the displacement on the single-restrained end were requested as outputs to construct the load-displacement curves.

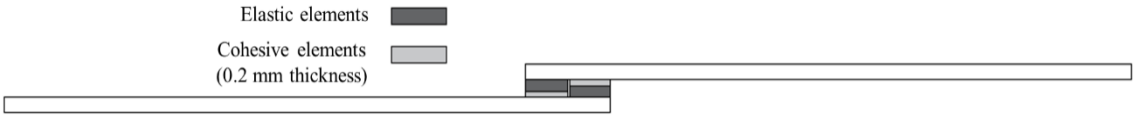

Fig. 8. Joint design used to model the behaviour of the SLJs with an adhesive thickness of 1.6 mm, with plain strain and cohesive elements being applied in the bonded region.

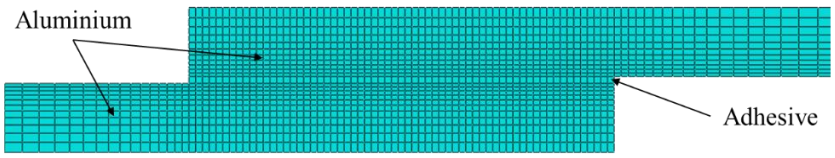

Fig. 9. Mesh refinement on the overlapped area, using the bias functionality.

3.1.2. 0.1 m/s modelling

The geometry, element types and concepts applied at the numerical model for the 0.1 m/s condition were similar to those presented for quasi-static. The only change applied focused on the triangular law used, which was now constructed with the properties corresponding to 0.1 m/s (Fig. 10b).

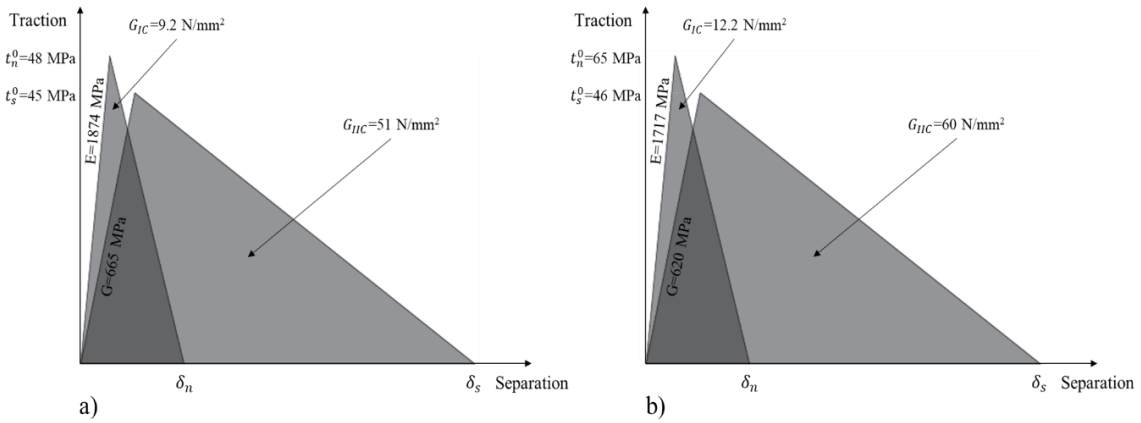

Fig. 10. CZM's traction-separation law for a) quasi-static and b) 0.1 m/s models.

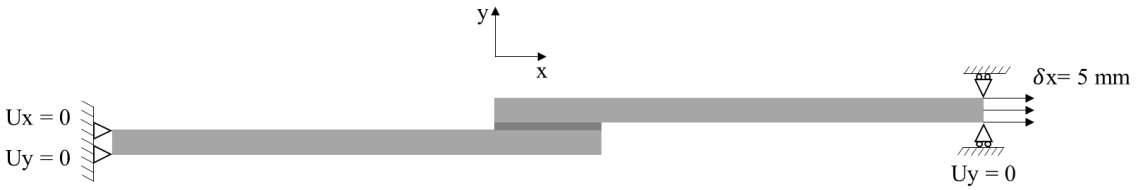

Fig. 11. Representation of the boundary conditions for quasi-static and 0.1 m/s conditions.

3.2. Automotive structure (front header)

The quasi-static numerical simulations of the front header were also carried out in ABAQUS®, with the mesh being imported from a model created in the HYPERMESH® software package. Shell elements with thicknesses of 1.7 and 1.2 mm were used to model the upper and lower aluminium substrates, respectively. The majority of these were linear quadrilateral elements (S4 in ABAQUS® nomenclature), but linear triangular elements (S3 in ABAQUS® nomenclature) were also employed due to the complex geometry of the structure. For modelling the adhesive bondlines, a single layer of linear, 8-node three-dimensional (3D) cohesive elements (COH3D8 in ABAQUS® nomenclature) was assigned and the properties at quasi-static conditions were used. Since the deformation and stress states on the impactor are negligible and not of interest, the same was modelled as a rigid body. To avoid penetration of the structure by the impactor, an interaction between the two was given, with a normal behaviour of the type “Hard contact” and a tangential behaviour with a friction coefficient of 0.61. As boundary conditions, the ends of the front header were encastred at both sides, simulating the service conditions (Fig. 12), and the impactor was allowed to move only in the vertical direction. A static, general

step was used to simulate the process and the SDEG parameter, the reaction forces at the encastre zones and the impactor's displacement were requested as outputs.

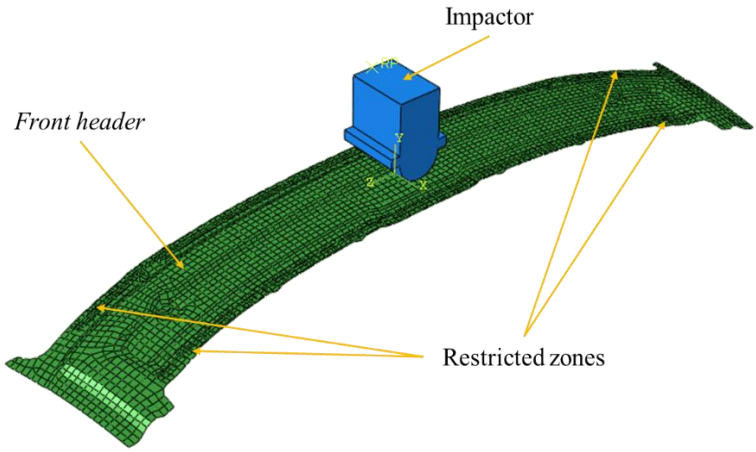

Fig. 12. Boundary conditions applied to the structure at static conditions.

4. Results and discussion

4.1. SLJ: experimental and numerical analysis

4.1.1. Quasi-static testing

The tests under quasi-static conditions for an adhesive thickness of 0.2 and 1.6 mm were found to lead to cohesive failure in the adhesive, as shown in Fig. 13.

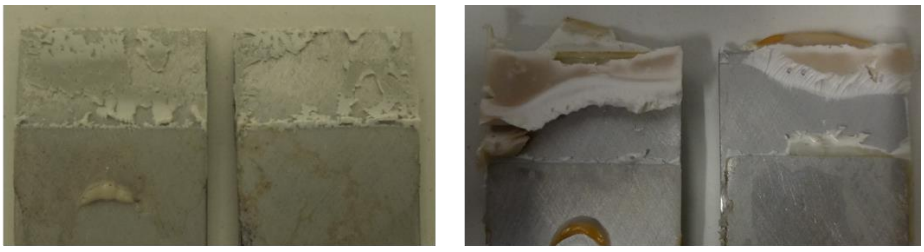

a) b)

Fig. 13. Cohesive failure in the adhesive for SLJs with a) 0.2 and b) 1.6 mm of adhesive layer thickness.

The SDEG parameter obtained in the numerical analysis, showing the degradation of the adhesive layer during the process, is displayed in Fig. 14 for the case of an adhesive thickness of 0.2 mm. The degradation was found to begin in the boundaries of the adhesive layer, continuously propagating until cohesive failure was reached. Similar results were obtained for a thickness of 1.6 mm.

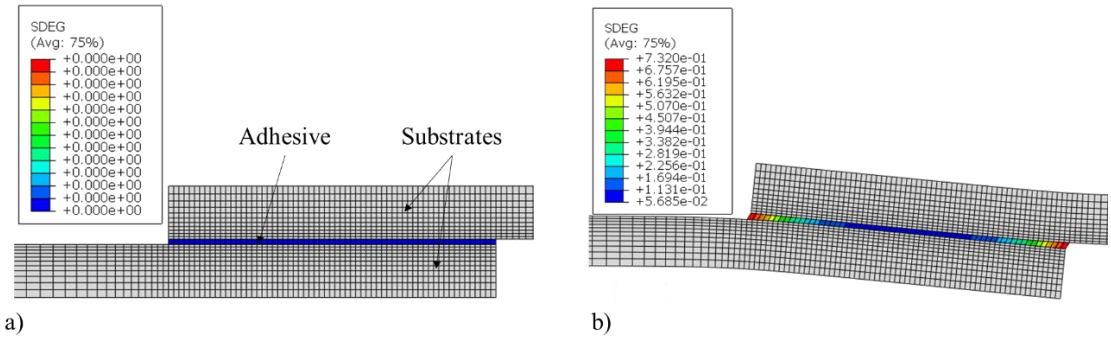

Fig. 14. Adhesive's numerical degradation for a thickness of 0.2 mm at a) the initial and b) an intermediate stage of the quasi-static loading process.

Comparisons between representative experimental load-displacement curves and the numerical results, for both thicknesses, are represented in Fig. 15.

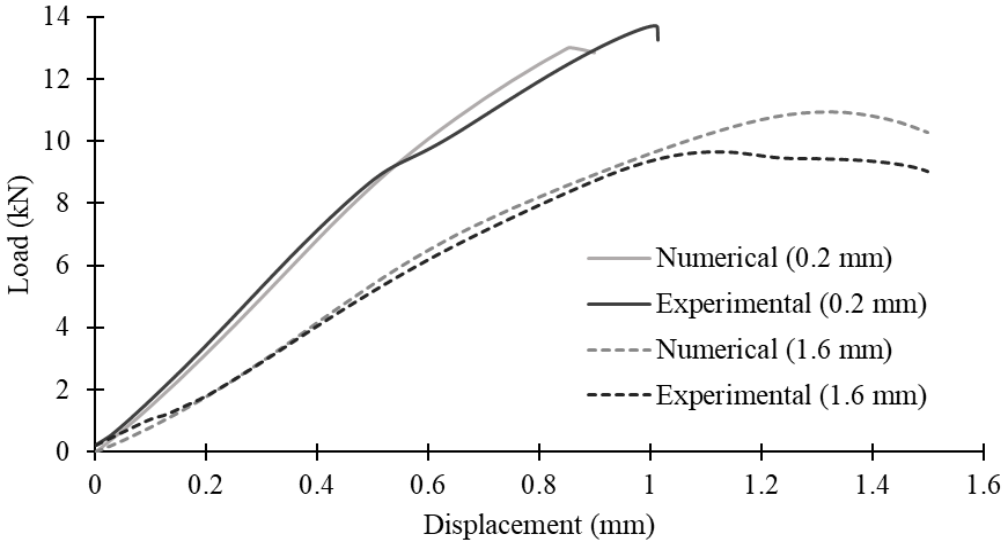

Fig. 15. Typical experimental and numerical load-displacement curves for the two tested adhesive thicknesses under quasi-static conditions.

The numerical curves can be considered to be in good agreement with the experimental data regarding the failure load, especially for a thickness of 0.2 mm. Concerning the 1.6 mm thickness, the prediction is not so accurate, but still reasonably good. This phenomenon can be explained by the higher susceptibility of the much thicker 1.6 mm joints to manufacturing defects, such as voids, leading to experimental failure loads lower than those expected by the FE models, where perfect material is assumed to exist. For a thickness of 0.2 mm, the experimental results show a slightly higher failure load than that predicted by the numerical analysis, which may be due to the intrinsic variation associated with the adhesive properties introduced in the model. The results

revealed that an increase in the adhesive thickness lead to a decrease in the failure load of the joint, as a better value was found for 0.2 mm. This observation is in accordance with the results obtained by Goglio et al. [30], when testing lap shear steel joints with an epoxy adhesive thickness of 0.5 and 1 mm, and by Banea et al. [31], when analysing SLJs with hard steel substrates bonded with a structural polyurethane adhesive with thicknesses ranging from 0.2 to 2 mm.

The complete results for the quasi-static loading can be found in Table 4, with the total absorbed energy being calculated as the area below the curves. Although they present worse results regarding the failure load, the joints with an adhesive thickness of 1.6 mm provide better energy absorption capabilities when compared to a thickness of 0.2 mm. Although larger bondline thicknesses are preferred in adhesively bonded automotive structures due to their better capability to deal with geometrical deviations in the substrates, they are also able to provide benefits to the mechanical behaviour. The strength, the energy absorption or a compromise between both can be the most important factor according to the application, being the adhesive thickness adjusted to fulfil the desired requirements.

Table 4. Failure load and energy absorption results for an adhesive thickness of 0.2 and 1.6 mm.

	0.2 mm		**1.6 mm**	
	Experimental	**Numerical**	**Experimental**	**Numerical**
Failure load (kN)	13.39 ± 0.36	13.03	9.20 ± 0.49	10.94
Absorbed energy (J)	8.64 ± 0.55	5.98	12.19 ± 3.02	13.14

4.1.2. 0.1 m/s testing

The failure surfaces for the 0.1 m/s condition are shown in Fig. 16, where it is possible to conclude that cohesive failure in the adhesive occurred also for this case. Regardless the thickness, the degradation process of the adhesive layer, obtained numerically, was found once again to initiate on its ends. Fig. 17 presents the SDEG parameter, now for the thickness of 1.6 mm.

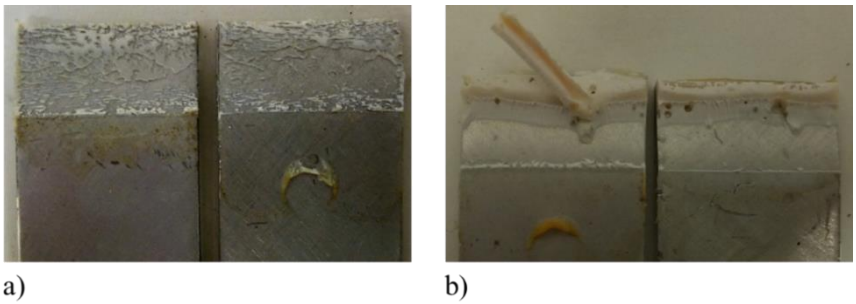

Fig. 16. Cohesive failure in the adhesive verified at 0.1 m/s: a) 0.2 mm and b) 1.6 mm adhesive thickness.

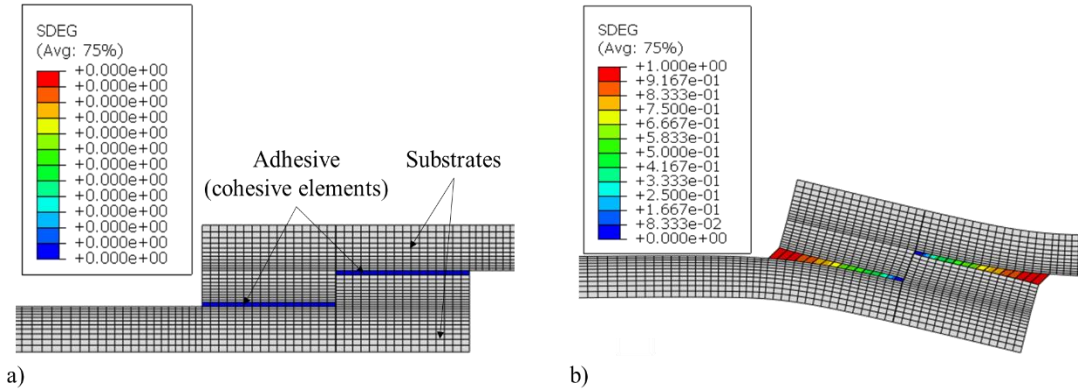

Fig. 17. Adhesive's numerical degradation for an adhesive thickness of 1.6 mm, at 0.1 m/s: a) initial and b) failure-imminent moments.

Fig. 18 shows the load-displacement evolutions (with representative experimental curves), where it is possible to conclude that the numerical results accurately predict the experimental data for both thicknesses.

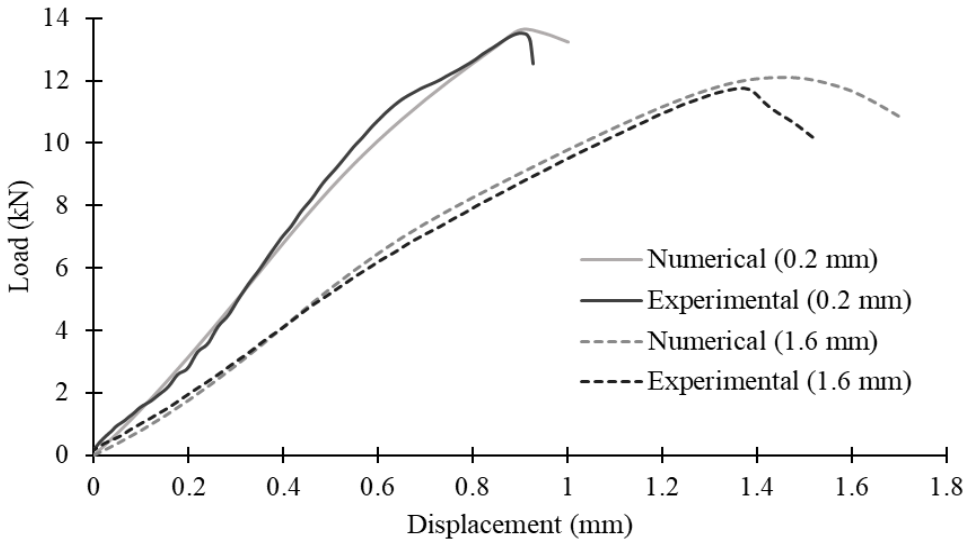

Fig. 18. Experimental and numerical load-displacement evolutions for both thicknesses at 0.1 m/s.

Also, for a displacement rate of 0.1 m/s, and in accordance with the quasi-static results, a higher joint strength and energy absorption were found for the lowest and highest thickness, respectively (Table 5).

Table 5. Summary of the failure load and energy absorption results obtained at 0.1 m/s.

	0.2 mm		**1.6 mm**	
	Experimental	**Numerical**	**Experimental**	**Numerical**
Failure load (kN)	13.99 ± 0.75	13.62	11.10 ± 0.86	12.12
Absorbed energy (J)	8.93 ± 3.13	6.58	14.60 ± 3.03	14.78

4.1.4. Displacement rate dependence

The SLJs strength appears to increase with the displacement rate for both adhesive layer thicknesses (Fig. 19), being the rise more pronounced for 1.6 mm. A similar conclusion was reached by Machado et al. [6] and [32] when testing joints composed of carbon-fibre reinforced plastic (CFRP) and AA6060-T6 alloy substrates, respectively, bonded with the same crash-resistant adhesive at RT.

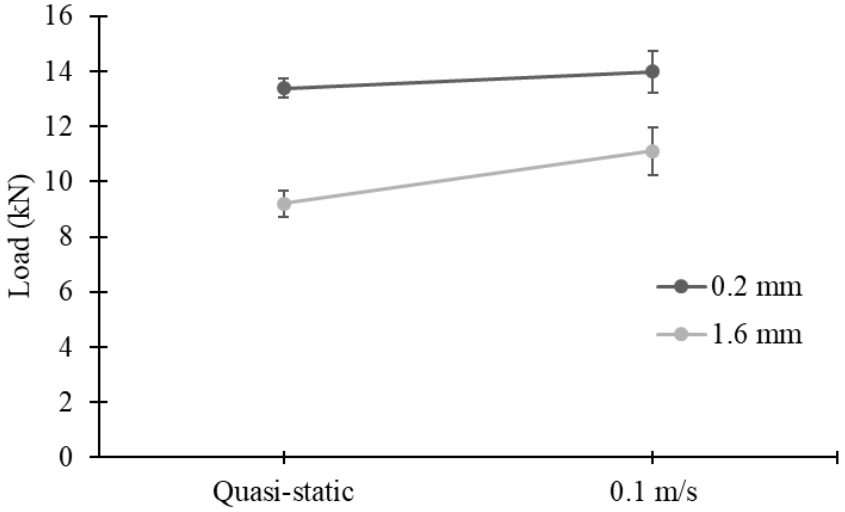

Fig. 19. Comparison of the average values and standard deviation of the failure load results for both adhesive thicknesses tested at quasi-static (1 mm/min) and 0.1 m/s conditions.

4.2. Automotive structure (front header): experimental and numerical analysis

When subjected to the quasi-static load, the two automotive specimens failed due to the high stress concentration around the central holes, which led to the initiation and propagation of a crack (Fig. 20). For this reason, it can be concluded that the behaviour

of the structure was ruled by the aluminium substrates, and that the adhesive used to bond them did not compromise structure's integrity. This can be observed by the shape of the representative experimental and numerical load-displacement curves (Fig. 21), which follow a typical elastic-plastic behaviour of aluminium. From the crack initiation moment forward, the load capacity of the front header abruptly decreases, being its total strength considerably low.

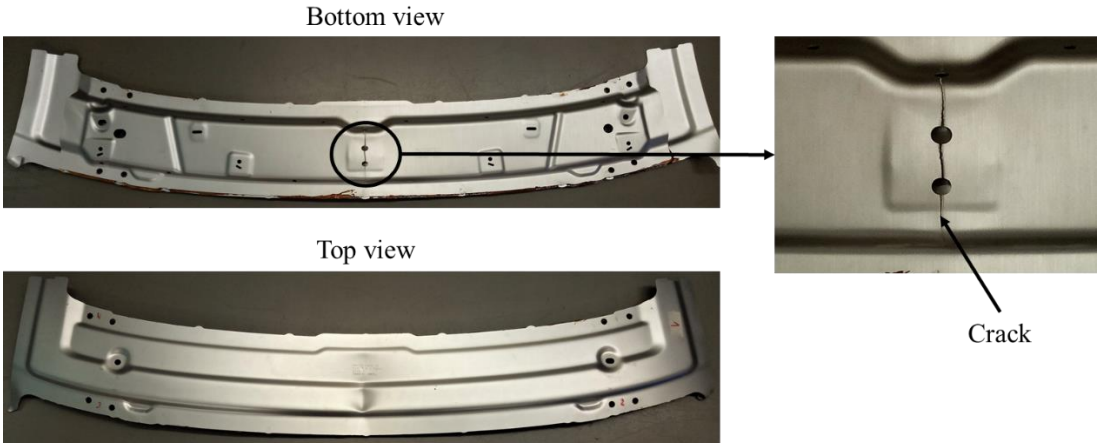

Fig. 20. Failure verified in both specimens at quasi-static conditions.

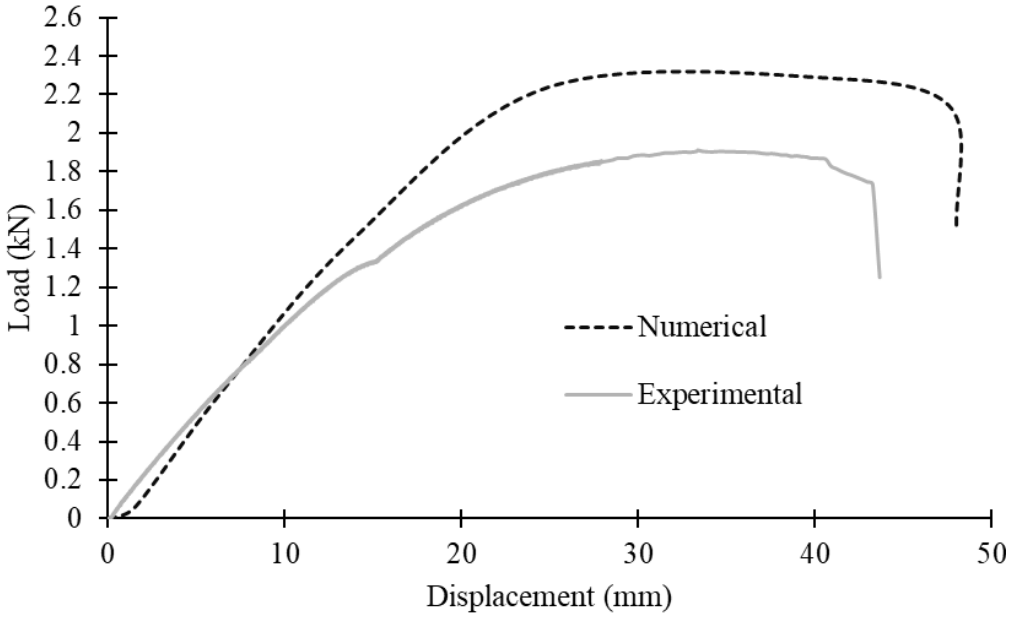

Fig. 21. Experimental and numerical results obtained for the quasi-static loading.

Since no information regarding the damage evolution of the aluminium substrates was available, the numerical analysis results were only considered until the moment when the ultimate stress of the aluminium was reached (shown in Fig. 4). The numerical model

shows relatively good results regarding the failure load prediction, but the displacement values are not as satisfactory, which can be due to the boundary conditions imposed to the structure. As mentioned before, encastre boundary conditions were applied to the ends of the component in the numerical analysis, something that is not exactly replied in the experimental procedures. Therefore, the specimens mounted in the assembly are less stiff than the model and can slightly move during the tests, leading to higher displacements. So that this effect could be compensated, the stiffness of the model in Fig. 21 was adjusted to the observations to better compare the results.

The numerical and experimental results regarding the failure load and the absorbed energy are shown in Table 6. The failure load predicted by the numerical model is slightly higher than the one observed in the experiments, which is usual as eventual manufacturing deviations and defects in both adhesive and aluminium substrates are not considered in the FE analysis.

Table 6. Failure load and absorbed energy of the automotive structure at quasi-static conditions.

	Experimental	**Numerical**
Failure load (kN)	1.78 ± 0.19	2.28
Absorbed energy (J)	60.23 ± 2.55	81.74

4.3. Influence of the adhesive system on the automotive structure response

Considering the failure mechanism observed in the automotive structure bonded with the crash-resistant epoxy, a new adhesive system was considered to join the aluminium substrates, namely a two-component, high-performance structural polyurethane with the reference SikaForce®-7818 L7, supplied by Sika®. The aim of this study was to determine the influence of the type of adhesive on the behaviour of the component. The general mechanical properties of this adhesive, given by the manufacturer, are shown in Table 7. For this case, only one specimen was manufactured and tested. The manufacturing process was the same as the one previously presented, excepting for the curing cycle. In opposition to the epoxy system that requires high curing temperatures, the polyurethane cures at RT by chemical reaction of the two components.

Table 7. General properties of the structural polyurethane adhesive.

Properties	
Density [kg/m^3]	1230
Tensile strength [MPa]	35
Young's modulus [MPa]	2500
Tensile lap-shear strength [MPa]	20
Elongation at break [%]	2.5
Glass transition temperature [°C]	45

Fig. 22 represents the experimental load-displacement curves for the specimens bonded with both adhesives, with a representative curve being used for the crash-resistant epoxy.

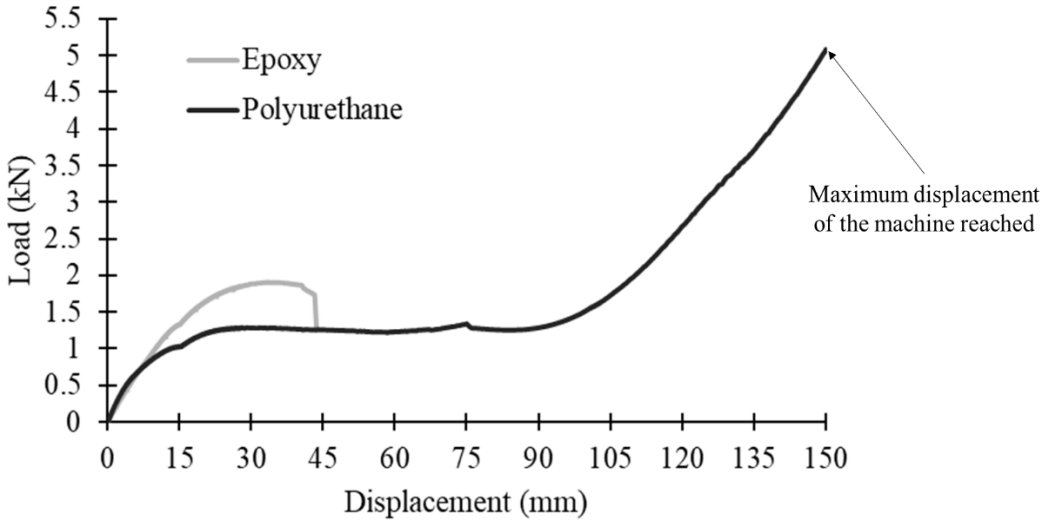

Fig. 22. Load-displacement curves for the automotive structure bonded with a crash-resistant epoxy and a high-performance polyurethane for quasi-static conditions.

When the automotive specimen was bonded with the structural polyurethane, no crack was found in the lower substrate (Fig. 23). The total strength of the component for this case was not found, as the maximum displacement that the universal testing machine is able to provide was reached before the failure load was verified. Although being weaker, the polyurethane is more flexible than the crash-resistant adhesive, absorbing more energy and transferring less load to the lower substrate, preventing its fracture. Therefore, in the context of a joint, the polyurethane adhesive seems to be more advantageous. Table 8 resumes the results of the specimens bonded with the two adhesives under quasi-static conditions.

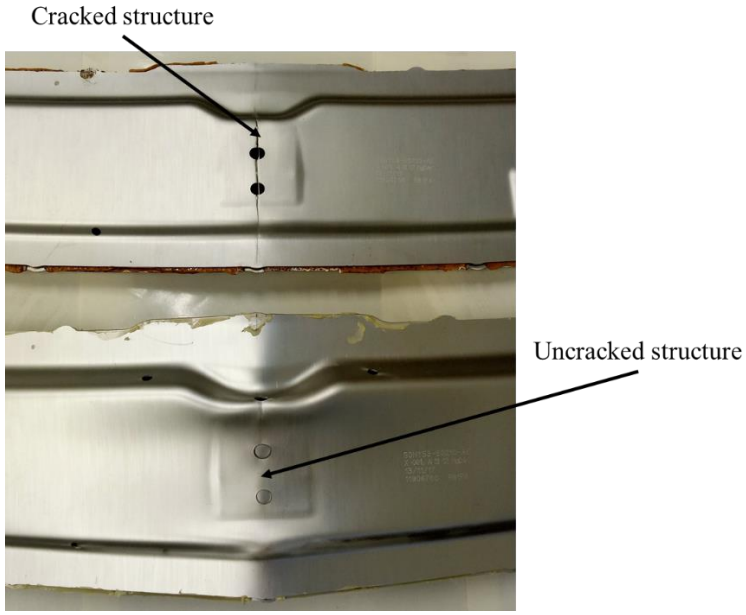

Fig. 23. Cracked and uncracked specimens, bonded with the crash-resistant epoxy and the structural polyurethane adhesive, respectively.

Table 8. Results of the automotive structure bonded with the two adhesive systems.

	Epoxy	**Polyurethane**
Failure load (kN)	1.78 ± 0.19	Not reached
Absorbed energy (J)	60.23 ± 2.55	(271.95)*

*Until the moment when the maximum displacement was reached and the test stopped

5. Conclusions

The main purpose of this work was to study the behaviour of an adhesively bonded automotive structure under quasi-static conditions, showing the applicability of adhesive bonding in real automotive applications. The tests, conducted at RT, revealed premature failure of the structure due to a crack initiation and propagation around the middle holes of the lower substrate, proving that the integrity of the component is ruled by the behaviour of the aluminium substrates. Therefore, it can be concluded that the crash-resistant adhesive was successfully capable of bonding the structure and transfer the loads to the aluminium adherends, being suited for automotive applications. The numerical simulation carried out in ABAQUS® was able to correctly predict the failure load of the structure, but the obtained displacement was not as precise. This can be explained by difficulty in accurately reproducing the boundary conditions experimentally applied to the specimens. While in the numerical model, where perfect conditions are considered,

the specimens were guaranteed not to move on their ends, in the experimental tests this was not exactly accomplished, leading to higher displacements. In order to verify if the aluminium fracture could be avoided, a high-performance polyurethane was used to bond the automotive structure as an alternative to the epoxy system. The specimen bonded with the polyurethane behaved better than those bonded with the epoxy, as the former adhesive is more ductile than the last, transferring less energy to the lower substrate and preventing its fracture.

The analysis of the SLJs, composed by similar aluminium substrates bonded with two different thicknesses of the same epoxy adhesive, showed that an increase in the adhesive thickness is followed by a decrease in the joint strength for the two tested conditions. However, the higher thickness led to an increase in the energy absorption capabilities. Additionally, as the displacement rate applied to the joints increased, the failure load was found to present higher values, for both thicknesses. The FE analysis carried out in ABAQUS® showed good accordance with the experimental data for the two loading conditions.

Acknowledgments

The authors gratefully acknowledge the funding provided by Project NORTE-01-0145-FEDER-000022 - SciTech - Science and Technology for Competitive and Sustainable Industries, co-financed by Programa Operacional Regional do Norte (NORTE2020), through Fundo Europeu de Desenvolvimento Regional (FEDER), and by PhD grant SFRH/BD/139341/2018 “Impact strength optimization with cohesive zone elements of multi-material bonded structures used in the automotive industry”, Project Nº 028473 POCI-01-0145-FEDER-028473 “Design methodology for impact resistant bonded multi-material automotive structures (ImpactBondDesign)”. The authors would also like to thank Nagase ChemteX® for the financial support provided, as well to Aston Martin Lagonda Limited® for supplying the aluminium substrates.

References

1. Barnes, T.A. and I.R. Pashby, *Joining techniques for aluminium spaceframes used in automobiles: Part II — adhesive bonding and mechanical fasteners.* Journal of Materials Processing Technology, 2000. **99**(1): p. 72-79.
2. Brooks, R., S.M. Shanmuga Ramanan, and S. Arun, *Composites in Automotive Applications: Design*, in *Reference Module in Materials Science and Materials Engineering*. 2017, Elsevier.
3. Beardmore, P. and C.F. Johnson, *The potential for composites in structural automotive applications.* Composites Science and Technology, 1986. **26**(4): p. 251-281.
4. Miller, W.S., et al., *Recent development in aluminium alloys for the automotive industry.* Materials Science and Engineering: A, 2000. **280**(1): p. 37-49.
5. Hirsch, J., *Recent development in aluminium for automotive applications.* Transactions of Nonferrous Metals Society of China, 2014. **24**(7): p. 1995-2002.
6. Machado, J.J.M., et al., *Adhesive joints using aluminium and CFRP substrates tested at low and high temperatures under quasi-static and impact conditions for the automotive industry.* Composites Part B: Engineering, 2019. **158**: p. 102-116.
7. C England, J., et al., *Design of Automotive Metal and Composite Chassis Structures.* Recent Patents on Mechanical Engineering, 2010. **3**(3): p. 211-225.
8. Galvez, P., et al., *Study of the behaviour of adhesive joints of steel with CFRP for its application in bus structures.* Composites Part B: Engineering, 2017. **129**: p. 41-46.
9. Borsellino, C., G. Di Bella, and V. Ruisi, *Adhesive joining of aluminium AA6082: The effects of resin and surface treatment.* International Journal of Adhesion and Adhesives, 2009. **29**(1): p. 36-44.
10. Costa, A.P.d., et al., *A Review of Welding Technologies for Thermoplastic Composites in Aerospace Applications.* Journal of Aerospace Technology and Management, 2012. **4**: p. 255-265.
11. Grujicic, M., et al., *An overview of the polymer-to-metal direct-adhesion hybrid technologies for load-bearing automotive components.* Journal of Materials Processing Technology, 2008. **197**(1-3): p. 363-373.

12. J. J. M. Machado, A.H., P. D. P. Nunes, E. A. S. Marques, R. J. C. Carbas, C. Sato, L. F. M. da Silva, *Strain rate dependence of a crash resistant adhesive as a function of temperature for the automotive industry.* 2018.
13. Banea, M.D., et al., *Effects of Temperature and Loading Rate on the Mechanical Properties of a High Temperature Epoxy Adhesive.* Journal of Adhesion Science and Technology, 2011. **25**(18): p. 2461-2474.
14. Bezemer, A.A., C.B. Guyt, and A. Vlot, *New impact specimen for adhesives: optimization of high-speed-loaded adhesive joints.* International Journal of Adhesion and Adhesives, 1998. **18**(4): p. 255-260.
15. Saldanha, D.F.S., et al., *Mechanical characterization of a high elongation and high toughness epoxy adhesive.* International Journal of Adhesion and Adhesives, 2013. **47**: p. 91-98.
16. Silva, L.F.M., A. Öchsner, and R. Adams, *Handbook of Adhesion Technology*. 2011. p. 1-7.
17. Neto, R.C., E. Sampaio, and J. Assis, *Numerical and experimental analysis of bonded joints with combined loading.* International Journal of Adhesion and Adhesives, 2019. **90**: p. 61-70.
18. Machado, J.J.M., et al., *Numerical study of impact behaviour of mixed adhesive single lap joints for the automotive industry.* International Journal of Adhesion and Adhesives, 2018. **84**: p. 92-100.
19. da Costa Mattos, H.S., E.M. Sampaio, and A.H. Monteiro, *Static failure analysis of adhesive corner joints.* International Journal of Adhesion and Adhesives, 2013. **47**: p. 110-116.
20. Lahaye, C., et al., *Development of an aluminium prototype bonnet for Saab 9-3*. 1998, SAE Technical Paper.
21. Cheon, S.S., D.G. Lee, and K.S. Jeong, *Composite side-door impact beams for passenger cars.* Composite Structures, 1997. **38**(1): p. 229-239.
22. Araújo, H., et al., *Dynamic behaviour of composite adhesive joints for the automotive industry.* Composite Structures, 2017. **171**: p. 549-561.
23. Yibo, P., et al., *Dynamic Mechanical Behaviors of 6082-T6 Aluminum Alloy.* Advances in Mechanical Engineering, 2013. **5**: p. 878016.
24. Oosterkamp, L.D., A. Ivankovic, and G. Venizelos, *High strain rate properties of selected aluminium alloys.* Materials Science and Engineering: A, 2000. **278**(1-2): p. 225-235.

25. Torca, I., et al., *Tensile Behaviour of 6082 Aluminium Alloy Sheet under Different Conditions of Heat Treatment, Temperature and Strain Rate*. Vol. 423. 2009. 105-112.
26. Chen, Y., et al., *Stress–strain behaviour of aluminium alloys at a wide range of strain rates.* International Journal of Solids and Structures, 2009. **46**(21): p. 3825-3835.
27. Gleich, D.M., M.J.L. Van Tooren, and A. Beukers, *Analysis and evaluation of bondline thickness effects on failure load in adhesively bonded structures.* Journal of Adhesion Science and Technology, 2001. **15**(9): p. 1091-1101.
28. Hillerborg, A., M. Modéer, and P.-E. Petersson, *Analysis of crack formation and crack growth in concrete by means of fracture mechanics and finite elements.* Cement and concrete research, 1976. **6**(6): p. 773-781.
29. Campilho, R.D.S.G., et al., *Modelling adhesive joints with cohesive zone models: effect of the cohesive law shape of the adhesive layer.* International Journal of Adhesion and Adhesives, 2013. **44**: p. 48-56.
30. Goglio, L. and M. Rossetto, *Impact rupture of structural adhesive joints under different stress combinations.* International Journal of Impact Engineering, 2008. **35**(7): p. 635-643.
31. Banea, M., L.F.M. Silva, and R. Campilho, *The Effect of Adhesive Thickness on the Mechanical Behavior of a Structural Polyurethane Adhesive*. Vol. 91. 2014. 331-346.
32. Machado, J., E. Marques, and L. da Silva, *Mechanical behaviour of adhesively bonded composite single lap joints under quasi-static and impact conditions with variation of temperature and overlap.* Journal of Composite Materials, 2018. **52**(26): p. 3621-3635.

Appendix B: Paper 2

Experimental and numerical study of the dynamic response of an adhesively bonded automotive structure

N.D.D. Silva[1], J.J.M. Machado[1], E.A.S. Marques[1], P.M.G.P. Moreira[1], L.F.M. da Silva[2,*]

[1]Instituto de Ciência e Inovação em Engenharia Mecânica e Engenharia Industrial (INEGI), Rua Dr. Roberto Frias, 4200-465 Porto, Portugal

[2]Departamento de Engenharia Mecânica, Faculdade de Engenharia (FEUP), Universidade do Porto, Rua Dr. Roberto Frias, 4200-465 Porto, Portugal

Abstract

Based on economic and environmental factors related to energy efficiency, the automotive industry is being increasingly encouraged to design lighter structures, making use of adhesive bonding in vehicle body frames. To meet the standards of the automotive sector, adhesive joints must provide high strength and stiffness, low cost and good energy absorption at a component level, therefore ensuring good impact strength and passenger safety. This work aims to study, at room temperature (24 ºC), the impact response of a real scale automotive structure bonded with a crash-resistant epoxy, allowing to access the suitability of adhesives for automotive structural purposes. The same component was also analysed through a finite element model, so that the numerical predictions could be compared with experimental data. The epoxy adhesive was found to successfully transfer the loads to the substrates and not to compromise the integrity of the structure, as its failure was dominated by the behaviour of the aluminium. Furthermore, the simulation showed good accordance with the experimental failure load, revealing that numerical analysis can be a viable tool to predict structure's behaviour. Additionally, a polyurethane was used as an alternative to the epoxy system to bond the structure, proving that the joint behaves better in the presence of a more flexible adhesive.

Keywords

Adhesively bonded automotive structure; High-performance crash-resistance adhesive; Aluminium; Impact; Single lap joints

[*] Corresponding author. Tel.: +351 22 508 17 06; fax: +351 22 508 14 45. *E-mail address:* lucas@fe.up.pt (L.F.M. da Silva)

1. Introduction

In an attempt to develop energy-efficient vehicles, the automotive industry has been encouraged to design lightweight structures, making use of low-density materials such as aluminium alloys and composites. Although offering a good compromise between weight and strength, the application of composite materials in large production structural automotive components is still facing some drawbacks. These are mainly caused by some uncertainty related to their long-term performance and by their high material and manufacturing costs [1, 2], which can be prohibitive for some applications. Aluminium alloys represent an economically advantageous solution and its excellent formability and corrosion resistance [3], allied with low weight, turns it particularly suitable for vehicle body frames. The lower strength and stiffness can be successfully compensated with the design of the spaceframe and the use of thicker cross-sections [4], with high strength aluminium alloys being able to satisfy the torsional stiffness requirements of an automotive component [5]. The aluminium alloys most commonly used in vehicle construction belong to the 5xxx and 6xxx series [6]. The former, highly deformable, are mostly used for inner panel applications, while the latter, heat-treatable, are preferred for outer panels [7]. Within the 6xxx series, the AA6016 (Europe) and AA6111 (USA) alloys are frequently used for body structures. The AA6016 alloy is preferred in Europe because it shows a superior formability and corrosion resistance compared to AA6111 [5, 8].

Lighter body frames, however, should not compromise mechanical strength, ensuring the simultaneous fulfilment of the requirements regarding fuel consumption and safety. Load bearing automotive structures must perform well under complex loading situations such as impact, which often leads to an increase in the complexity and manufacturing difficulties [9]. Such factors encouraged the expansion of adhesive bonding in this industry, as this technique is able to tolerate damage, presents low manufacturing costs, allows the reduction of vibrations [10] and lead to an uniform stress distribution in the bonded area, reducing the stress concentration [11] and improving the fatigue behaviour [12, 13]. Several vehicle manufacturers have shown the benefits of adhesive bonding with the production of several concept cars [8, 10]. The 2002 Aston Martin's V12 Vanquish, one of the most technically advanced cars of its time, had a space-frame made of extruded aluminium and adhesive bonding was chosen to join the entire vehicle together [14].

Structural polyurethanes and epoxies represent the most common adhesive systems in the automotive industry. The first are often chosen due to their peel strength, good

fatigue behaviour and high durability [15], while the last are often selected to bond structural automotive components due to their capability to guarantee a strong and stiff bond, as well as joint stability. These epoxy characteristics allowed their application, for instance, in the load carrying components of the Lamborghini's Murcièlago model [16] and in the extruded aluminium sections that shape the chassis of Lotus' Elise and Evora models [2]. However, conventional epoxy adhesives are very brittle and therefore have insufficient energy-absorption properties, leading to reduced shear strength and peel resistance under impact [17, 18]. Toughened, crash-resistant epoxy adhesives have been recently introduced in the market, possessing superior energy absorption capabilities and good strength at high strain rates [19]. The toughening process is usually achieved with the addiction of flexible polymer or rubber particles to epoxy-based formulations. Crash-resistant epoxy adhesives are able to combine high ductility with high strength and stiffness, allowing the absorption of significant amounts of energy in comparison to standard adhesives [12].

Over the years, finite element (FE) analysis has become a viable and accurate tool for prediction the behaviour of structures subjected to a large variety of loading conditions, including impact. This method stands as a complement or even an alternative to experimental procedures, which are sometimes undesirable or impossible to perform. Within the field of adhesive bonding, cohesive zone modelling (CZM) has been used as an add-in to FE to model the behaviour of the adhesive using cohesive elements. This damage mechanics technique, based in energetic concepts, has already been successfully applied to simple joint configurations, such as single lap joints (SLJs) [20] and corner joints [21], providing good results when compared to experimental data.

The test and analysis of real-scale automotive structures, especially of bonded construction, under impact loads is not common in the literature and few examples can be found regarding this matter. Golzar et al. [22] manufactured a prototype of a composite body cover structure to replace steel in an automobile model and a FE study was carried out in ABAQUS® to analyse its behaviour under impact. Although no experimental tests were conducted, a composite body cover with 1.6 mm thickness was found to have higher energy absorption performance in comparison to steel, while allowing a 42% weight saving. The crash behaviour of thin-walled aluminium extrusions, which represent the base of the aluminium space-frame concept, was studied by Langseth et al. [23]. The extrusions were subjected to axial loading conditions and three different configurations were tested, namely non-filled extrusions and aluminium foam-filled extrusions with and

without an epoxy adhesive between the foam and the walls of the extrusion. Results suggested that the presence of the foam filler drastically changes the energy absorption behaviour, with the use of adhesive increasing the mass specific energy absorption. The non-linear finite element simulations conducted in the computer code LS-DYNA® over the AA6060 alloy non-filled extrusions (the only numerical simulations presented) were in accordance with the experimental results. The response of a composite side-door impact beam was studied by Cheon et al. [24], as an alternative to the traditional steel version. The new beam showed higher energy absorption capabilities when subjected to the dynamic load. A similar automotive component was analysed by Li et al. [25] exclusively using a numerical approach with the software LS-DYNA®. The goal was to optimize the design of the beam so that energy absorption could be maximized in a lateral crash accident. The results of the new beam design showed improvements of 18% in the impact energy absorption and 14% in the impact load peak.

The work developed in this article aims to analyse the impact behaviour of a full-scale, adhesively bonded automotive structure, by numerical and experimental approaches. The behaviour of the joint was predicted using a FE model with CZM being applied in the crash-resistant epoxy adhesive. The mechanical properties of the epoxy that allowed the construction of the cohesive law were determined in previous works [26, 27]. The experimental tests were conducted at room temperature (RT) and with an impact velocity of 3 m/s. Furthermore, a polyurethane adhesive was also considered to bond the component, so that the influence of the adhesive type on the behaviour of the structure could be analysed. As a complement, the dynamic response (at 3 m/s) of SLJs bonded with two adhesive layer thicknesses, namely 0.2 and 1.6 mm, was studied to evaluate the effect of this parameter on the behaviour of the joints.

2. Experimental details

2.1. SLJ

2.1.1. Material and properties

The SLJ specimens tested in the context of this work consisted of similar substrates of an aluminium alloy bonded with a crash-resistant, highly ductile one-component epoxy adhesive, well suited for impact loads.

2.1.1.1. Aluminium

The initial research plan was to use the AA6016-T4 aluminium alloy for the substrates of the SLJs, as this represents the material used in the substrates of the automotive structure. Unfortunately, this was not possible due to difficulty in obtaining this specific alloy. The contacted aluminium manufacturers only supply this material in industrial quantities, not compatible with those desired for this project. Additionally, its storage in a naturally aged temper (T4) is not common, as prolonged exposure to environmental agents often leads to the degradation of this treatment.

In the presence of this information, the AA6082-T6 aluminium alloy was selected for this purpose as alternative, due to its reasonably identical general mechanical properties (Table 1) and easier obtainment in the market.

The strain rate sensitivity of AA6082-T6 was reported in the literature to be low at RT [28-31]. Yibo et al. [31] studied its plastic behaviour for quasi-static to moderate strain rates (0.001-100 s^{-1}) and noticed a slightly increase in yield and tensile strengths within this range. Therefore, the considered plastic behaviour of AA6082-T6 under impact was adapted from his work and is represented Fig. 1.

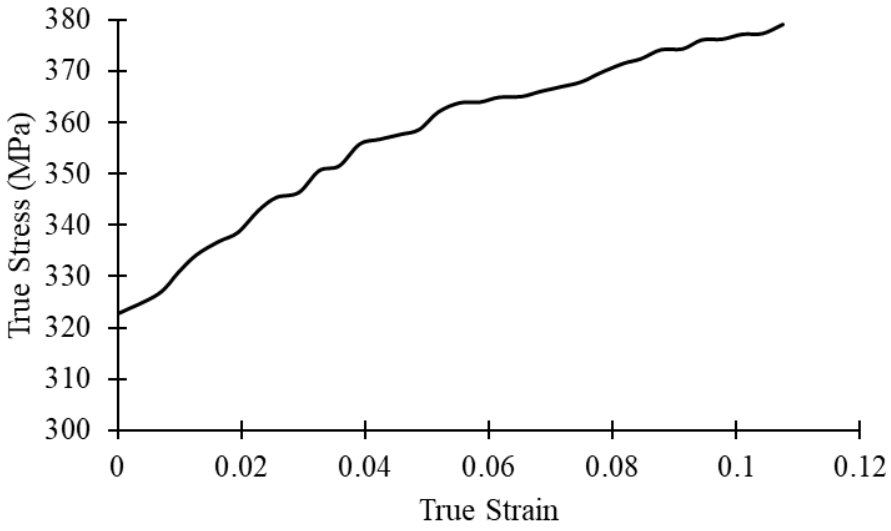

Fig. 1. Plastic behaviour of AA6082-T6 under impact (adapted from [31]).

Table 1. General mechanical properties of the AA6082-T6 aluminium alloy.

Properties	
Density, ρ [kg/m^3]	2700
Young's modulus, E [MPa]	69000
Shear modulus, G [MPa]	26000
Poisson's ratio, ν	0.33
Tensile strength, σ_n [MPa]	360
Yield strength, σ_y [MPa]	310
Shear strength, τ [MPa]	220
Elongation at break, ε [%]	9.8

2.1.1.2. Adhesive

The aluminium substrates in the SLJs specimens were bonded with the same crash-resistant epoxy adhesive applied in the automotive component, with the reference XNR6852 E-3, supplied by Nagase ChemteX®. Aside from high mechanical strength, a crash-resistant adhesive should also support significant plastic deformation before failure, allowing the structure to remain bonded and transferring the load to the metallic substrates, leading to large absorption of energy and ensuring the safety of the structure in a crash situation.

The mechanical properties of this adhesive at RT under impact condition (3 m/s) were already determined by Machado et al. [26] and Araújo et al. [27], being summarized in Table 2. Its density was considered to be 1550 kg/m^3.

Table 2. Mechanical properties of XNR6852 E-3 adhesive.

Properties	**Impact (3 m/s)**
Glass transition temperature, T_g [°C]	132
Cohesive tensile strength, t_n^0 [MPa]	72
Young's modulus, E [MPa]	3667
Cohesive shear strength, t_s^0 [MPa]	43
Shear modulus, G [MPa]	603
Critical strain energy release rate in mode I, G_{IC} [N/mm]	13.3
Critical strain energy release rate in mode II, G_{IIC} [N/mm]	64

2.1.2. Fabrication and testing

Aluminium adherends with a thickness of 2 mm were used in the SLJs, due to the proximity of this value with the thickness of the automotive structure substrates. An overlap length of 12.5 mm was applied to avoid plasticity of aluminium and ensure failure in the bonded region, as the adhesive presents high ductility. With the goal of analysing the influence of the adhesive layer thickness on the response of the joints, two configurations were produced, with thicknesses of 0.2 and 1.6 mm. The last value was chosen because it corresponds to the approximate thickness of the adhesive in the automotive component, while the first is commonly used in the study of SLJs [32].

The specimens were initially drilled and the adherends anodised using phosphoric acid anodizing. The purpose of this superficial treatment was to improve the adhesion between the aluminium and the adhesive, in an attempt to avoid interfacial failure. So that thermal expansion differentials between the joints and the mould could be minimized, an aluminium mould was used to manufacture the joints. Pins were applied to ensure the correct alignments of the joints and spacers, with a length of 77.5 mm, were positioned into the mould assembly to obtain the desired overlap length of 12.5 mm. Tapes with calibrated thicknesses were selected to ensure the correct thickness of the adhesive. Its application was achieved using a spatula for an adhesive thickness of 0.2 mm and using a pressure gun for the 1.6 mm thickness, so that voids inside the adhesive layer could be avoided. Finally, the mould assembly was introduced in a hot plate press to perform the curing cycle of this epoxy, set as 4h at 165 °C by the manufacturer.

An in-house developed drop-weight testing machine was used to perform the impact tests. In this device, the specimen is assembled in a grip and a mass is dropped from a certain height, impacting the lower section of the grip and loading the specimen in tension-shear. The impact velocity (V) is controlled by the drop height (H), making use of the energy conservation principle:

$$V = \sqrt{2gH} \tag{1}$$

where g is the acceleration of gravity. For these impact tests, a mass of 26 kg and an impact velocity of 3 m/s were defined, providing an impact energy of 117 J. At least three specimens (which dimensions are shown in Fig. 2) were tested for each configuration.

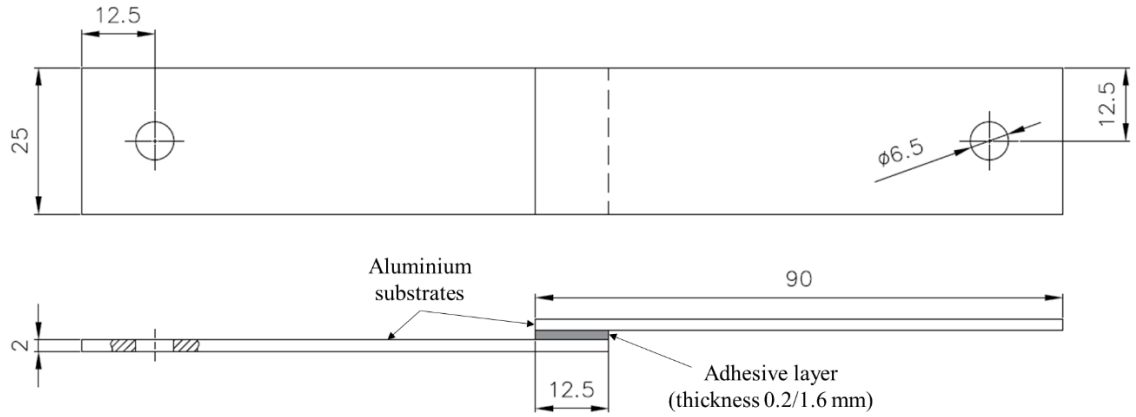

Fig. 2. Configuration and dimensions of the manufactured SLJs.

2.2. Automotive structure (front header)

The location of the adhesively bonded automotive component in the body structure of the vehicle is shown in Fig. 3.

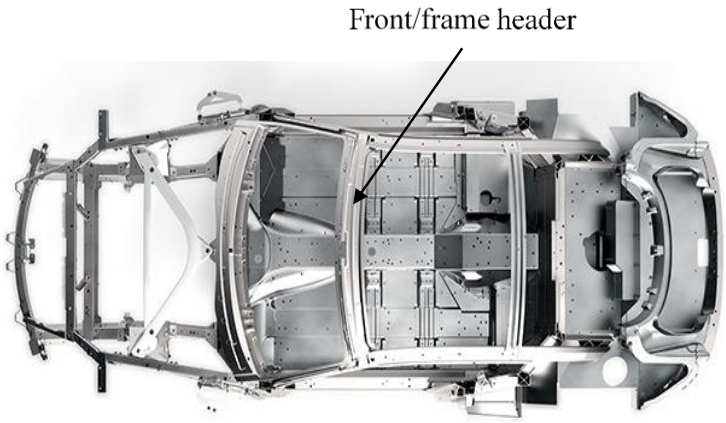

Fig. 3. Automotive front header in the body frame of the Aston Martin's DB11.

2.2.1. Material and properties

2.2.1.1. Aluminium

The adhesively bonded automotive structure, often named as front header, was manufactured with AA6016-T4 substrates, which were already provided in an anodised state. In terms of mechanical behaviour, this alloy was referred by the supplier to become close to the AA6016-T6 alloy after the structure being subjected to the curing cycle of the adhesive. Therefore, the properties of both alloys are represented in Table 3, being the plastic behaviour of the substrates in the final stage of manufacture shown in Fig. 4.

Table 3. General mechanical properties of the AA6016-T4 and AA6016-T6 aluminium alloys.

Properties	**AA6016-T4**	**AA6016-T6**
Density, ρ [kg/m^3]	2700	2700
Young's modulus, E [MPa]	69000	69000
Shear modulus, G [MPa]	26000	26000
Poisson's ratio, ν	0.33	0.33
Tensile strength, σ_n [MPa]	200	280
Yield strength, σ_y [MPa]	110	210
Shear strength, τ [MPa]	130	170
Elongation at break, ε [%]	27	11

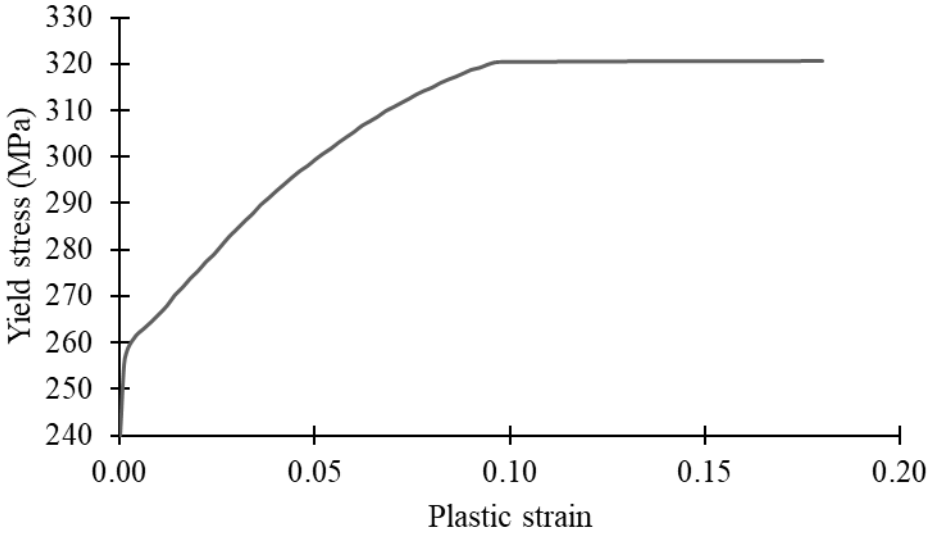

Fig. 4. Plastic behaviour of AA6016-T6, used as substrates in the automotive structure.

2.2.1.2. Adhesive

The XNR6852 E-3 adhesive was initially chosen to bond the structure, due to its crash resistance and high energy absorption capabilities. Its properties under impact were already introduced in Table 2.

2.2.2. Fabrication and testing

To ensure a good adhesion with the adhesive and remove undesirable particles on its surfaces, the aluminium substrates were initially cleaned with isopropanol alcohol. A total of 14 spacers, constructed by assembling layers of calibrated tape, were joined to the edges of the lower substrate to guarantee the thickness of the adhesive bead, which

dimensions were set as approximately 17 mm wide and 1.6 mm thick throughout the bondlines. The locations of these spacers were chosen in order to disturb the adhesive the least as possible. For each specimen, about 70 g of adhesive were applied in both sides of the lower substrate, using a pressure gun. The next steps consisted in assembling the upper substrate on the top of the lower substrate and positioning clamps in the locations of the spacers to restrain the structure and apply pressure. The manufacturing process was completed by placing the whole structure in an oven to perform the curing cycle of the adhesive. A resume of all the described steps is represented in Fig. 5.

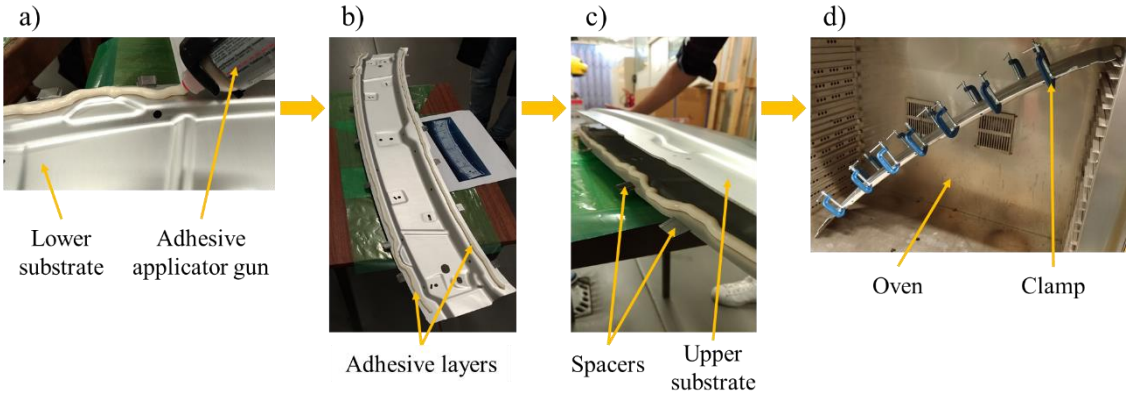

Fig. 5. Steps in the manufacturing of the automotive structure: a) adhesive application using a pressure gun; b) adhesive layers on the top of the lower substrate; c) assembling of the upper substrate; d) structure with clamps inside the oven, to perform the curing cycle of the adhesive.

A drop-weight testing machine was used to conduct the impact tests, with an impact mass and velocity of 30 kg and 3 m/s, respectively, providing an impact energy of 135 J. The contact with the structure was made by an impactor, as presented in the configuration of Fig. 6. The fixation of the automotive component in the structural support, designed for this purpose, was accomplished by a total of eight typical screw-nut connections. The impact load was recorded by the machine, while the vertical displacement was measured with a high-speed video camera. Two automotive structures were tested at this condition.

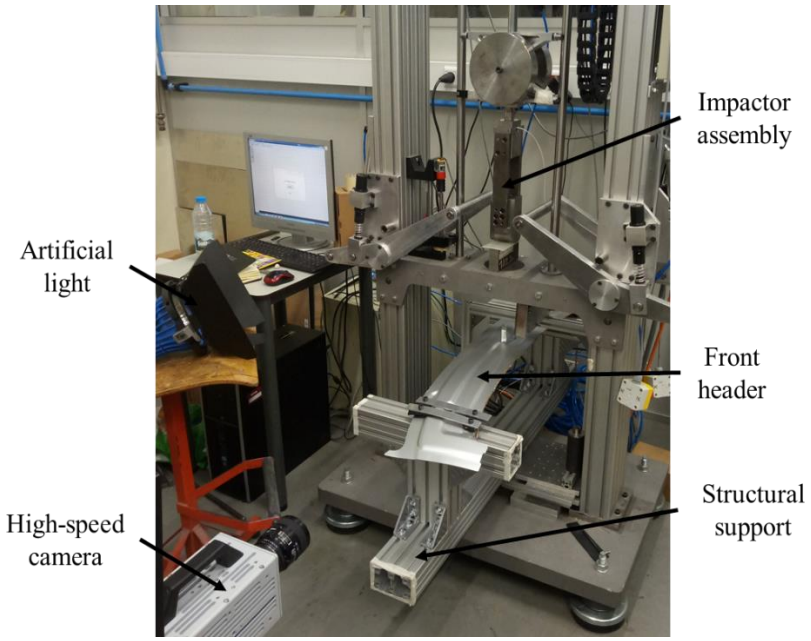

Fig. 6. Testing configuration for the impact load.

3. Numerical details

The numerical models using CZM have been increasingly used in the prediction of adhesive joints behaviour, as they represent an accurate tool and serve as an alternative or complement to experimental procedures. This method is able to simulate damage growth, and therefore determine the strength of a joint, by using energetic principles and parameters, combining concepts of elasticity and fracture mechanics.

Traction-separation laws are constructed to model the behaviour of the cohesive elements that simulate the adhesive, by establishing a relation between stresses and displacements throughout the process [27]. Of all common shapes of these laws (triangular, trapezoidal and exponential), the triangular shape (Fig. 7) is often preferred, as it is the simplest, tends to present less convergence problems and is readily implemented in most FE software [33].

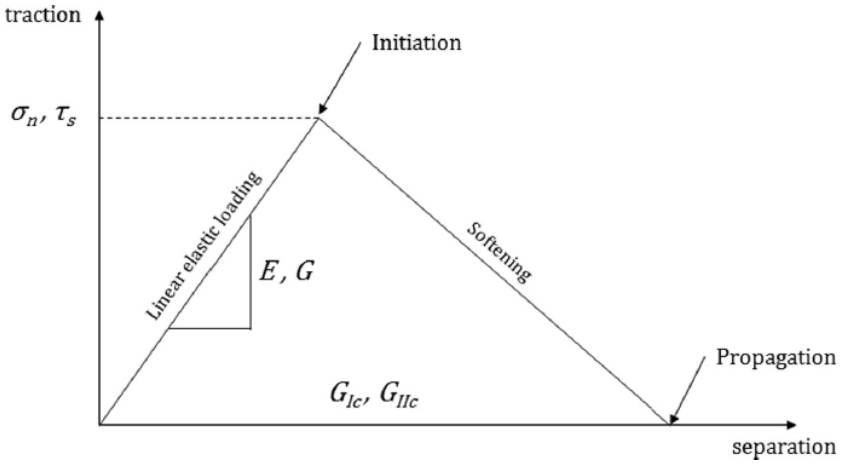

Fig. 7. Traction-separation law with a triangular shape for mode I, mode II [27].

For the construction and implementation of these laws, the mechanical properties of the adhesive in study are needed, according to the type of the loading condition. Thus, the values of the cohesive tensile strength (σ_n)/cohesive shear strength (τ_s), Young's modulus (E)/shear modulus (G) and critical strain energy release rate in mode I (G_{IC})/critical strain energy release rate in mode II (G_{IIC}) are required for mode I/mode II loading conditions, respectively.

3.1. SLJ

The numerical analysis of the SLJs under impact was carried out in ABAQUS® software package. A two-dimensional (2D) geometry was considered due to the simplicity of the joint configuration and reduced computational time, without prejudice of the results. The properties of the adhesive and aluminium at this condition were used, as well as material densities. A movement restriction in both in-plane directions was applied to one end of the joint, while in the opposite end a restriction was made regarding the vertical movement only. To model the dropped mass and the impact velocity, a new geometrical feature with a mass of 26 kg was added to the SLJ configuration and subjected to a boundary condition that specified its initial velocity as 3 m/s (Fig. 8).

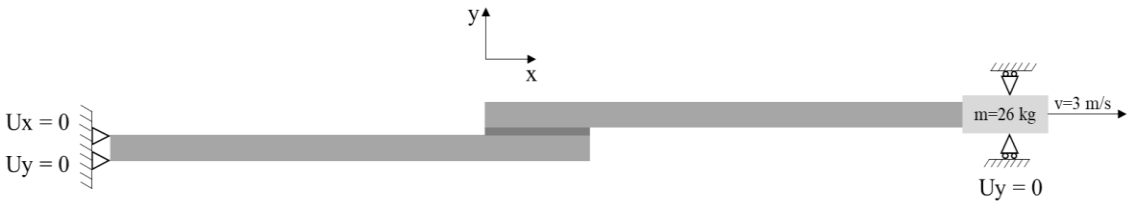

Fig. 8. Boundary conditions applied to the SLJs model.

So that a good compromise between the accuracy of the results and computational time could be achieved, different mesh refinements were created in the most critical regions using the bias functionality, with explicit, 4-node bilinear plain strain quadrilateral elements (CPE4R in ABAQUS® nomenclature) being applied to the adherends and explicit, 4-node two-dimensional cohesive elements (COH2D4 in ABAQUS® nomenclature) being used in the adhesive. A triangular law, shown in Fig. 9, was used to model the cohesive elements.

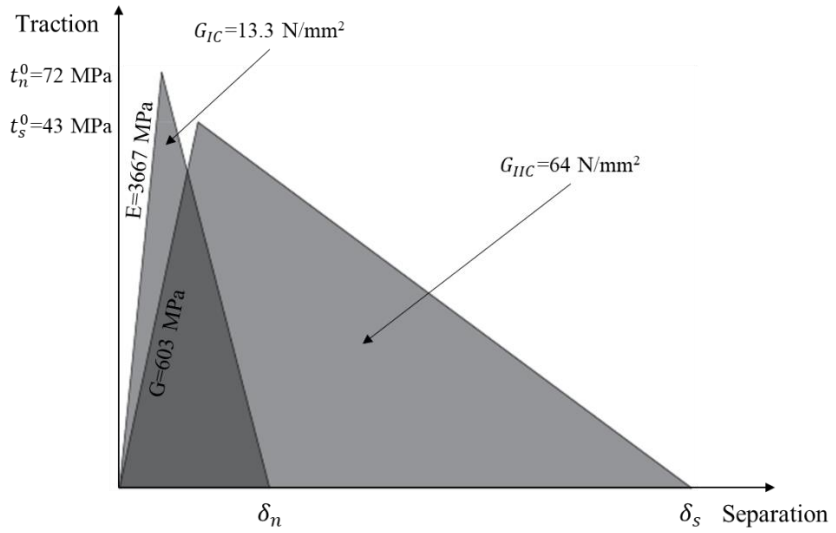

Fig. 9. CZM's traction-separation law for impact conditions.

While a single layer of cohesive elements was applied to model the adhesive region for a thickness of 0.2 mm, a different design was considered for the 1.6 mm thickness (Fig. 10). For this case, intercalated layers of cohesive and plain strain elements were used, with the elastic properties of the adhesive being attributed to the elastic areas. This new configuration was applied instead because better results were achieved regarding the failure load prediction, as the failure process is replicated more accurately. A dynamic, explicit step was selected to solve the model and the SDEG parameter, that shows the adhesive degradation along the process, the reaction forces in the bi-restrained end and the displacement in the end where the solicitation was applied were requested as outputs, in order to construct the load-displacement curve.

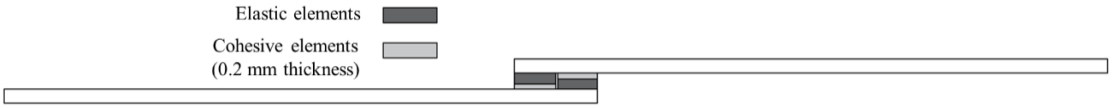

Fig. 10. Adhesive layer configuration used to model the behaviour of the SLJ with an adhesive thickness of 1.6 mm, with cohesive and plain strain elements being applied.

3.2. Automotive structure (front header)

The FE analysis of the front header was also conducted in ABAQUS®, with the mesh and geometry being imported from the HYPERMESH® software package. The properties under impact and material densities were applied and solid elements were assigned to both substrates and adhesive. Therefore, explicit, 8-node 3D cohesive elements (COH3D8 in ABAQUS® nomenclature) were assigned to the adhesive layers, while explicit, 8-node linear 3D stress elements (C3D8R in ABAQUS® nomenclature) were applied to the upper and lower aluminium substrates, with a thickness of 1.7 and 1.2 mm, respectively. Due to the complex geometry of the frame, explicit, 6-node linear triangular 3D stress elements (C3D6 in ABAQUS® nomenclature) were used to complement the mesh in the adherends. Encastre boundary conditions were given to the ends of the automotive structure to simulate the experimental procedure (Fig. 11) and the impactor, which was only allowed to move vertically, was modelled as a rigid body, since its stress state was not of interest. As the total mass and impact velocity of the dropping structure in the experimental tests were 30 kg and 3 m/s, respectively, these mass parameters were attributed to the impactor body. An interaction between the impactor and the structure was created to avoid penetration and ensure the correct contact between the two bodies, with a normal behaviour of the type "Hard contact" and a tangential behaviour with friction coefficient of 0.61. A dynamic, explicit step was used to run the model and the SDEG, the reaction forces at the restricted zones and the impactor's displacement were requested as outputs.

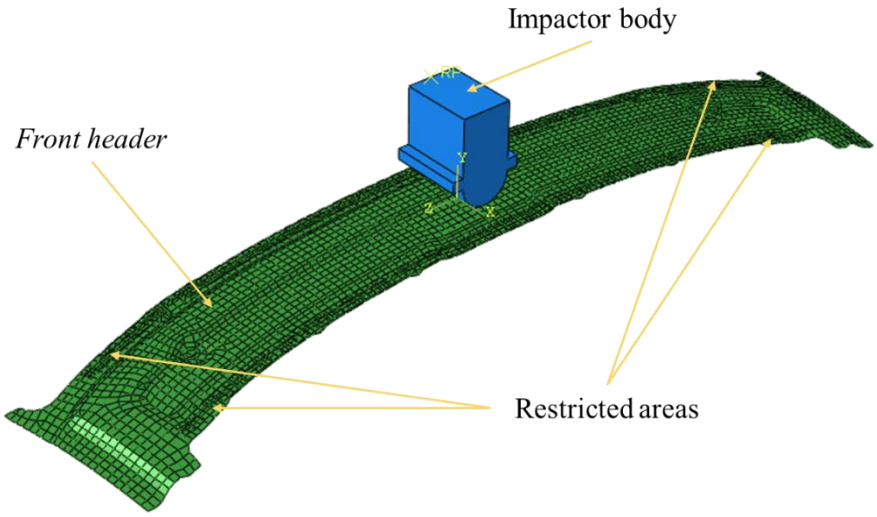

Fig. 11. Configuration of the numerical model used to simulate the behaviour of the automotive structure under impact.

4. Results and discussion

4.1. SLJ: experimental and numerical analysis

Fig. 12 shows a representative experimental load-displacement curve for both thicknesses, together with the numerical evolutions.

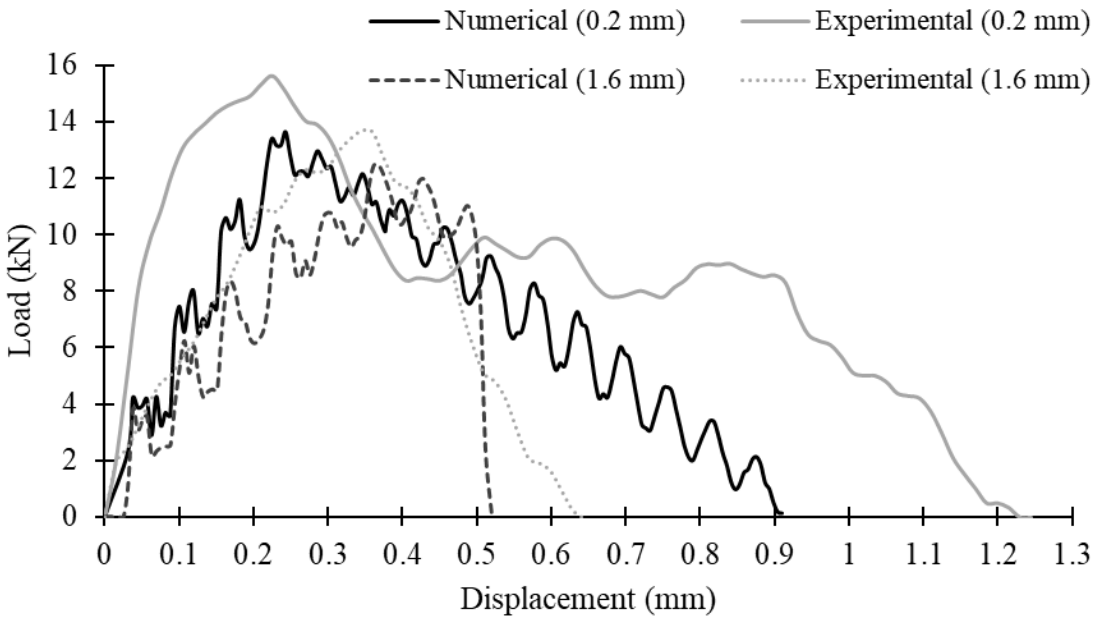

Fig. 12. Comparison between the experimental and numerical curves at impact conditions for an adhesive thickness of 0.2 and 1.6 mm.

As the impactor hits the fixture where the joints are assembled during the tests, high load peaks were observed in the initial stages of the raw experimental data. These are induced by acceleration peaks that occur due to contact between the impactor and the metal grip and do not correspond to the real strength of the joint. The information provided by the machine was therefore treated and filtered to remove this initial noise, resulting in the experimental data presented in Fig. 12. The failure loads predicted by the numerical models show relatively good accuracy with the experimental ones. The deviations can be explained by the fact that some adhesive properties were extrapolated for impact in [26] and [27]. The stiffness of the numerical models was slightly adjusted to compensate possible errors induced by clearances in the fixtures.

The SDEG parameter given by the numerical analysis is shown in Fig. 13 for both adhesive thicknesses, where it is possible to state that the degradation of the adhesive started in the edges and propagated to the middle of the adhesive layer, until cohesive failure was reached in the two configurations.

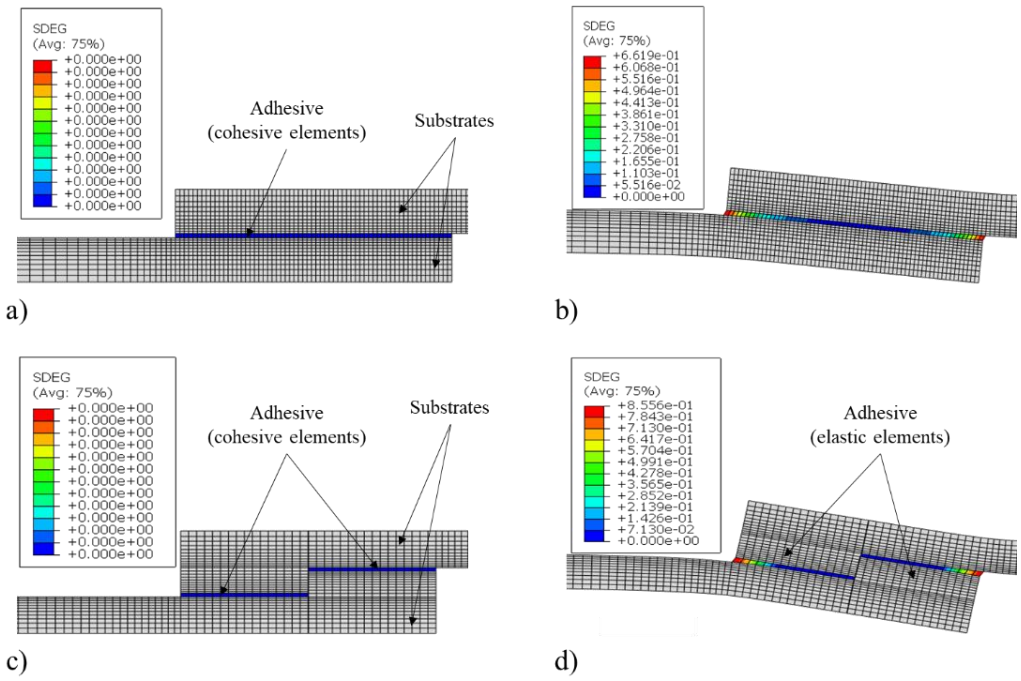

Fig. 13. Adhesive's degradation for a thickness of 0.2 mm (a) initial and b) intermediate stages) and 1.6 mm (c)initial and d) intermediate stages).

The results for impact are summarized in Table 4. A decrease in the joint strength was found with the increase of the adhesive thickness. Some general theories have been proposed to explain the reduction of strength for higher thicknesses. Gleich et al. [32] proposed, using a FE analysis, that the peel and shear stresses at the interface increase as the bondline gets thicker, leading to lower failure loads. Adams and Peppiatt [34] stated that thicker bondlines have tendency to contain more voids and microcracks, which cause premature failure of the joints. However, FE simulations conducted by Liao et al. [35] on SLJs subjected to impact tensile loads revealed that the maximum principal stress in the joint interface increases as the adhesive layer thickness decreases, suggesting lower failure loads for thinner thicknesses. These results appear to be in opposition to what was mentioned above and with the numerical and experimental results found in this work. Thus, the effect of bondline thickness on the strength of SLJs under impact conditions is still an open issue.

Table 4. Failure load results for the impact load.

	0.2 mm		**1.6 mm**	
	Experimental	**Numerical**	**Experimental**	**Numerical**
Failure load (kN)	17.18 ± 1.51	13.65	13.58 ± 1.46	12.50

4.2. Automotive structure (front header): experimental and numerical analysis

During the impact tests, the automotive structure specimens were found to fail due to high stress concentration around the middle holes present in the lower substrate. Such phenomenon led to the initiation and propagation of a crack (Fig. 14), which caused the decreasing of the load carrying capacity of the component. The response of the structure can therefore be said to be highly dependent of the behaviour of the aluminium substrates, with the adhesive being responsible by transferring the loads between the substrates. The load-displacement curves for the numerical analysis and a representative experimental specimen are shown in Fig. 15. Due to the failure mechanism described above, it can be concluded that the load the automotive structure is able to withstand is relatively low. Due to the lack of information regarding the damage evolution of the aluminium substrates, the FE analysis results were only considered until the ultimate stress (Fig. 4) was reached. The numerical model was able to correctly predict the maximum load of the front header, but the displacement was not so accurate. This was due to the boundary conditions assigned to the numerical analysis and the ones verified in the experimental procedure: while in the FE analysis perfect conditions were considered, truly restraining the ends of the component from moving, such condition was not exactly replied during the tests. In fact, the structure and its assembly during the impact load were less stiff than the numerical model, allowing small movements and therefore leading to higher displacements in the load-displacement curve. In order to compensate these observations, the stiffness of the FE model was slightly corrected to allow a more realistic comparison with the experimental data.

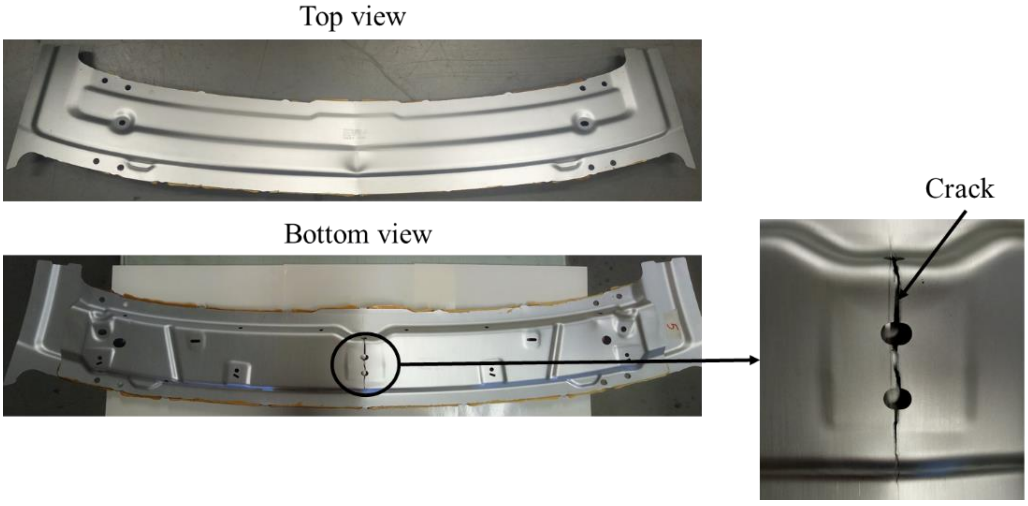

Fig. 14. Failure mechanism observed in the specimens during the impact tests.

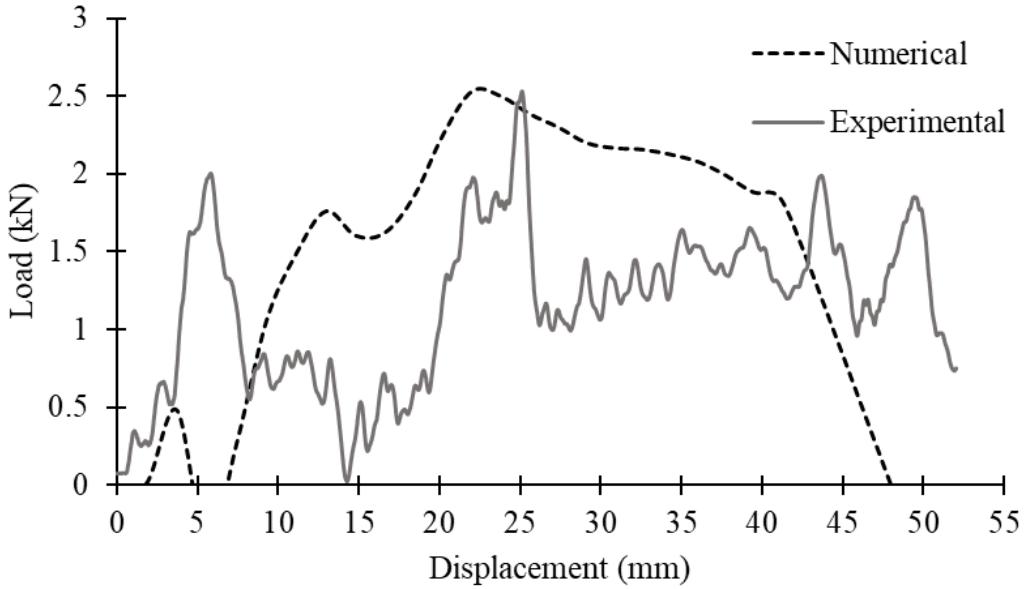

Fig. 15. Load-displacement curves for the impact loading.

Table 5 summarizes the results obtained for the dynamic testing, in terms of failure load and absorbed energy, the last calculated as the area below the curves. The values of the simulation are slightly higher than those measured experimentally as ideal conditions are considered in the software, something that is practically impossible to obtain during the tests.

Table 5. Failure load and absorbed energy of the automotive structure under impact conditions.

	Experimental	**Numerical**
Failure load (kN)	2.32 ± 0.30	2.53
Absorbed energy (J)	60.22 ± 0.06	72.30

4.3. Influence of adhesive type on the dynamic response of the automotive structure

Since fracture was observed in the front header specimens bonded with the crash-resistant epoxy system, another adhesive was selected to verify if this phenomenon could be avoided. Therefore, a high-performance structural polyurethane was chosen, supplied by Sika® and with the reference SikaForce®-7818 L7 (Table 6). The manufacturing process previously described for the epoxy remains valid for the polyurethane-bonded specimens, excepting for the curing cycle. This adhesive cures at RT by chemical reaction of two components, dispensing the use of the oven.

Table 6. General properties of the SikaForce®-7818 L7 polyurethane adhesive.

Properties	
Density [kg/m^3]	1230
Tensile strength [MPa]	35
Young's modulus [MPa]	2500
Tensile lap-shear strength [MPa]	20
Elongation at break [%]	2.5
Glass transition temperature [°C]	45

For the case of the automotive structure bonded with the polyurethane, no failure was found in the component, in opposition to what was verified with the specimens bonded with the crash-resistant adhesive (Fig. 16).

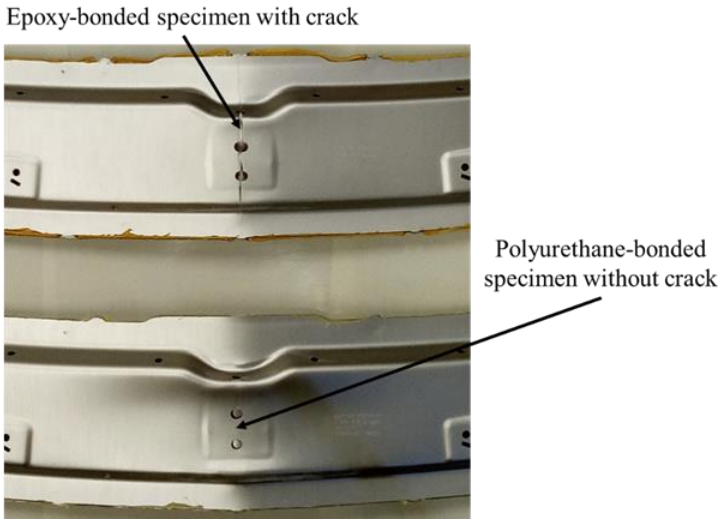

Fig. 16. Front header specimens tested under impact condition, showing that aluminium fracture does not occur when polyurethane is used.

Fig. 17 represents the evolutions of the load in the structure and the displacement of the impactor with time. Its analysis allows to conclude that the load in the structure increases as the impact moves downwards (its displacement is considered positive in this direction) and starts to decrease from the moment when the impactor starts to rebound (its displacement evolves in the opposite direction). This is, the maximum load in Fig. 17 do not correspond to the strength of the joint. This value was not possible to find because the impact conditions (30 kg and 3 m/s) were insufficient to cause the failure of the new specimen. The same impact conditions were considered for both epoxy and polyurethane so that comparisons between the results could be made.

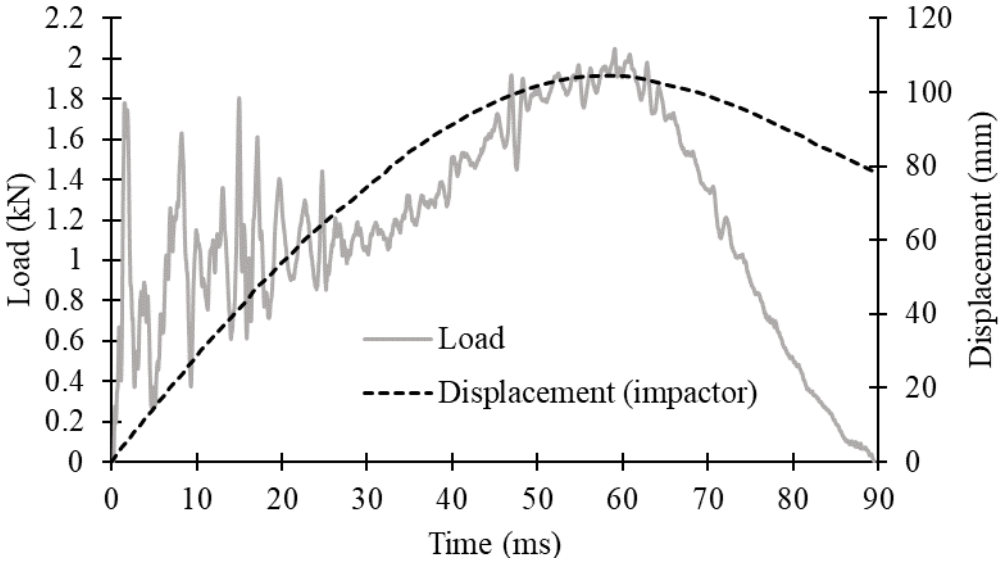

Fig. 17. Evolutions of the load in the structure and the displacement on the impactor for the polyurethane-bonded automotive structure.

The load-displacement evolutions for the automotive structures bonded with the two adhesives are shown in Fig. 18. As two epoxy-bonded specimens were tested, a representative experimental curve is presented for this case. Only one structure bonded with polyurethane was tested due to specimens' availability.

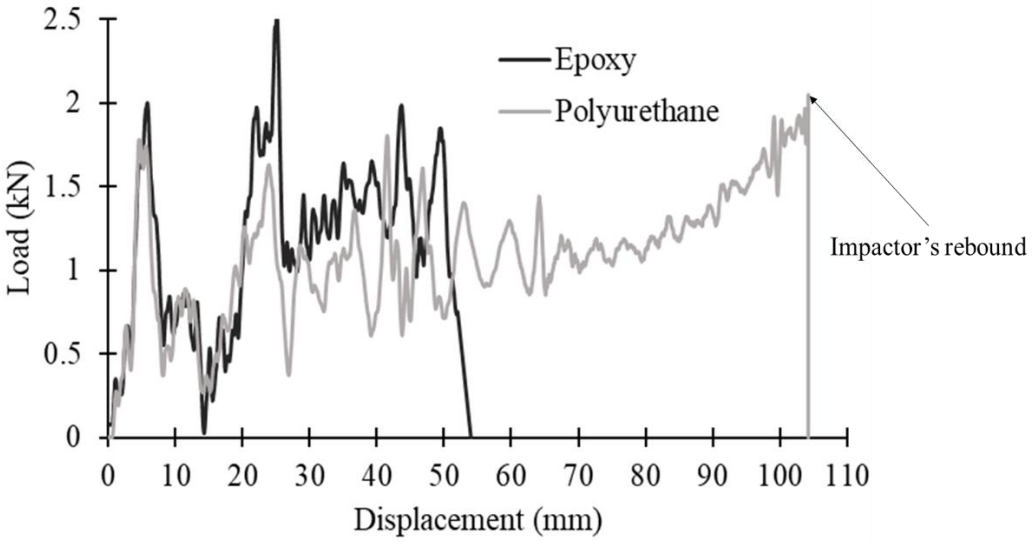

Fig. 18. Load-displacement curves for the automotive structure bonded with the two adhesives.

The curves present a similar shape until the moment when the specimen bonded with the epoxy adhesive starts to fail due to the initiation of the crack. The structural polyurethane seems to be more suited than the crash-resistant epoxy in the context of the joint, as it leads to higher energy-absorption capabilities (Table 7) and no failure for the

same boundary conditions. Such observation can be explained by the fact that the polyurethane, although weaker, is more flexible than the epoxy. This means higher absorption energy in the adhesive and less transmitted load to the lower substrate, avoiding the appearance of the high stress concentrations in the middle holes that caused the crack.

Table 7. Failure load and absorbed energy for the specimens bonded with the two adhesives.

	Epoxy	**Polyurethane**
Failure load (kN)	2.32 ± 0.30	Not reached
Absorbed energy (J)	60.22 ± 0.06	(113.75)*

*Until impactor's rebounding moment

5. Conclusions

In this work, a real, adhesively bonded automotive structure was tested under impact condition (3 m/s), with the main goal of showing that adhesive bonding behaves well during crash situations. The analysis conducted at RT, corresponding to the temperature verified in most service situations, allowed to conclude that failure in the specimens bonded with the crash-resistant epoxy adhesive occurred due to the formation and further propagation of a crack in the middle of the lower substrate, caused by the presence of holes which led to high stress concentrations. Therefore, the adhesive can be concluded to successfully transfer the loads between the adherends and not to compromise the response of the structure, as its behaviour is predominantly ruled by the aluminium substrates. The simulation carried out in ABAQUS® software package correctly predicted the maximum load of the front header, while its displacement was not as accurate. This was attributed to the boundary conditions applied to the model and to the specimens, as the assembly of the last was less stiff and allowed some movement, leading to higher displacements than those obtained numerically. When a more flexible adhesive was used instead, namely a high-performance structural polyurethane, the joint performance was found to improve under the same conditions. This is due to the higher ductility of the polyurethane, which is responsible for absorbing higher amounts of energy and transferring less of it to the lower substrate, avoiding its fracture. Still, even in the presence of a crack, the adhesion capabilities of the epoxy system were not affected, as the structure remained perfectly bonded (but with its load carrying capabilities lost). Thus,

it is possible to state that the behaviour of the adhesive influences the response of the structure, but in neither case the adhesive bonding compromised the integrity of the joint, being therefore a trustworthy solution to join real automotive components subjected to impact loads.

As a complement, SLJs with aluminium adherends similar to those used in the automotive structure were bonded with the same crash-resistant epoxy adhesive, in an attempt to study the influence of the adhesive layer thickness on the behaviour of the joints. Two thicknesses were tested at RT, namely 0.2 and 1.6 mm, allowing to conclude that the joint strength decreases with increasing thickness for impact. The numerical results, also conducted in ABAQUS®, showed relatively good accordance with the experimental observations. The considerably difference regarding the 0.2 mm thickness can be explained by possible variations in the properties used to model the adhesive under impact, as some of them were obtained by extrapolation.

Acknowledgments

The authors gratefully acknowledge the funding provided by Project NORTE-01-0145-FEDER-000022 - SciTech - Science and Technology for Competitive and Sustainable Industries, co-financed by Programa Operacional Regional do Norte (NORTE2020), through Fundo Europeu de Desenvolvimento Regional (FEDER), and by PhD grant SFRH/BD/139341/2018 "Impact strength optimization with cohesive zone elements of multi-material bonded structures used in the automotive industry", Project Nº 028473 POCI-01-0145-FEDER-028473 "Design methodology for impact resistant bonded multi-material automotive structures (ImpactBondDesign)". The authors would also like to thank Nagase ChemteX® for the financial support provided, as well to Aston Martin Lagonda Limited® for supplying the aluminium substrates.

References

1. Thornton, P. and R. Jeryan, *Crash energy management in composite automotive structures.* International Journal of Impact Engineering, 1988. **7**(2): p. 167-180.
2. C England, J., et al., *Design of Automotive Metal and Composite Chassis Structures.* Recent Patents on Mechanical Engineering, 2010. **3**(3): p. 211-225.

3. Khan, A.S. and H. Liu, *Variable strain rate sensitivity in an aluminum alloy: Response and constitutive modeling.* International Journal of Plasticity, 2012. **36**: p. 1-14.
4. Barnes, T.A. and I.R. Pashby, *Joining techniques for aluminium spaceframes used in automobiles: Part II — adhesive bonding and mechanical fasteners.* Journal of Materials Processing Technology, 2000. **99**(1): p. 72-79.
5. Tisza, M. and I. Czinege, *Comparative study of the application of steels and aluminium in lightweight production of automotive parts.* International Journal of Lightweight Materials and Manufacture, 2018. **1**(4): p. 229-238.
6. Hirsch, J., *Aluminium Alloys for Automotive Application*. Vol. 242. 1997. 33-50.
7. Miller, W.S., et al., *Recent development in aluminium alloys for the automotive industry*. Materials Science and Engineering: A, 2000. **280**(1): p. 37-49.
8. Hirsch, J., *Recent development in aluminium for automotive applications.* Transactions of Nonferrous Metals Society of China, 2014. **24**(7): p. 1995-2002.
9. Henning, F., et al., *Fast processing and continuous simulation of automotive structural composite components.* Composites Science and Technology, 2019. **171**: p. 261-279.
10. Borsellino, C., G. Di Bella, and V. Ruisi, *Adhesive joining of aluminium AA6082: The effects of resin and surface treatment.* International Journal of Adhesion and Adhesives, 2009. **29**(1): p. 36-44.
11. Galvez, P., et al., *Study of the behaviour of adhesive joints of steel with CFRP for its application in bus structures.* Composites Part B: Engineering, 2017. **129**: p. 41-46.
12. Machado, J.J.M., E.A.S. Marques, and L.F.M. da Silva, *Adhesives and adhesive joints under impact loadings: An overview*. The Journal of Adhesion, 2018. **94**(6): p. 421-452.
13. He, X., *A review of finite element analysis of adhesively bonded joints.* International Journal of Adhesion and Adhesives, 2011. **31**(4): p. 248-264.
14. Hill, J., *Adhesively Bonded Structural Composites for Aston Martin Vehicles.* Ford Motor Company Research and Advanced Engineering, 2003.
15. Silva, L.F.M., A. Öchsner, and R. Adams, *Handbook of Adhesion Technology*. 2011. p. 1-7.

16. Feraboli, P. and A. Masini, *Development of carbon/epoxy structural components for a high performance vehicle.* Composites Part B: Engineering, 2004. **35**(4): p. 323-330.
17. Silva, M.R.G., E.A.S. Marques, and L.F.M.d. Silva, *Behaviour under Impact of Mixed Adhesive Joints for the Automotive Industry.* Latin American Journal of Solids and Structures, 2016. **13**: p. 835-853.
18. Saldanha, D.F.S., et al., *Mechanical characterization of a high elongation and high toughness epoxy adhesive.* International Journal of Adhesion and Adhesives, 2013. **47**: p. 91-98.
19. Adams, R.D., *Adhesive bonding: science, technology and applications*. 2005: Elsevier.
20. Machado, J.J.M., et al., *Numerical study of impact behaviour of mixed adhesive single lap joints for the automotive industry.* International Journal of Adhesion and Adhesives, 2018. **84**: p. 92-100.
21. Neto, R.C., E. Sampaio, and J. Assis, *Numerical and experimental analysis of bonded joints with combined loading.* International Journal of Adhesion and Adhesives, 2019. **90**: p. 61-70.
22. Golzar, M. and M. Poorzeinolabedin, *Prototype fabrication of a composite automobile body based on integrated structure.* The International Journal of Advanced Manufacturing Technology, 2010. **49**(9-12): p. 1037-1045.
23. Langseth, M., O.S. Hopperstad, and A.G. Hanssen, *Crash behaviour of thin-walled aluminium members.* Thin-Walled Structures, 1998. **32**(1): p. 127-150.
24. Cheon, S.S., D.G. Lee, and K.S. Jeong, *Composite side-door impact beams for passenger cars.* Composite Structures, 1997. **38**(1): p. 229-239.
25. Li, Q.F., et al., *Optimum Design and Numerical Simulation of Automotive Front Side-Door Impact Beam.* Key Engineering Materials, 2011. **452-453**: p. 169-172.
26. J. J. M. Machado, A.H., P. D. P. Nunes, E. A. S. Marques, R. J. C. Carbas, C. Sato, L. F. M. da Silva, *Strain rate dependence of a crash resistant adhesive as a function of temperature for the automotive industry.* 2018.
27. Araújo, H., et al., *Dynamic behaviour of composite adhesive joints for the automotive industry*. Composite Structures, 2017. **171**: p. 549-561.
28. Oosterkamp, L.D., A. Ivankovic, and G. Venizelos, *High strain rate properties of selected aluminium alloys.* Materials Science and Engineering: A, 2000. **278**(1-2): p. 225-235.

29. Torca, I., et al., *Tensile Behaviour of 6082 Aluminium Alloy Sheet under Different Conditions of Heat Treatment, Temperature and Strain Rate*. Vol. 423. 2009. 105-112.
30. Chen, Y., et al., *Stress–strain behaviour of aluminium alloys at a wide range of strain rates.* International Journal of Solids and Structures, 2009. **46**(21): p. 3825-3835.
31. Yibo, P., et al., *Dynamic Mechanical Behaviors of 6082-T6 Aluminum Alloy.* Advances in Mechanical Engineering, 2013. **5**: p. 878016.
32. Gleich, D.M., M.J.L. Van Tooren, and A. Beukers, *Analysis and evaluation of bondline thickness effects on failure load in adhesively bonded structures.* Journal of Adhesion Science and Technology, 2001. **15**(9): p. 1091-1101.
33. Campilho, R.D.S.G., et al., *Modelling adhesive joints with cohesive zone models: effect of the cohesive law shape of the adhesive layer.* International Journal of Adhesion and Adhesives, 2013. **44**: p. 48-56.
34. Adams, R.D. and N.A. Peppiatt, *Stress analysis of adhesive-bonded lap joints.* Journal of Strain Analysis, 1974. **9**(3): p. 185-196.
35. Liao, L., et al., *3-D FEM stress analysis and strength evaluation of single-lap adhesive joints subjected to impact tensile loads.* International Journal of Adhesion and Adhesives, 2011. **31**(7): p. 612-619.